MODELING AND DESIGN OF AN AC MAGNETOHYDRODYNAMIC MICROPUMP USING LORENTZ FORCE

By
Mustafa Rasheed Abdullah

Supervisor
Dr. Hamzeh Duwairi

This Dissertation was Submitted in Partial Fulfillment of the Requirements for the Doctor of Philosophy Degree in Mechanical Engineering

Faculty of Graduate Studies
The University of Jordan

August, 2007

Dedication

To my father, mother, wife and family for their love, encouragement and support

Acknowledgement

My first thanks go to my advisor, Dr. Hamzeh Duwairi, for guiding me during my work. I also wish to thank my committee members, Professor Mahmood Hammad, Professor Ali Badran and Professor Burhan Tashtoush for reviewing my dissertation.

Many thanks go to my family, friends and colleagues for their encouragement and support.

Special thanks to Dr. Jamal Nazzal for his continuous support and help during my education.

List of Contents

List of Tables

List of Figures

List of Symbols

$a_{m,n}$, $b_{i,j}$	Separation variables
B	Magnetic flux density (*Tesla*)
C_p	Specific heat (*kJ/kg.K*)
E	Electric field intensity (*Volt/m*)
Ec	Eckert number, $Ec=u_0^2/C_pT_w$
f,g	Separation variables
F_L	Lorentz force, (*Newton*)
h	Height of micro-channel (*m*)
H	Separation variable
Ha	Hartman number, $Ha=wB\sqrt{\sigma/\mu}$
J	Electric current density ($Amper/m^2$)
K	Thermal conductivity (*W/m.K*)
L	Length of micro-channel (m)
P	Pressure (N/m^2)
Pr	Prandtl number, $\Pr=\mu C_p/k$
P^*	Dimensionless pressure gradient
p^*	Dimensionless pressure
q	Charge (Coulombs)
Re	Reynold's number, $\mathrm{Re}=\frac{u_0L}{\nu}$
S	Source term in energy equation
St	Stanton number, $St=\frac{w}{\sqrt{\nu T^*}}$
t	Time (*s*)
T	Temperature (*K*)
T^*	Period of alternations in electric and magnetic fields (*s*)
T_w	Wall temperature (*K*)
u,v	Velocity components in the x, and y directions (*m/s*)
u^*,v^*	Dimensionless velocity components in x, and y directions
u_m	Mean velocity (*m/s*)
u_m^*	Dimensionless mean velocity
V	Potential difference (*Volts*)
w	Width of micro-channel (*m*)
x, y, z	Cartesian coordinates
x^*,y^*,z^*	Dimensionless coordinates

Greek Symbols

μ	Dynamic viscosity ($N \cdot s/m^2$)
ρ	Density (kg/m^3)
υ	Kinematic viscosity (m^2/s)
σ	Liquid's conductivity ($Siemens/m$)
α	Aspect ratio
τ	Dimensionless time
θ	Dimensionless temperature
γ, λ, η	Separation constants
ψ, δ, ϕ	Separation variables
ω	Angular frequency (*rad/s*)
ϕ	Phase shift angle (*rad*)

MODELLING AND DESIGN OF AN AC MAGNETOHYDRODYNAMIC MICROPUMP USING LORENTZ FORCE

By
Mustafa Rashied Abdullah

Supervisor
Dr. Hamzeh Duwairi

Abstract

A theoretical model describing a magnetohydrodynamic (MHD) micropump is presented. The micropump is driven by the Lorentz force which is induced as a result of interaction between an applied electric field and a perpendicular magnetic field. The Lorentz force is used to pump an electrically conducting liquids along a microchannel.

A two-dimensional transient fully developed laminar flow and temperature distribution is modeled, where the velocity and temperature profiles under the effect of Lorentz force are solved both analytically and numerically. The governing equations are solved analytically by an eigenfunction expansion method, and numerically by a finite-difference (ADI) method. The numerical and analytical results are found to be in good agreement with each other. The effect of different parameters on the transient and steady flow velocity and temperature, such as aspect ratio, Hartman number, Prandtl number, and Eckert number is studied. The results obtained showed that controlling the flow and the temperature can be achieved by controlling the potential difference, the magnetic flux, and by a good choice of the electrical conductivity.

The transient, laminar, incompressible, and developing flow equations are numerically solved using the finite difference method and the SIMPLE algorithm. The effect of Hartman number on the transient velocity profile and the entrance region length is studied. It is found that controlling the electrical conductivity and magnetic flux density will allow to control the entrance region length.

The effect of fluctuating Lorentz force on the AC magnetohydrodynamic micropump is studied for both developing and fully developed flow. It was found that at high frequency, the pulsed volume is small, which yields a continuous flow instead of pulsating flow. The magnitude and direction of the flow can be controlled by the phase shift between the electrical and magnetic fields.

Chapter 1
Introduction

1.1 Micro-Electromechanical systems (MEMS)

Micro-electromechanical systems (MEMS) is a technology used to create small integrated devices or systems that combine mechanical and electrical components. They can range in size from a few micrometers to millimetres. These systems have the ability to sense, control and actuate on the micro scale, and generate effects on the macro scale. The advantages following from the use of microsystems compared to macrosystems are:

1. Smaller size of the devices (bringing analysis closer to the process)

2. Reduced fabrication costs (depending on the volume of production)

3. Lower energy consumption (due to smaller size of the device, provides suitability for wireless solutions)

4. Smaller volumes of expensive reagents (or also suitable for situations, where sample is not available in large enough volume)

5. Better performance

In the most general form, MEMS consist of mechanical microstructures, microsensors, microactuators and microelectronics, all integrated onto the same silicon chip. Microsensors detect changes in the system's environment by measuring mechanical, thermal, magnetic, chemical or electromagnetic information or phenomena. Microelectronics process this information and signal the microactuators to react and create some form of changes to the environment.

1.2 Microfluidics

Micro-fluidic systems were one of MEMS developed in recent years. In these years, many papers that studied very small devices controlling or sensing flow named microflow devices have been published.

Microflow systems consist of nozzles, pumps, reservoirs, mixers, valves, sensors etc., can be used for many applications including drug dispensing, ink-jet printing and general transport, analysis and production of liquids, gases and their mixtures. In addition, the medical industry has shown interest in microfluidics technology.

.1.3 Micropumps

One of the most common devices in microfluidic systems is the micro pump, which plays an important role in a micro-fluidic system, and can be used in many application fields, such as fluid distribution, medical transportation, and micro cooling of electronic components.

Clearly, the need to precisely control gas and fluid flow is critical for biomedical systems. Hence, there have been many efforts to develop low-cost high-precision microneedles, microfilters, microvalves and micropumps.

Several methods of microactuation have been used to drive micropumps. They depend on electrostatic, magnetic, and piezoelectric forces.

Figure (1.1) illustrates the classification of micropumps. The typical operation range of displacement micropumps lies between 10 μl/min and several milliliters per minute. For flow rates less than 10 μl/min, alternative dynamic pumps or non-mechanical pumps are needed for an accurate control of these small fluid amounts .

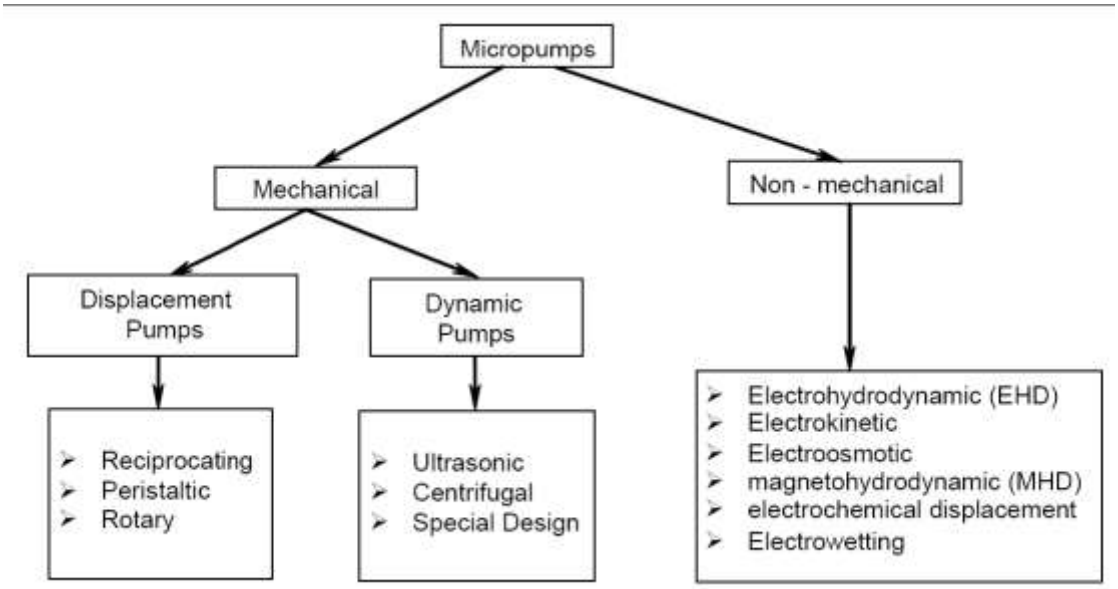

Figure 1.1: Classification of micropumps

1.3.1 Mechanical micropumps

Mechanical pumps can be divided according to the principles by which mechanical energy is applied to the fluid. Mechanical pumps are divided into two major categories: displacement pumps and dynamic pumps. In displacement pumps, such as peristaltic, reciprocating and rotary pumps, energy is periodically added by the application of force to a movable boundary. In dynamic pumps, such as ultrasonic pumps and centrifugal pumps, energy is continuously added to increase the fluid velocities within the pump.

Reciprocating pumps

A reciprocating pump consists of a pressure chamber with an actuated diaphragm and two check valves. The actuator can be a piezoelectric, pneumatic or electrostatic actuator, for example. In the first phase of pumping, liquid is sucked into the chamber and in the next phase, pumped out. The check valves prevent flow to the wrong direction.

A valve-less reciprocating pump contains diffuser/nozzle units instead of check valves. In valve-less reciprocating valves, there is always flow to both directions but the parameters of the diffusers and nozzles determine the direction and volume of the net flow. The operating principle of the valve-less micropump is presented in Figure (1.2).

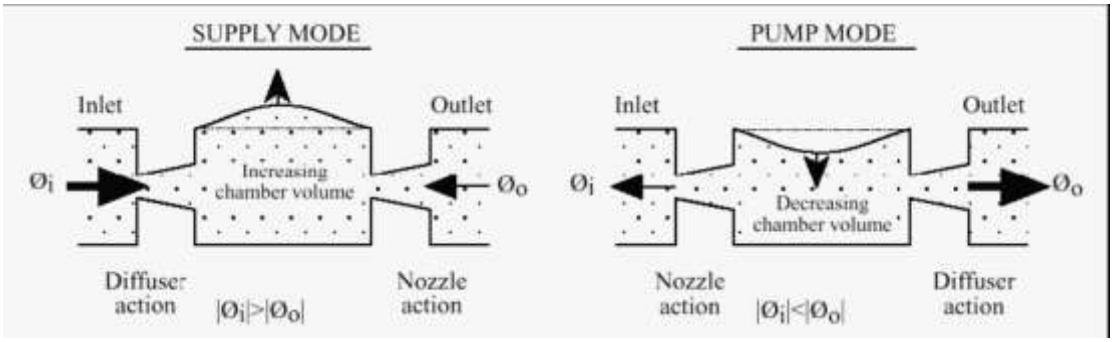

Figure 1.2: Operating principle of diffuser based micropump (Woias 2005)

Peristaltic pumps

In peristaltic pumps, the pumping concept is based on the peristaltic motion of the pump chambers which squeezes the fluid in the desired direction. Peristaltic pumps need three or more pump chambers with actuating membrane.

Rotary pumps

In rotary pumps, the liquid is actuated using rotating gears which mesh together. One gear is turned by an external or internal actuator and it drives the other gear. The space between the gear teeth moves the liquid through the pump chamber.The operation principle can be seen in Figure (1.3)

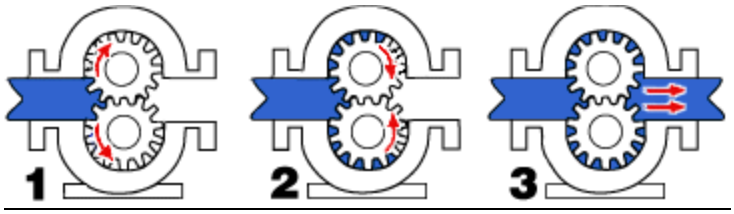

Figure 1.3: An operation principle of a gear pump (Nguyen et al, 2002)

1.3.2 Non-mechanical micropumps

Non-mechanical micropumps add momentum to the fluid by directly converting non-mechanical energy into kinetic energy without mechanical movement of a structure. While mechanical pumping is mostly used in macroscale pumps and micropumps with a relatively large size and high flow rates, the non-mechanical pumps have advantages when used in the microscale. The driving forces can be electric, magnetic, thermal, chemical or surface tension forces. The non-mechanical micropumps can be categorized into electrohydrodynamic (EHD) pumps, electrokinetic pumps, and magnetohydrodynamic (MHD) pumps.

Electro-hydro dynamic (EHD) pumps

Electrohydrodynamic pumps are based on electrostatic forces acting on nonconductive fluids. EHD pumps can be categorized as EHD injection pumps (static) and EHD induction pumps (dynamic).

Electrokinetic pump

Electrokinetic pumps use a static electric field for pumping conductive fluid. The electrokinetic phenomenon can be divided into electrophoresis and electro-osmosis. Electrokinetic flow results from the effect of electrical field on charged particles in the fluid and fluid itself, when the fluid is placed in a narrow capillary. The force on the particles in the fluid leads to electrophoresis while the force on the fluid in a narrow capillary leads to electro-osmosis. Since electrophoresis and electro-osmosis occur at the same time, electro-osmosis usually determines the overall direction of the fluid.

Magneto-hydro dynamic (MHD) pump

The magnetohydrodynamic (MHD) micropump is one of the important micropumps which has no moving parts, generates continuous flow, and has potential applications in biomedical studies. The pumping source in the (MHD) micropumps is the Lorentz force which is produced as a result of interaction between the magnetic and electric fields. The magnitude of the force depends on the electric current across the channel, the magnetic flux density and the width of the channel. The resulting Lorentz force affects the ions in the solution and thus, propels the fluid. Because the Lorentz force acts on the bulk fluid and creates a pressure gradient, MHD pumps generate a parabolic velocity profile similar to pressure-driven flows. Figure (1.4) shows a schematic diagram of the MHD micropump.

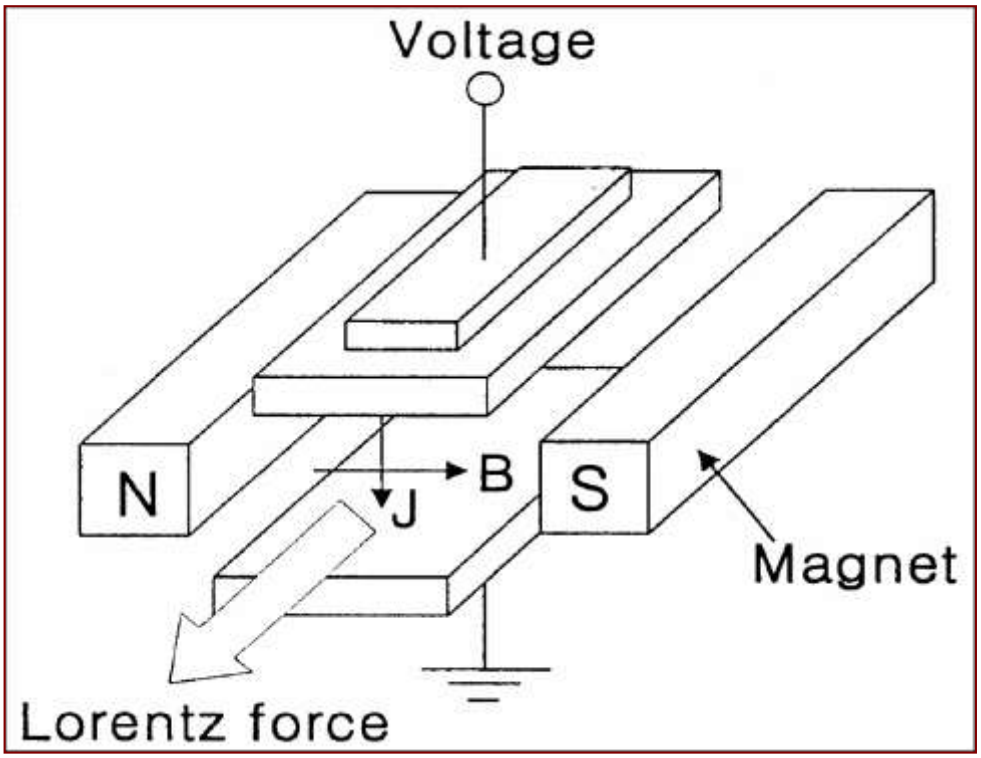

Figure 1.4: A schematic diagram of the MHD micropump

Compared with other types of non-mechanical micropumps, the MHD micropump has several advantages, such as

1- The MHD micropumps operate without moving parts.

2- The pumps require low actuation voltages (less than 10 V).

3- Similar to pressure-driven flows, forword and reverse flows can be obtained.

4- The solution with least slight electrical conductivity can be pumped.

5- The fabrication process is simple.

6- The pumps produce continuous fluid flow.

Hence, it is believed that the MHD micropump can be used in biomedical devices such as a drug delivery system or it can be used to propel highly conducting fluids such as liquid metals and ionized gases and it can be used in fluid stirring and mixing.

Chapter 2
Literature survey

2.1 MHD micropumps

A review study of microflow devices and systems was presented by (Shoji and Esashi, 1994). In the study, microflow devices including microvalves, micropumps and microflow sensors fabricated by micromachining were reviewed. Schomburg *et al*.(1993) and Schomburg *et al*.(1994) developed pumps and valves for microfluidic systems using advanced micromachining technology.

A review studies of micropumps were presented by (Nguyen *et al*., 2002) and (Woias, 2005). Nguyen *et al*.(2002) divided the micropumps into two categories: Mechanical micropumps which have moving mechanical parts, and non-mechanical micropumps without moving parts. Woias (2005) divided micropumps into two groups: Reciprocating micropumps which use the oscilaory or rotational movement of fluid, and continuous flow micropmp (including magnetohydrodynamic, electrohydrodynamic, electroosmatic and electrochemical actuation mechanisms) which are based on a direct transformation of non-mechanical or mechanical energy into a continuous fluid movement.

According to these studies the micropumps can be divided into two large groups, mechanical micropumps and non-mechanical micropumps. Koch *et al*.(1998), Ullmann (1998), Richter *et al*.(1998), Jun and Kim(1998), Bohm *et al*.(1999), Zeng *et al*.(2001), Yun *et al*.(2001), and Debesset *et al*.(2004) studied some of these micropumps that are used to propel fluid for different applications.

In the last century, the MHD principle has been widely used and studied and there are many studies of the MHD channel flows in macroscopic scale. Ramos and Winowich (1986) analyzed the steady state MHD channel flow using a finite difference method. The results of the calculations indicate that the electromagnetic forces yield M-shaped velocity profiles.

Ueno (1991) studied the inertia effect in two dimensional MHD channel flow under a traveling sine wave magnetic field. He concluded that the inertia effect to the power output is very small. Also, Ueno (1993) studied the effect of turnaround lines of magnetic flux in two dimensional MHD channel flow. It was concluded that a set of turnaround lines of magnetic flux cause a set of recirculating flows. Bessaih and Kadji (1999) studied MHD flow of a liquid metal Flow driven by a rotating disk. The results obtained showed that the flow can be controlled by a good choice of electrical conductivity.

Attia (2001) studied the effect of variable viscosity on the transient MHD flow of dusty fluid with heat transfer. He found that some important effects for the variable viscosity are indicated.

West *et al*.(2002) studied application of MHD actuation to continuous flow chemistry where fluid propulsion was achieved using AC MHD actuation. Wang *et al*.(2003) designed a programmable diffusion bioassays based on MHD microfluidic system.

Brener and Park(2004) studied and discussed the design and fabrication of electromagnetic actuators and their application to affect the wall shear stress on a fully turbulent channel flow. Satou *et al*.(2004) developed a new AC MHD calculation for electromagnetic stirring.

Khalzov and Smolyakov (2006) proposed a new numerical method to calculate two-dimensional steady state MHD flows of incompressible liquid metals in linear and circular thin-wall ducts of a rectangular cross section.

Recently, theoretical and experimental studies on DC and AC MHD micropumps were investigated. An MHD micropump using a DC current and a permanent magnet was firstly described by (Jang and Lee, 1998).

Jang and Lee, (2000) studied theoretically and experimentally an MHD micropump. They obtained the performance of the micropump by measuring head difference and flow rate. In this study, bubble generation by the electrolysis of the conducting liquid was observed.

The use of magnetohydrodynamic (MHD) to circulate fluids in conduits fabricated with ceramic tapes was described by (Zhong *et al*., 2002). The experiments described used mercury slags, saline solution and deionized water as the conducting fluid.

To avoid gas bubbles, Homsy *et al*. (2005) described the operation of DC (MHD) micropump at a high current densities where the gas bubbles was not observed in the pumping channel. They have discussed experimental observations where they noted that the flow velocity was higher than that calculated. One explanation is that the temperature in the channel began to rise because of Joule heating occurring in the channel. Above a certain threshold the temperature will decrease the viscosity of the pumped solution, leading to an increase in flow velocity.

Patel and Kassegne (2006) developed a numerical frame work to investigate different flow channel geometries influenced by the micromachining process, effects of non-uniform magnetic and electric fields, Joule heating, and electroosmatics in MHD micropumps.

In a DC (MHD) micropump with permenant magnet, the electrolytic reaction that enables current conduction also produces gas bubbles that impede fluid flow and causes electrodes to dissolve. This limits the practical application of such a device to non electrolytic conductors, such as liquid metals. When an AC current of sufficiently high frequency is passed through an electrolytic solution, the chemical reactions are reversed rapidly enough that bubbles never have a chance to form and no electrode degradation can occur (Lemoff *et al.*, 1999).

Lemoff and Lee (2000) described the theory, fabrication method and experimental results of an AC (MHD) micropump. Pumping was demonstrated in several different electrolytic solutions. Eijkel *et al.*(2003) developed and fabricated an AC magnetohydrodynamic micropump for chromatographic application.

A new study of (MHD) flow is presented by (Qian *et al.*, 2005). They studied theoretically the (MHD) flow of a RedOx electrolyte in a straight conduit, and solved the coupled momentum and advection equation.

In addition to (MHD) pumping, study of mixing systems and microfluidic networks using (MHD) pumping has been made. Bau et al. (2001) and Yi *et al*. (2002) constructed and analyzed two types of a magnetohydrodynamic stirrers experimentally and theoretically. An active micromixer has been developed that uses electric and magnetic fields to create Lorentz forces that induced MHD flows in a solution of an electrolyte (Bau *et al.*, 2001). The device was fabricated from ceramic tapes. Electrodes were created with gold paste, and were placed parallel to the channel. A permanent magnet was placed under the mixing

device. The mixing chamber was 1 mm deep, 4.7 mm wide, and 22.3 mm long (volume ~100 μL). When potential difference was applied to the electrodes, Lorentz forces were generated parallel to the axis of the chamber, and the solution was mixed within several seconds. Yi *et al.* (2002) investigated experimentally and theoretically a magnetohydrodynamic (MHD) stirrer that exhibits chaotic advection .

The area of micrototal analysis systems, also called (lab on a chip) is grawing rapidly (Reyes *et al*., 2002). Lemoff and Lee (2003) presented an MHD microfluidic switch which could form the basis for general microfluidic circuits. The switch uses an AC MHD pumping mechanism.

2.2 Present contributions to the previous work

The above previous researches presented and analyzed different models of the MHD micropumps which can be used in biomedical devices and microfluidic propulsion applications. Most of these researches studied the micropump flow experimentally or theoretically by assuming one dimensional steady fully developed flow, where the Poiseuille condition which neglects the side-wall frictional effects was used to solve for velocity distribution.

In this study a theoretical model of a DC and AC MHD micropump flow will be analyzed. The present contributions to the previous work are:

1- A transient two dimensional fully developed flow in a DC MHD micropump is modeled and analyzed. The dimensionless governing equations are solved numerically using suitable numerical technique and analytically using eigenfunction expansion method. The numerical and analytical results are compared with each other to enhance the solution.

2- A transient two dimensional developing flow in a DC MHD micropump is also modeled, and the dimensionless governing equations are solved numerically using pressure-correction method and SIMPLE algorithm. The results are verified by comparing them with analytical solutions of the fully developed region in the pump channel.

3- The effect of fluctuating Lorentz force on the transient behavior of an AC MHD micropump is studied for both fully developed and developing flow. A sinusoidal electric field with a perpendicular sinusoidal magnetic field with phase shift are applied. The difference between the DC and AC transient flow behavior is shown and studied.

4- The effect of dimensionless parameters such as Hartmann number, aspect ratio and prandtl number on the DC and AC MHD flow is studied.

5- It is noticed previously that there is an important effect of heat generation on other types of micropumps. Hence the effect of the heat generation produced by constant and fluctuating Lorentz force on temperature profile is studied in this work. The dimensionless energy equation is solved numerically and analytically and the effect of different parameters on temperature distribution such as Hartmann number, Stanton number, Eckert number and Prandtl number is discussed.

6- To design the MHD micropump, a good selection of the magnitude of certain parameters must be done. Hence the effect of different dimensional parameters such as: cross-sectional dimensions, magnetic flux, electric current density, frequency, phase angle and applied voltage on controlling the transient and steady flow and temperature rise for both DC and AC MHD pumping is studied.

7- The obtained results for the numerical analysis of a DC and AC MHD flow are compared with exact analytical solutions of the same governing equations or reduced forms of them.

Chapter 3
Mathematical Modeling

3.1 MHD theory

An inclined view of the MHD micropump and the coordinate system used are shown in Figure (3.1). A conductive liquid with a density ρ , a dynamic viscosity μ , and an electrical conductivity σ fills a rectangular cross-section channel of width *w*, height *h*, and length *L*. The coordinates *x*, *y*, and *z* are aligned, respectively, along the channel's axis, width, and height.

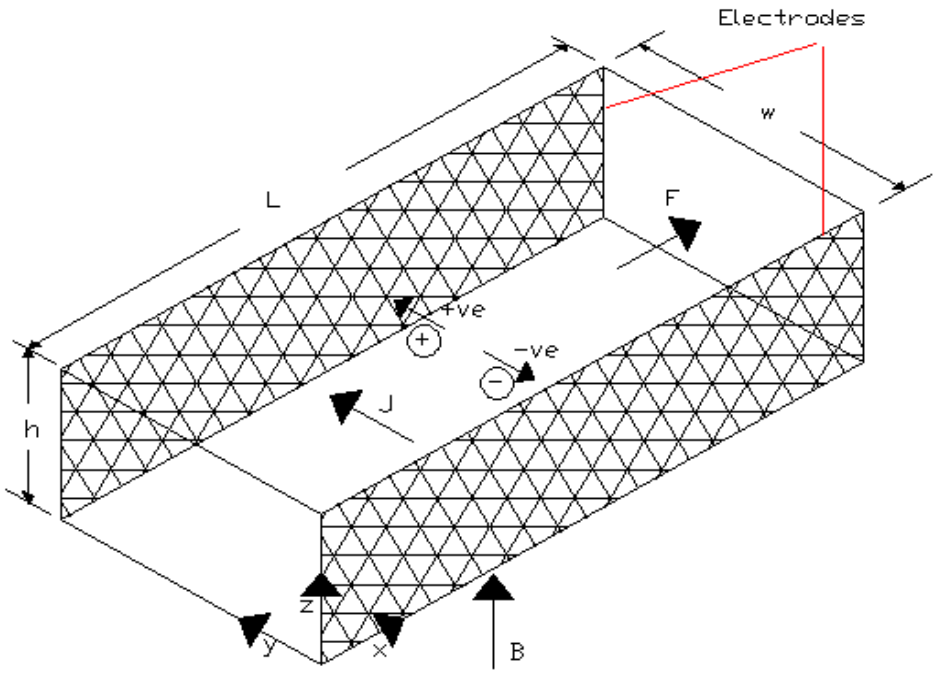

Figure 3.1: Inclined view of an MHD micropump

The channel is subjected to a potential difference *V* imposed across the opposing electrodes that induces an electric current of density *J*. The channel is placed in a uniform magnetic field of flux density *B* in the *z* direction.

The interaction between the magnetic and electric fields produces a body Lorentz force $J \times B$ that is perpendicular to both J and B. The Lorentz force is used to pump the conducting liquids along the microchannel.

To illustrate the pumping mechanism in details, the forces exerted as a result of the interaction between the electric and the magnetic field will be analyzed. As the electric current is carried between the electrodes across the channel, positive and negative ions will be formed and moved with opposite transverse velocities as shown in figure (3.1). The force exerted on every ion of species (*i*) in the solution will equal:

$$F_i = F_{el} + F_L \qquad (3.1)$$

Where F_{el} is the electrical field force and F_L is the Lorentz force. The electrical field force on every ion is:

$$F_{el} = Z_i q E \qquad (3.2)$$

Where Z is the valance, q is the unit charge. Due to the electroneutrality of the bulk solution $F_{el,total} = E\sum_i Z_i q N_i = 0$ (Eijkel et al. 2003), Where N_i is the number of ions of species i in the channel.

Now the second term in equation (3.1) is the Lorentz force:

$$F_L = Z_i q \vec{v}_i \times B \qquad (3.3)$$

Where $\vec{v}_i$ is the velocity of the ion.

The velocity has two components, one parallel to the electrical field and one along the channel length axis. The velocity component parallel to the electrical field exerts the first component of the Lorentz force:

$$F_{L1} = E \times B \sum_i Z_i q \mu_i N_i \qquad (3.4)$$

Where μ_i is the electrophoretic mobility (m^2/sV) and $\mu_i E$ is the migration velocity.

But $\sum_i Z_i q \mu_i N_i$ is the electrical conductivity multiplied by it's volume. Hence

$$F_{L1} = \sigma V_c E \times B \tag{3.5}$$

Where V_c is the channel volume, E is the electric field intensity and σ is the electrical conductivity, or $F_{L1} = V_c J \times B$ Where J is the current density.

Now the velocity component along the channel length axis will exert the second component of the Lorentz force (which is the magnetic force exerted on a current carrying conductor) which is

$$F_{L2} = J \times B \tag{3.6}$$

Where the current $J = \sigma(v \times B)$ induced when the magnetic field induces a voltage in the conductor of magnitude $v \times B$, then the total conduction current is now defined as:

$$J = \sigma(E + v \times B) \tag{3.7}$$

Then the total Lorentz force will be

$$F_L = J \times B = \sigma(E + v \times B) \times B \tag{3.8}$$

And the work done on the system per unit time by the Lorentz force is

$W = F_L . v$

Or $W = J \times B \cdot v$ (3.9)

But the magnetic field induces a voltage in the conductor of magnitude $v \times B = J/\sigma$ then

$$W = \frac{J \cdot J}{\sigma} \tag{3.10}$$

In this work, a DC and AC Lorentz force will be used to propel fluid in MHD micropump. In AC pumping, a sinusoidal electric current with a perpendicular sinusoidal magnetic field will be used. The electric current and magnetic fields will have equal frequency and a phase difference between them.

To illustrate the AC phase difference concept, figure (3.2) shows the relation between two AC voltages or currents that are out of step with each other, which means that the two waveforms are not synchronized; that their peaks and zero points do not match up at the same points in time.

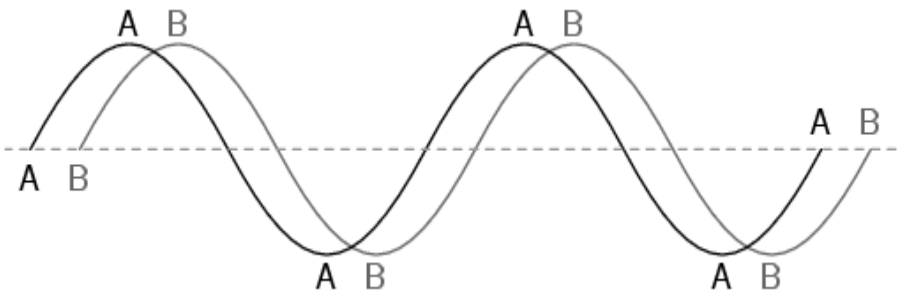

Figure 3.2: Out of phase waveforms

The two waves shown above (A versus B) are of the same amplitude and frequency, but they are out of step with each other. In technical terms, this is called a phase shift.

3.2 General Governing Equations

The governing equations of the MHD micropump that present the fluid motion are:

The **Ohm's Law**:

$$J=\sigma(E+u\times B) \tag{3.11}$$

The **continuity equation**:

$$\nabla . \vec{u} = 0 \tag{3.12}$$

The time dependent **momentum equation**:

$$\rho \frac{\partial \vec{u}}{\partial t} + \rho (\vec{u} . \nabla) \vec{u} = -\nabla p + \mu \nabla^2 \vec{u} + \vec{J} \times \vec{B} \tag{3.13}$$

And the **energy equation**:

$$\rho c_p \frac{\partial T}{\partial t} + \rho c_p \left(\vec{u} . \nabla T \right) = K \nabla^2 T + \frac{\vec{J} . \vec{J}}{\sigma} \tag{3.14}$$

In the above equations, $\vec{u}$ is the fluid velocity, ρ is the density, μ is the viscosity, C_p is the specific heat, k is the thermal conductivity and T is the temperature.

In the following sections, the governing equations of two dimensional fully developed flow and developing flow are presented, where the fluid can be propelled by constant or fluctuating Lorentz force. Various assumptions are set to develop the model:

1- Two-dimensional.

2- Laminar flow.

3- Incompressible fluid.

4- Constant fluid properties.

5- Negligible radiation heat transfer.

6- Negligible gravitational effects.

7- The current flow is assumed to be one dimensional.

3.3 Governing Equations of the Fully Developed Flow

In this section, the governing equations of the transient incompressible two-dimensional fully developed flow with both constant and fluctuating Lorentz force are studied. The velocity components in the *y*, and *z* directions are neglected compared with the velocity along the conduit's axis.

For the fully developed flow the nonlinear term in equation (3.13) goes to zero, and the continuity equation goes to zero since $\frac{\partial u}{\partial x}=0$.

The induced current in the channel is

$$J=\sigma(E+v\times B) \tag{3.15}$$

It can be written as:

$$J=\sigma E+\sigma v\times B=\sigma E_k+\sigma(u_i)\times B_j \tag{3.16}$$

Then $J=\sigma E_k+\sigma u B_k$ (3.17)

Now the Lorentz force is:

$$F_L=J\times B=\sigma E_k\times B_j+\sigma u B_k\times B_j=(\sigma EB-\sigma uB^2)_i \tag{3.18}$$

By introducing the Lorentz force given in equation (3.18), the two dimensional x-momentum equation will be:

$$\rho\frac{\partial u}{\partial t}=-\frac{\partial p}{\partial x}+\mu\left(\frac{\partial^2 u}{\partial y^2}+\frac{\partial^2 u}{\partial z^2}\right)+\sigma(E-uB)B \tag{3.19}$$

In the energy equation, the flow is assumed thermally fully developed, and the viscous dissipation effects are neglected because the fluid velocity is very small. Hence the energy equation will be:

$$\frac{\partial T}{\partial t}=\frac{\nu}{P_r}\left(\frac{\partial^2 T}{\partial y^2}+\frac{\partial^2 T}{\partial z^2}\right)+\frac{\sigma(E+uB)^2}{\rho C_p} \tag{3.20}$$

Now the governing equations of transient fully developed flow using an AC magnetohydrodynamic MHD pumping mechanism will be studied. A sinusoidal electric current with a perpendicular sinusoidal magnetic field are used. The electric current and magnetic fields applied have equal frequency and a phase difference between them.

When applying the AC current field and magnetic field with a phase shift ϕ and equal angular frequency ϖ the two dimensional transient fully developed momentum equation will be:

$$\rho\frac{\partial u}{\partial t}=-\frac{dp}{dx}+\mu\left(\frac{\partial^2 u}{\partial y^2}+\frac{\partial^2 u}{\partial z^2}\right)+\sigma\left(E\sin(\omega t+\phi)-uB\sin\omega t\right)B\sin\omega t \qquad (3.21)$$

And the energy equation becomes:

$$\frac{\partial T}{\partial t}=\frac{\nu}{P_r}\left(\frac{\partial^2 T}{\partial y^2}+\frac{\partial^2 T}{\partial z^2}\right)+\frac{\sigma\left(E\sin(\omega t+\phi)+uB\sin\omega t\right)^2}{\rho C_p} \qquad (3.22)$$

To write the governing equations in dimensionless form, the following dimensionless variables can be used:

$$y^*=\frac{y}{w},\ z^*=\frac{z}{w},\ u^*=\frac{u}{u_0},\ \tau=\frac{t}{T^*},\ P^*=\frac{dp/dx}{\sigma EB},\ \theta=\frac{T-T_w}{T_w}$$

Where $u_0=\sigma VBw/\mu$, T^* is the period of the alternations in the electric field and magnetic field, and T_w is the wall temperature. Substituting the above dimensionless variables leads to the following dimensionless equations:

Momentum equation:

$$St^2\frac{\partial u^*}{\partial\tau}=\frac{\partial^2 u^*}{\partial y^{*2}}+\frac{\partial^2 u^*}{\partial z^{*2}}+\sin(2\pi\tau)\sin(2\pi\tau+\phi)-Ha^2u^*\sin^2(2\pi\tau)-P^* \qquad (3.23)$$

With the following boundary conditions:

$$u^*(0,z^*,\tau)=u^*(1,z^*,\tau)=0$$
$$u^*(y^*,0,\tau)=u^*(y^*,\alpha,\tau)=0$$

And the **energy equation**:

$$St^2\frac{\partial\theta}{\partial\tau}=\frac{1}{p_r}\left(\frac{\partial^2\theta}{\partial y^{*2}}+\frac{\partial^2\theta}{\partial z^{*2}}\right)+S\left(y^*,z^*,\tau\right) \tag{3.24}$$

Where the source term is:

$$S\left(y^*,z^*,\tau\right)=Ha^2Ec\left(\frac{\sin\left(2\pi\tau+\phi\right)}{Ha^2}+u^*\sin\left(2\pi\tau\right)\right)^2$$

In the above equations, $Ha=wB\sqrt{\frac{\sigma}{\mu}}$ is the Hartman number which is the ratio of the magnetic body force to the viscous force, $St=w\sqrt{\frac{1}{\nu T^*}}$ is the Stanton number which is the ratio of the diffusion time to the forcing period, P_r is the Prandtl number which is ratio of the rate of diffusion of viscous effects to rate of diffusion of heat, $Ec=u_0^2/C_pT_w$ is the Eckert number which is the ratio of kinetic energy to enthalpy change, and $\alpha=h/w$ is the conduit's aspect ratio.

Now using $\tau=\frac{t}{w^2/\nu}$ as the dimensionless time, the above dimensionless equations can be reduced to be applicable for the DC fully developed flow:

Momentum equation

$$\frac{\partial u^*}{\partial\tau}=\frac{\partial^2u^*}{\partial y^{*2}}+\frac{\partial^2u^*}{\partial z^{*2}}+1-Ha^2u^*-P^* \tag{3.25}$$

With boundary conditions:
$$\begin{aligned}u^*\left(0,z^*,\tau\right)&=u^*\left(1,z^*,\tau\right)=0\\ u^*\left(y^*,0,\tau\right)&=u^*\left(y^*,\alpha,\tau\right)=0\end{aligned} \tag{3.26}$$

And the **energy equation**

$$\frac{\partial\theta}{\partial\tau}=\frac{1}{P_r}\left(\frac{\partial^2\theta}{\partial y^{*2}}+\frac{\partial^2\theta}{\partial z^{*2}}\right)+Ha^2E_c\left(\frac{1}{Ha^2}+u^*\right)^2 \tag{3.27}$$

With boundary conditions: $$\begin{matrix}\theta(0,z^*,\tau)=\theta(1,z^*,\tau)=0\\ \theta(y^*,0,\tau)=\theta(y^*,\alpha,\tau)=0\end{matrix} \tag{3.28}$$

3.4 Governing equations of the developing flow

In our model, the width of the channel is assumed to be much larger than it's height (w/h>>1), hence we studied the transient incompressible two-dimensional developing flow.

The following dimensionless variables can be used to non-dimensionalize the governing equations:

$$x^*=\frac{x}{w},\ y^*=\frac{y}{w},\ u^*=\frac{u}{u_0},\ \tau=\frac{t}{w^2/\nu},\ p^*=\frac{p}{\sigma EBv}$$

Where $u_0=\sigma EBw^2/\mu$ is the reference velocity. Substituting the above dimensionless variables leads to the following dimensionless form of continuity and Navier-Stokes equations for an incompressible, two-dimensional developing flow.

Continuity equation

$$\frac{\partial u^*}{\partial x^*}+\frac{\partial v^*}{\partial y^*}=0 \tag{3.29}$$

X-momentum equation

$$\frac{\partial u^*}{\partial\tau}+\left(\frac{\alpha+1}{2\alpha}\right)R_{eD}\left(u^*\frac{\partial u^*}{\partial x^*}+v^*\frac{\partial u^*}{\partial y^*}\right)=-\frac{\partial p^*}{\partial x^*}+\frac{\partial^2u^*}{\partial x^{*2}}+\frac{\partial^2u^*}{\partial y^{*2}}+1-Ha^2u^* \tag{3.30}$$

Y-momentum equation

$$\frac{\partial v^*}{\partial \tau}+\left(\frac{\alpha+1}{2\alpha}\right)R_{eD}\left(u^*\frac{\partial v^*}{\partial x^*}+v^*\frac{\partial v^*}{\partial y^*}\right)=-\frac{\partial p^*}{\partial y^*}+\frac{\partial^2 v^*}{\partial x^{*2}}+\frac{\partial^2 v^*}{\partial y^{*2}} \tag{3.31}$$

In the above equations, u^* and v^* are the dimensionless velocity components in x and y directions, τ is the dimensionless time, x^* and y^* are the dimensionless coordinates, $Ha=wB\sqrt{\frac{\sigma}{\mu}}$ is the Hartman number, $\mathrm{Re}=\frac{u_0 D_h}{\nu}$ is the Reynolds number which is the ratio of inertia force to viscous force and D_h is the hydraulic diameter.

The boundary conditions can be specified as follows. The velocity is zero at all boundaries except the channel outlet.

$$\begin{aligned} u^*(0,y^*)&=v^*(0,y^*)=0\\ u^*(x^*,0)&=v^*(x^*,0)=0\\ u^*(x^*,1)&=v^*(x^*,1)=0 \end{aligned} \tag{3.32}$$

The flow is fully developed at the channel outlet

$$\frac{\partial u^*}{\partial x^*}\left(\frac{L}{w},y^*\right)=\frac{\partial v^*}{\partial x^*}\left(\frac{L}{w},y^*\right)=0 \tag{3.33}$$

Initially, at $\tau=0$, $u^*(x^*,y^*)=v^*(x^*,y^*)=0$

Now similar to the study of the AC fully developed flow the electric and magnetic field applied in an AC MHD micropump are sinusoidal and have phase shift and equal angular frequency. So the governing equations that suitable for developing flow are

$$\nabla.u=0 \tag{3.34}$$

$$\rho\frac{\partial u}{\partial t}+\rho(u.\nabla)u=-\nabla p+\mu\nabla^2 u+J\times B\sin\omega t\sin(\omega t+\phi) \tag{3.35}$$

The following dimensionless variables can be used to non-dimensionalize the governing equations:

$$x^*=\frac{x}{w},\ y^*=\frac{y}{w},\ u^*=\frac{u}{u_0},\ \tau=\frac{t}{T^*},\ p^*=\frac{p}{\sigma EBv}$$

Then the dimensionless form of continuity and Navier-Stokes equations for an incompressible, two-dimensional AC developing flow can be written as:

Continuity equation

$$\frac{\partial u^*}{\partial x^*}+\frac{\partial v^*}{\partial y^*}=0 \tag{3.36}$$

X-momentum equation

$$\begin{aligned}&St^2\frac{\partial u^*}{\partial \tau}+\left(\frac{\alpha+1}{2\alpha}\right)\mathrm{Re}_D\left(u^*\frac{\partial u^*}{\partial x^*}+v^*\frac{\partial u^*}{\partial y^*}\right)=\\&-\frac{\partial p^*}{\partial x^*}+\frac{\partial^2 u^*}{\partial x^{*2}}+\frac{\partial^2 u^*}{\partial y^{*2}}+\sin(2\pi\tau)\sin(2\pi\tau+\phi)-Ha^2u^*\sin^2(2\pi\tau)\end{aligned} \tag{3.37}$$

Y-momentum equation

$$St^2\frac{\partial v^*}{\partial \tau}+\left(\frac{\alpha+1}{2\alpha}\right)\mathrm{Re}_D\left(u^*\frac{\partial v^*}{\partial x^*}+v^*\frac{\partial v^*}{\partial y^*}\right)=-\frac{\partial p^*}{\partial y^*}+\frac{\partial^2 v^*}{\partial x^{*2}}+\frac{\partial^2 v^*}{\partial y^{*2}} \tag{3.38}$$

The boundary conditions can be specified as follows. The velocity is zero at all boundaries except the channel outlet.

$$\begin{aligned} u^*(0,y^*)=v^*(0,y^*)=0 \\ u^*(x^*,0)=v^*(x^*,0)=0 \\ u^*(x^*,1)=v^*(x^*,1)=0 \end{aligned} \tag{3.39}$$

The flow is fully developed at the channel outlet

$$\frac{\partial u^*}{\partial x^*}\left(\frac{L}{w},y^*\right)=\frac{\partial v^*}{\partial x^*}\left(\frac{L}{w},y^*\right)=0 \tag{3.40}$$

Initially, at $\tau=0$, $u^*(x^*,y^*)=v^*(x^*,y^*)=0$

In this work, the previous dimensionless governing equations (23-27) are going to be solved for velocity and temperature distributions for both DC and AC fully developed flow to illustrate the effect of *Ha*, *Pr*, *Ec*, and *St* numbers on the MHD flow. The equations will be solved numerically and analytically and a comparison between them will be presented. The dimensionless governing equations (29-31) and (36-38) will be solved numerically using suitable method to show the effect of *Ha* and *St* numbers on the developing flow for both DC and AC pumping. The following chapters illustrate these solutions.

Chapter 4
Fully developed flow solution

4.1 Introduction

In this chapter a numerical alternating direct implicit (ADI) technique and analytical eigen-function expansion method will be used to solve the transient fully developed flow for both constant and fluctuating Lorentz force.

4.2 DC (MHD) pumping

4.2.1 Analytical approach

In this section the analytical approach using the eigenfunction expansion method is used to solve the momentum equation of the transient DC fully developed flow.

The dimensionless momentum equation is

$$\frac{\partial u^*}{\partial \tau} = \frac{\partial^2 u^*}{\partial y^{*2}} + \frac{\partial^2 u^*}{\partial z^{*2}} - Ha^2 u^* + N \tag{4.1}$$

Where $N = 1 - p^*$

With boundary conditions:
$$\begin{matrix} u^*(0, z^*, \tau) = u^*(1, z^*, \tau) = 0 \\ u^*(y^*, 0, \tau) = u^*(y^*, \alpha, \tau) = 0 \end{matrix} \tag{4.2}$$

Consider the eigenfunctions of the related homogeneous problem:

$$\frac{\partial u^*}{\partial \tau} = \frac{\partial^2 u^*}{\partial y^{*2}} + \frac{\partial^2 u^*}{\partial z^{*2}} - Ha^2 u^* \tag{4.3}$$

$$\begin{matrix} u^*(0, z^*, \tau) = u^*(1, z^*, \tau) = 0 \\ u^*(y^*, 0, \tau) = u^*(y^*, \alpha, \tau) = 0 \end{matrix} \tag{4.4}$$

Since the partial differential equation (4.2) and the boundary conditions are linear and homogeneous, we apply the method of separation of variables.

Let $u^*(y^*,z^*,\tau)=\delta(\tau)\phi(y^*,z^*)$

Taking the derivatives and substituting into equation (4.3) yields

$$\frac{1}{\delta}\frac{\partial\delta}{\partial\tau}+Hd^2=\frac{1}{\phi}\left(\frac{\partial^2\phi}{\partial y^{*2}}+\frac{\partial^2\phi}{\partial z^{*2}}\right)=-\lambda^2 \tag{4.5}$$

Where λ^2 is the separation constant.

From this equation the two-dimensional eigenvalue problem is

$$\frac{\partial^2\phi}{\partial y^{*2}}+\frac{\partial^2\phi}{\partial z^{*2}}+\lambda^2\phi=0 \qquad \begin{matrix}\phi(0,z^*)=\phi(1,z^*)=0\\ \phi(y^*,0)=\phi(y^*,\alpha)=0\end{matrix} \tag{4.6}$$

To solve equation (4.6) let $\phi(y^*,z^*)=f(y^*)g(z^*)$ (4.7)

Take the derivatives and substitute into equation(4.6) yields

$$\frac{1}{f}\frac{d^2f}{dy^{*2}}=\frac{-1}{g}\frac{d^2g}{dz^{*2}}-\lambda^2=-\gamma^2 \tag{4.8}$$

Two ordinary differential equations result from separation of variables of equation (4.6) with two independent variables:

$$\frac{d^2f}{dy^{*2}}+\gamma^2 f=0 \tag{4.9}$$

With $f(0)=f(1)=0$

And

$$\frac{d^2g}{dz^{*2}}-(\gamma^2-\lambda^2)g=0 \tag{4.10}$$

With $g(0)=g(\alpha)=0$

Now equation (4.9) with it's boundary conditions can be solved, and the solution will be

$$f_n(y^*)=\sin n\pi y^* \text{ with } \gamma_n=n\pi \qquad (4.11)$$

Where $n=1,2,\cdots\infty$

Now in solving equation (4.10), for each value of γ_n is still an eigenvalue problem, then there are an infinite number of eigenvalues λ for each n.

$$\Rightarrow\lambda=\lambda_{mn}$$

Eq.(4.8) can be written as:

$$\frac{d^2g}{dz^{*2}}+(\lambda^2-\gamma^2)g=0 \qquad (4.12)$$

The solution of this equation is

$$g(z^*)=c_1\sin\sqrt{\lambda^2-\gamma^2}z^*+c_2\cos\sqrt{\lambda^2-\gamma^2}z^* \qquad (4.13)$$

By applying the boundary conditions, the solution will be

$$g_{mn}(z^*)=\sin\frac{m\pi}{\alpha}z^* \qquad (4.14)$$

And $\lambda_{mn}^2=\frac{m^2\pi^2}{\alpha^2}+(n\pi)^2$

Where $m=1,2,\ldots,\infty$ and $n=1,2,\cdots\infty$

From equation (4.1):

$$\phi_{mn}(y^*,z^*)=\sin n\pi y^*\sin\frac{m\pi}{\alpha}z^* \qquad (4.15)$$

Now assume the solution of equation (4.1) as the following:

$$u^*(y^*,z^*,\tau)=\sum_{m=1}^{\infty}\sum_{n=1}^{\infty}a_{mn}(\tau)\phi_{mn}(y^*,z^*) \tag{4.16}$$

Which will satisfy the non-homogeneous equation with initial condition $u^*(y^*,z^*,0)=0$ .Substituting $u^*(y^*,z^*,\tau)$ and it's derivatives from equation (4.16) into equation (4.1) yields:

$$\sum_{m=1}^{\infty}\sum_{n=1}^{\infty}\left(\frac{da_{mn}}{d\tau}+\left(\lambda_{mn}^2+Ha^2\right)a_{mn}(\tau)\right)\phi_{mn}(y^*,z^*)=N \tag{4.17}$$

where N=1-P* with $a_{mm}(0)=0$

In equation (4.17), we have a double Fourier series. To solve for $a_{mm}(\tau)$

Let: $V_{mn}=\frac{da_{mn}}{d\tau}+\left(\lambda_{mn}^2+Ha^2\right)a_{mn}(\tau)$ (4.18)

This yields

$$\sum_{m=1}^{\infty}\sum_{n=1}^{\infty}V_{mn}\sin n\pi y^*\sin\frac{m\pi}{\alpha}z^*=N \tag{4.19}$$

Let $K_m(z^*)=\sum_{m=1}^{\infty}V_{mn}\sin\frac{m\pi}{\alpha}z^*$ (4.20)

Then equation (4.20) can be written as:

$$\sum_{n=1}^{\infty}K_m(z^*)\sin n\pi y^*=N \tag{4.21}$$

For fixed z this is the Fourier sine series of N. From equation (4.21):

$$K_m(z^*)=2\int_0^1 N\sin n\pi y^*dy^* \tag{4.22}$$

Perform the integral yields

$$K_m(z^*)=\frac{2N}{n\pi}(1-\cos n\pi) \tag{4.23}$$

Now substitute equation (4.23) into (4.20) :

$$\frac{2N}{n\pi}(1-\cos n\pi)=\sum_{m=1}^{\infty}V_{mn}\sin\frac{m\pi}{\alpha}z^{*} \tag{4.24}$$

Then,

$$V_{mn}=\frac{2}{\alpha}\int_{0}^{\alpha}\frac{2N}{n\pi}(1-\cos n\pi)\sin\frac{m\pi}{\alpha}z^{*}dz^{*} \tag{4.25}$$

$$V_{mn}=\frac{4N}{mn\pi^{2}}\left(1-\cos\frac{m\pi}{\alpha}\right)(1-\cos n\pi) \tag{4.26}$$

Then V_{mn} can be written as

$$V_{mn}=\begin{cases}\dfrac{16N}{mn\pi^{2}} & m,\text{and } n \text{ odd}\\ 0 & m,\text{or } n \text{ even}\end{cases} \tag{4.27}$$

Now equation (4.18) is a first order ordinary differential equation and can be solved for a_{mm}

$$a_{mn}(\tau)=ce^{-\left(\lambda_{mn}^{2}+Ha^{2}\right)\tau}+\left(\frac{V_{mn}}{\lambda_{mn}^{2}+Ha^{2}}\right) \tag{4.28}$$

The initial condition is:

$$a_{mm}(0)=0$$

Then the solution is:

$$a_{mn}(\tau)=\left(\frac{V_{mn}}{\lambda_{mn}^{2}+Ha^{2}}\right)\left(1-e^{-\left(\lambda_{mn}^{2}+Ha^{2}\right)\tau}\right) \tag{4.29}$$

Substituting into equation (4.16) yields :

$$u^*(y^*,z^*,\tau)=\sum_{m=1}^{\infty}\sum_{n=1}^{\infty}\frac{V_{mn}}{(\lambda_{mn}^2+Hd^2)}\left(1-e^{-(\lambda_{mn}^2+Hd^2)\tau}\right)\sin n\pi y^*\sin\frac{m\pi}{\alpha}z^* \qquad (4.30)$$

In dimensional form, the velocity can be written as:

$$u(x,y,t)=u_0u^*(y^*,z^*,\tau)=u_0\sum_{m=1}^{\infty}\sum_{n=1}^{\infty}\frac{V_{mn}}{(\lambda_{mn}^2+Hd^2)}\left(1-e^{-(\lambda_{mn}^2+Hd^2)\frac{t}{w^2/\nu}}\right)\sin n\pi\frac{y}{w}\sin\frac{m\pi}{\alpha}\frac{z}{w}$$

(4.31)

The mean velocity in the micro-channel can be determined from the equation (White, 1979):

$$u_m=\int_{Ac}\frac{\rho u(y,z,t)dA_c}{\rho Ac} \qquad (4.32)$$

Where A_c is the cross-sectional area of the channel.

The density here is assumed to be constant, then

$$u=\int_{Ac}\frac{u(y,z)dA_c}{Ac} \qquad (4.33)$$

Substitute the velocity from equation (4.31) yields

$$u_m=u_0\frac{\int_0^h\int_0^w\sum_{m=1}^{\infty}\sum_{n=1}^{\infty}\frac{V_{mn}}{(\lambda_{mn}^2+Hd^2)}\left(1-e^{-(\lambda_{mn}^2+Hd^2)\frac{t}{w^2/\nu}}\right)\sin\frac{n\pi y}{w}\sin\frac{m\pi z}{h}\frac{dydz}{w^2}}{hw}$$

Perform the integrals to obtain

$$u_m=u_0\sum_{m=1}^{\infty}\sum_{n=1}^{\infty}\frac{4V_{mn}}{mn\pi^2w^2(\lambda_{mn}^2+Hd^2)}\left(1-e^{-(\lambda_{mn}^2+Hd^2)\frac{t}{w^2/\nu}}\right) \qquad (4.34)$$

And then the volume flow rate will be

$$Q=u_0\sum_{m=1}^{\infty}\sum_{n=1}^{\infty}\frac{4\alpha V_{mn}}{mn\pi^2(\lambda_{mn}^2+Hd^2)}\left(1-e^{-(\lambda_{mn}^2+Hd^2)\frac{t}{w^2/\nu}}\right) \qquad (4.35)$$

4.2.2 Numerical modeling

The finite difference alternating-direction (ADI) technique which is a time marching method is applied to solve the dimensionless Navier-Stokes equation. A uniform grid of a number of nodes in the *y* and *z* directions is used. The method with about 1000 time steps is employed until the steady state solution is achieved. At each time the implicit solutions using the Crank-Niclson scheme are directly obtained from the use of Thomas Algorithm. Different time step size ($\Delta\tau$),(ΔY), and (ΔZ) are taken to ensure stability, the results show that the numerical solution is always stable.

The numerical (ADI) technique is used to solve

$$\frac{\partial u^*}{\partial \tau} = \frac{\partial^2 u^*}{\partial y^{*2}} + \frac{\partial^2 u^*}{\partial z^{*2}} - Hd^2 u^* + N \tag{4.36}$$

Where $N = 1 - p^*$

Firstly, we treat the *y* derivative in equation (4.36) implicitly using finite difference method.

$$\frac{u^{*n+1}_{i,j} - u^{*n}_{i,j}}{\Delta\tau} = \frac{u^{*n+1}_{i+1,j} - 2u^{*n+1}_{i,j} + u^{*n+1}_{i-1,j}}{\Delta y^{*2}} + \frac{u^{*n}_{i,j+1} - 2u^{*n}_{i,j} + u^{*n}_{i,j-1}}{\Delta z^{*2}} - Hd^2 u^{*n+1}_{i,j} + N \tag{4.37}$$

This equation can be written as:

$$Au^{*n+1}_{i-1,j} - Bu^{*n+1}_{i,j} + Au^{*n+1}_{i+1,j} = K^n_i \tag{4.38}$$

Where

$$A = \frac{\Delta\tau}{\Delta y^{*2}}$$

$$B = \frac{2\Delta\tau}{\Delta y^{*2}} + 1 + Hd^2\Delta\tau$$

$$K_i^n = -\left(u_{i,j}^{*n} + \frac{\Delta\tau}{\Delta z^{*2}} \left(u_{i,j+1}^{*n} - 2u_{i,j}^{*n} + u_{i,j-1}^{*n} \right) + N\Delta\tau \right)$$

Now by using finite difference method treat the *z* derivative in equation (4.36) implicitly

$$\frac{u_{i,j}^{*n+2} - u_{i,j}^{*n+1}}{\Delta\tau} = \frac{u_{i+1,j}^{*n+1} - 2u_{i,j}^{*n+1} + u_{i-1,j}^{*n+1}}{\Delta y^{*2}} + \frac{u_{i,j+1}^{*n+2} - 2u_{i,j}^{*n+2} + u_{i,j-1}^{*n+2}}{\Delta z^{*2}} - Ha^2 u_{i,j}^{*n+2} + N \quad (4.39)$$

This equation can be written as:

$$Cu_{i,j-1}^{*n+2} - Du_{i,j}^{*n+2} + Cu_{i,j+1}^{*n+2} = L_j^{n+1} \quad (4.40)$$

Where

$$C = \frac{\Delta\tau}{\Delta z^{*2}}$$

$$B = \frac{2\Delta\tau}{\Delta z^{*2}} + 1 + Ha^2\Delta\tau$$

$$L_j^{n+1} = -\left(u_{i,j}^{*n+1} + \frac{\Delta\tau}{\Delta y^{*2}} \left(u_{i+1,j}^{*n+1} - 2u_{i,j}^{*n+1} + u_{i-1,j}^{*n+1} \right) + N\Delta\tau \right)$$

4.3.AC (MHD) pumping

4.3.1 Numerical modeling

Similar to the solution of the DC fully developed flow, the finite difference alternating-direction (ADI) technique can be used to solve the dimensionless momentum equation.

$$St^2 \frac{\partial u^*}{\partial \tau} = \frac{\partial^2 u^*}{\partial y^{*2}} + \frac{\partial^2 u^*}{\partial z^{*2}} + \sin(2\pi\tau)\sin(2\pi\tau + \phi) - Ha^2 u^* \sin^2(2\pi\tau) - P^* \quad (4.41)$$

Firstly, we treat the y derivative in equation (4.41) implicitly.

$$St^2\frac{u^{*n+1}_{i,j}-u^{*n}_{i,j}}{\Delta\tau}=\frac{u^{*n+1}_{i+1,j}-2u^{*n+1}_{i,j}+u^{*n+1}_{i-1,j}}{\Delta y^{*2}}+\frac{u^{*n}_{i,j+1}-2u^{*n}_{i,j}+u^{*n}_{i,j-1}}{\Delta z^{*2}}$$
$$-Hd^2u^{*n+1}_{i,j}\sin^2(2\pi\tau)+\sin(2\pi\tau^{n+1})\sin(2\pi\tau^{n+1}+\phi)-P^* \quad (4.42)$$

This equation can be written as:

$$Au^{*n+1}_{i-1,j}-Bu^{*n+1}_{i,j}+Au^{*n+1}_{i+1,j}=K^n_i \quad (4.43)$$

Where

$$A=\frac{\Delta\tau}{St^2\Delta y^{*2}}$$

$$B=\left(1+\frac{2\Delta\tau}{St^2\Delta y^{*2}}+\frac{Hd^2\Delta\tau}{St^2}\sin^2(2\pi\tau^{n+1})\right)$$

$$K^n_i=-\left(u^{*n}_{i,j}+\frac{\Delta\tau}{St^2\Delta z^{*2}}\left(u^{*n}_{i,j+1}-2u^{*n}_{i,j}+u^{*n}_{i,j-1}\right)+\frac{\Delta\tau}{St^2}\left(\sin(2\pi\tau^{n+1})\sin(2\pi\tau^{n+1}+\phi)-P^*\right)\right)$$

The descritization in *z* direction yields

$$St^2\frac{u^{*n+2}_{i,j}-u^{*n+1}_{i,j}}{\Delta\tau}=\frac{u^{*n+1}_{i+1,j}-2u^{*n+1}_{i,j}+u^{*n+1}_{i-1,j}}{\Delta y^{*2}}+\frac{u^{*n+2}_{i,j+1}-2u^{*n+2}_{i,j}+u^{*n+2}_{i,j-1}}{\Delta z^{*2}}$$
$$-Hd^2u^{*n+2}_{i,j}\sin^2(2\pi\tau^{n+2})+\sin(2\pi\tau^{n+2})\sin(2\pi\tau^{n+2}+\phi)-P^* \quad (4.44)$$

This equation can be written as:

$$Cu^{*n+2}_{i,j-1}-Du^{*n+2}_{i,j}+Cu^{*n+2}_{i,j+1}=L^{n+1}_j \quad (4.45)$$

Where

$$C=\frac{\Delta\tau}{St^2\Delta z^{*2}}$$

$$B=\left(1+\frac{2\Delta\tau}{St^2\Delta z^{*2}}+\frac{Ha^2\Delta\tau}{St^2}\sin^2\left(2\pi\tau^{n+2}\right)\right)$$

$$L_j^{n+1}=-\left(u_{i,j}^{*n+1}+\frac{\Delta\tau}{St^2\Delta y^{*2}}\left(u_{i+1,j}^{*n+1}-2u_{i,j}^{*n+1}+u_{i-1,j}^{*n+1}\right)+\frac{\Delta\tau}{St^2}\left(\sin\left(2\pi\tau^{n+2}\right)\sin\left(2\pi\tau^{n+2}+\phi\right)-P^*\right)\right)$$

The ADI method produce a tri-diagonal matrix which can be solved for velocity using Thomas Algorithm which depend on Gauss elimination method. The Thomas Algorithm and the program used to solve for velocity and temperature is included in appendix A.

4.3.2 Steady state analytical solution

In this section, the analytical approach using the eigenfunction expansion method is used to solve the momentum equation of the steady state AC fully developed flow.

The dimensionless time independent Navier-Stokes equation is

$$\frac{\partial^2u^*}{\partial y^{*2}}+\frac{\partial^2u^*}{\partial z^{*2}}+\sin\left(2\pi\tau\right)\sin\left(2\pi\tau+\phi\right)-Ha^2u^*\sin^2\left(2\pi\tau\right)-P^*=0 \tag{4.46}$$

With boundary conditions:
$$\begin{matrix}u^*\left(0,z^*\right)=u^*\left(1,z^*\right)=0\\ u^*\left(y^*,0\right)=u^*\left(y^*,\alpha\right)=0\end{matrix} \tag{4.47}$$

Consider the eigenfunctions of the related homogeneous problem:

$$\frac{\partial^2u^*}{\partial y^{*2}}+\frac{\partial^2u^*}{\partial z^{*2}}-Ha^2u^*\sin^2\left(2\pi\tau\right)=0 \tag{4.48}$$

Since the partial differential equation (4.48) and the boundary conditions are linear and homogeneous, we apply the method of separation of variables.

Let $u^*\left(y^*,z^*\right)=\delta(y)\phi(z^*)$

Taking the derivatives and substituting into equation (4.48) yields

$$-\frac{1}{\delta}\frac{\partial^2\delta}{\partial y^2}-Ha^2u^*\sin^2(2\pi\tau)=\frac{1}{\phi}\frac{\partial^2\phi}{\partial z^{*2}}=-\lambda^2 \tag{4.49}$$

Where λ^2 is the separation constant.

From this equation the eigenvalue problem is::

$$\frac{\partial^2\phi}{\partial z^{*2}}+\lambda^2\phi=0 \qquad \phi(0)=\phi(\alpha)=0 \tag{4.50}$$

The solution of the above equation is:

$$\phi(z^*)=c_1\sin\lambda z^*+c_2\cos\lambda z^* \tag{4.51}$$

By applying the boundary conditions, the solution is:

$$\phi_n(z^*)=\sin\frac{n\pi}{\alpha}z^* \tag{4.52}$$

With

$$\lambda_n^2=\frac{n^2\pi^2}{\alpha^2}$$

Where $n=1,2,\cdots\infty$. Now assume the solution of equation (4.46) as the following:

$$u^*(y^*,z^*)=\sum_{n=1}^{\infty}a_n(y)\phi_n(z^*) \tag{4.53}$$

Which will satisfy the non-homogeneous equation with boundary conditions $u^*(0,z^*)=u^*(1,z^*)=0.$

Substituting $u^*(y^*,z^*)$ and it's derivatives from equation (4.53) into equation (4.46) yields:

$$\sum_{n=1}^{\infty}\left(\frac{d^2a_n}{dy^2}-\left(\lambda_n^2+Ha^2\sin^2(2\pi\tau)\right)a_n(y)\right)\sin\left(\frac{n\pi z^*}{\alpha}\right)=p^*-\sin(2\pi\tau)\sin(2\pi\tau+\phi) \tag{4.54}$$

$$\text{Let: } V_n = \frac{d^2 a_n}{dy^2} - \left(\lambda_n^2 + Ha^2 \sin^2(2\pi\tau)\right) a_n(y) \tag{4.55}$$

This yields

$$\sum_{n=1}^{\infty} V_n \sin\frac{n\pi}{\alpha} z^* = p^* - \sin(2\pi\tau)\sin(2\pi\tau+\phi) \tag{4.56}$$

$$V_n(y^*) = \frac{2}{\alpha}\int_0^{\alpha} \left(p^* - \sin(2\pi\tau)\sin(2\pi\tau+\phi)\right)\sin\frac{n\pi}{\alpha} z^* dz^* \tag{4.57}$$

Perform the integral yields

$$V_n = \frac{-4\left(p^* - \sin(2\pi\tau)\sin(2\pi\tau+\phi)\right)}{n\pi} \tag{4.58}$$

Where $n = 1,3,5,\cdots\infty$

Now equation (4.55) is a second order ordinary differential equation and can be solved for a_n

$$a_n(y) = c1e^{m1y^*} + c2e^{m2y^*} - \frac{V_n}{\left(\lambda_n^2 + Ha^2 \sin^2(2\pi\tau)\right)} \tag{4.59}$$

Where $m1,2 = \pm\sqrt{\left(\lambda_n^2 + Ha^2 \sin^2(2\pi\tau)\right)}$

And $c1 = \frac{V_n\left(e^{m2} - 1\right)}{\left(\lambda_n^2 + Ha^2 \sin^2(2\pi\tau)\right)\left(e^{m2} - e^{m1}\right)}$

$$c2 = \frac{V_n\left(1 - e^{m1}\right)}{\left(\lambda_n^2 + Ha^2 \sin^2(2\pi\tau)\right)\left(e^{m2} - e^{m1}\right)}$$

Chapter 5

Fully developed energy analysis

In this chapter the dimensionless energy equation will be solved analytically using eigen-function expansion method and numerically using ADI method in the same way which was followed when solving the momentum equation. From these solutions the temperature distribution will be given for both DC and AC pumping.

5.1 DC (MHD) pumping

5.1.1 Analytical approach

The energy equation can be written as

$$\frac{\partial\theta}{\partial\tau}=\frac{1}{\mathrm{Pr}}\left(\frac{\partial^2\theta}{\partial y^{*2}}+\frac{\partial^2\theta}{\partial z^{*2}}\right)+S(y^*,z^*,\tau) \tag{5.1}$$

Where the source term is:

$$S(y^*,z^*,\tau)=Ha^2E_c\left(\frac{1}{Ha^2}+\sum_{m=1}^{\infty}\sum_{n=1}^{\infty}\frac{V_{mn}}{(\lambda_{mn}^2+Ha^2)}\left(1-e^{-(\lambda_{mn}^2+Ha^2)\tau}\right)\sin n\pi y^*\sin\frac{m\pi}{\alpha}z^*\right)^2$$

Take the homogeneous part of equation (5.1):

$$\frac{\partial\theta}{\partial\tau}=\frac{1}{\mathrm{Pr}}\left(\frac{\partial^2\theta}{\partial y^{*2}}+\frac{\partial^2\theta}{\partial z^{*2}}\right) \tag{5.2}$$

Let $\theta(y^*,z^*,\tau)=H(\tau)\psi(y^*,z^*)$

Differentiate and substitute into equation (5.2) to yield:

$$\frac{\mathrm{Pr}}{H}\frac{dH}{d\tau}=\frac{1}{\psi}\left(\frac{\partial^2\psi}{\partial y^{*2}}+\frac{\partial^2\psi}{\partial z^{*2}}\right)=-\eta^2$$

Then the two dimensional eigenvalue problem is:

$$\frac{\partial^2\psi}{\partial y^{*2}}+\frac{\partial^2\psi}{\partial z^{*2}}+\eta^2\psi=0 \qquad \begin{matrix}\psi(0,z^*)=\psi(1,z^*)=0\\ \psi(y^*,0)=\psi(y^*,\alpha)=0\end{matrix} \tag{5.3}$$

Equation (5.3) is similar to equation (4.6) in previous velocity analysis.

So the solution is:

Eigenvalues: $\eta_{ij}^2 = (i\pi)^2 + \left(\frac{j\pi}{\alpha}\right)^2$ (5.4)

Where $i = 1,2,\ldots,\infty$ and $j = 1,2,\cdots\infty$

With eigenfunctions:

$$\psi_{ij}(y^*, z^*) = \sin i\pi y^* \sin\frac{j\pi}{\alpha} z^* \quad (5.5)$$

Now refer to the nonhomogeneous equation (5.1) and assume:

$$\theta(y^*, z^*, \tau) = \sum_{i=1}^{\infty}\sum_{j=1}^{\infty} b_{ij}(\tau)\psi_{ij}(y^*, z^*) \quad (5.6)$$

Which will satisfy the non-homogeneous equation with initial condition $\theta^*(y^*, z^*, 0) = 0$

Take the derivatives of equation (5.6) and substitute into equation (5.1) yields:

$$\sum_{i=1}^{\infty}\sum_{j=1}^{\infty}\left(\frac{db_{ij}}{d\tau} + \frac{\eta_{ij}^2}{\mathrm{Pr}} b_{ij}(\tau)\right)\psi_{ij}(y^*, z^*) =$$
$$Ha^2 Ec\left(\frac{1}{Ha^2} + \sum_{m=1}^{\infty}\sum_{n=1}^{\infty}\frac{V_{mn}}{(\lambda_{mn}^2 - Ha^2)}\left(1 - e^{-(\lambda_{mn}^2 - Ha^2)\tau}\right)\sin n\pi y^* \sin\frac{m\pi}{\alpha} z^*\right)^2 \quad (5.7)$$

With

$$b_{ij}(0) = 0$$

The above equation can be written as:

$$\sum_{i=1}^{\infty}\sum_{j=1}^{\infty}\left(\frac{db_{ij}}{d\tau}+\frac{\eta_{ij}^2}{\Pr}b_{ij}(\tau)\right)\psi_{ij}(y^*,z^*)=\frac{E_c}{Ha^2}+$$
$$2E_c\sum_{m=1}^{\infty}\sum_{n=1}^{\infty}\left(\frac{V_{mn}}{(\lambda_{mn}^2-Ha^2)}\right)\left(1-e^{-(\lambda_{mn}^2-Ha^2)\tau}\right)\sin n\pi y^*\sin\frac{m\pi}{\alpha}z^*$$
$$+Ha^2Ec\sum_{m=1}^{\infty}\sum_{n=1}^{\infty}\sum_{k=1}^{\infty}\sum_{l=1}^{\infty}\left(\frac{V_{mn}}{(\lambda_{mn}^2-Ha^2)}\right)\left(1-e^{-(\lambda_{mn}^2-Ha^2)\tau}\right)\left(\frac{V_{kl}}{(\lambda_{kl}^2-Ha^2)}\right)\left(1-e^{-(\lambda_{kl}^2-Ha^2)\tau}\right) \quad (5.8)$$
$$\sin n\pi y^*\sin\frac{m\pi}{\alpha}z^*\sin l\pi y^*\sin\frac{k\pi}{\alpha}z^*$$

Let: $$E_{ij}=\frac{db_{ij}}{d\tau}+\frac{\eta_{ij}^2}{\Pr}b_{ij}(\tau) \quad (5.9)$$

Then

$$\sum_{i=1}^{\infty}\sum_{j=1}^{\infty}E_{ij}\sin i\pi y^*\sin\frac{j\pi}{\alpha}z^*=S(y^*,z^*,\tau) \quad (5.10)$$

Let $$L_j(z^*)=\sum_{j=1}^{\infty}E_{ij}\sin\frac{j\pi}{\alpha}z^* \quad (5.11)$$

The equation (5.11) can be written as:

$$\sum_{i=1}^{\infty}L_i(z^*)\sin i\pi y^*=S(y^*,z^*,\tau) \quad (5.12)$$

For fixed z this is the Fourier sine series of S.

From equation (5.12):

$$L_j(z^*)=2\int_0^1 S\sin i\pi y^*dy^*$$

$$L_j(z^*)=\frac{2Ec}{Ha^2}\frac{(1-\cos i\pi)}{i\pi}+2E_c\sum_{m=1}^{\infty}\sum_{n=1}^{\infty}A_{mn}(\tau)\sin\frac{m\pi}{\alpha}z^*$$
$$2Ha^2E_c\sum_{m=1}^{\infty}\sum_{n=1}^{\infty}\sum_{k=1}^{\infty}\sum_{l=1}^{\infty}A_{mn}(\tau)A_{kl}(\tau)M_{inl}\sin\frac{m\pi}{\alpha}z^*\sin\frac{k\pi}{\alpha}z^* \quad (5.13)$$

Where

$$A_{mn}(\tau)=\left(\frac{r_{mn}}{\left(\lambda_{mn}^2-Ha^2\right)}\right)\left(1-e^{-\left(\lambda_{mn}^2-Ha^2\right)\tau}\right)$$

$$A_{kl}(\tau)=\left(\frac{r_{kl}}{\left(\lambda_{kl}^2-Ha^2\right)}\right)\left(1-e^{-\left(\lambda_{kl}^2-Ha^2\right)\tau}\right)$$

$$M_{inl}=\frac{1}{4\pi}\left[\frac{\cos(l+i+n)\pi-1}{(l+i+n)}+\frac{\cos(l-i-n)\pi-1}{(l-i-n)}-\frac{\cos(l+i-n)\pi-1}{(l+i-n)}-\frac{\cos(l-i+n)\pi-1}{(l-i+n)}\right]$$

Now

$$L_j(z^*)=\sum_{j=1}^{\infty}E_{ij}\sin\frac{j\pi}{\alpha}z^*$$

Then

$$E_{ij}=\frac{2}{\alpha}\int_0^{\alpha}L_j(z^*)\sin\frac{j\pi}{\alpha}z^*dz^*$$

$$E_{ij}=\frac{4E_c}{ij\pi^2Ha^2}(1-\cos i\pi)(1-\cos j\pi)+2E_c\sum_{m=1}^{\infty}\sum_{n=1}^{\infty}A_{mn}(\tau)$$
$$+4Ha^2E_c\sum_{m=1}^{\infty}\sum_{n=1}^{\infty}\sum_{k=1}^{\infty}\sum_{l=1}^{\infty}A_{mn}(\tau)A_{kl}(\tau)M_{inl}M_{jmk} \qquad (5.14)$$

But

$$E_{ij}=\frac{db_{ij}}{d\tau}+\frac{n_{ij}^2}{\Pr}b_{ij}(\tau)$$

$$\frac{db_{ij}}{d\tau}+\frac{n_{ij}^2}{\Pr}b_{ij}(\tau)=\frac{16E_c}{ij\pi^2Ha^2}+2E_c\sum_{m=1}^{\infty}\sum_{n=1}^{\infty}A_{mn}(\tau)$$
$$+4Ha^2E_c\sum_{m=1}^{\infty}\sum_{n=1}^{\infty}\sum_{k=1}^{\infty}\sum_{l=1}^{\infty}A_{mn}(\tau)A_{kl}(\tau)M_{inl}M_{jmk} \qquad (5.15)$$

With initial condition: $b_{ij}(0)=0$

The solution of the first order ordinary differential equation (3.54) is

$$b_{ij}(\tau)=\frac{\mathrm{Pr}}{\eta_{ij}^2}Q1_{ij}\left(1-e^{-\frac{\eta_{ij}^2}{\mathrm{Pr}}\tau}\right)$$
$$+\sum\sum Q2_{mn}\left(\frac{\mathrm{Pr}}{\eta_{ij}^2}\left(1-e^{-\frac{\eta_{ij}^2}{\mathrm{Pr}}\tau}\right)-\frac{\left(e^{-\left(\lambda_{mn}^2+Ha^2\right)\tau}-e^{-\frac{\eta_{ij}^2}{\mathrm{Pr}}\tau}\right)}{\frac{\eta_{ij}^2}{\mathrm{Pr}}-\left(\lambda_{mn}^2+Ha^2\right)}\right)$$
$$+\sum_{m=1}^{\infty}\sum_{n=1}^{\infty}\sum_{k=1}^{\infty}\sum_{l=1}^{\infty}Q3_{ijklmn}\left(\frac{\mathrm{Pr}}{\eta_{ij}^2}\left(1-e^{-\frac{\eta_{ij}^2}{\mathrm{Pr}}\tau}\right)-\frac{\left(e^{-\left(\lambda_{kl}^2+Ha^2\right)\tau}-e^{-\frac{\eta_{ij}^2}{\mathrm{Pr}}\tau}\right)}{\frac{\eta_{ij}^2}{\mathrm{Pr}}-\left(\lambda_{kl}^2+Ha^2\right)}-\frac{\left(e^{-\left(\lambda_{mn}^2+Ha^2\right)\tau}-e^{-\frac{\eta_{ij}^2}{\mathrm{Pr}}\tau}\right)}{\frac{\eta_{ij}^2}{\mathrm{Pr}}-\left(\lambda_{mn}^2+Ha^2\right)}+\frac{\left(e^{-\left(\lambda_{kl}^2+\lambda_{mn}^2+2Ha^2\right)\tau}-e^{-\frac{\eta_{ij}^2}{\mathrm{Pr}}\tau}\right)}{\frac{\eta_{ij}^2}{\mathrm{Pr}}-\left(\lambda_{kl}^2+\lambda_{mn}^2+2Ha^2\right)}\right)$$

(5.16)

Where

$$Q1_{ij}=\frac{16Ec}{ij\pi^2Ha^2}$$

$$Q2_{mn}=\begin{cases}2Ec\left(\frac{V_{mn}}{\lambda_{mn}^2+Ha^2}\right) & when\ m=n\\ 0 & when\ m\neq n\end{cases}$$

$$Q3_{ijklmn}=4Ha^2EcM_{inl}M_{jmk}\left(\frac{V_{mn}}{\lambda_{mn}^2+Ha^2}\right)\left(\frac{V_{kl}}{\lambda_{kl}^2+Ha^2}\right)$$

And the indices: $i,j,k,l,m,n=1,3,5,\cdots;\infty$

Finally,

$$\theta(y^*,z^*,\tau)=\sum_{i=1}^{\infty}\sum_{j=1}^{\infty}b_{ij}(\tau)\sin i\pi y^*\sin\frac{j\pi}{\alpha}z^* \qquad (5.17)$$

5.1.2 Numerical modeling

Now the ADI method can be used to solve the energy equation

$$\frac{\partial\theta}{\partial\tau}=\frac{1}{p_r}\left(\frac{\partial^2\theta}{\partial y^{*2}}+\frac{\partial^2\theta}{\partial z^{*2}}\right)+S\left(y^*,z^*,\tau\right) \tag{5.18}$$

Where the source term is:

$$S\left(y^*,z^*,\tau\right)=Ha^2E_c\left(\frac{1}{Ha^2}+u^*\right)^2$$

Firstly, we treat the y derivative in equation (5.18) implicitly using finite difference method.

$$\frac{\theta_{i,j}^{n+1}-\theta_{i,j}^{n}}{\Delta\tau}=\frac{1}{\mathrm{Pr}}\left(\frac{\theta_{i+1,j}^{n+1}-2\theta_{i,j}^{n+1}+\theta_{i-1,j}^{n+1}}{\Delta y^{*2}}+\frac{\theta_{i,j+1}^{n}-2\theta_{i,j}^{n}+\theta_{i,j-1}^{n}}{\Delta z^{*2}}\right)+S_{i,j}^{n+1} \tag{5.19}$$

This equation can be written as:

$$A\theta_{i-1,j}^{n+1}-B\theta_{i,j}^{n+1}+A\theta_{i+1,j}^{n+1}=K_i^n \tag{5.20}$$

Where

$$A=\frac{\Delta\tau}{\mathrm{Pr}\Delta y^{*2}}$$

$$B=\frac{2\Delta\tau}{\mathrm{Pr}\Delta y^{*2}}+1$$

$$K_i^n=-\left(\theta_{i,j}^{n}+\frac{\Delta\tau}{\mathrm{Pr}\Delta z^{*2}}\left(\theta_{i,j+1}^{n}-2\theta_{i,j}^{n}+\theta_{i,j-1}^{n}\right)+S_{i,j}^{n+1}\Delta\tau\right)$$

Now treat the z derivative in equation (5.18) implicitly.

$$\frac{\theta_{i,j}^{n+2}-\theta_{i,j}^{n+1}}{\Delta\tau}=\frac{1}{\mathrm{Pr}}\left(\frac{\theta_{i+1,j}^{n+1}-2\theta_{i,j}^{n+1}+\theta_{i-1,j}^{n+1}}{\Delta y^{*2}}+\frac{\theta_{i,j+1}^{n+2}-2\theta_{i,j}^{n+2}+\theta_{i,j-1}^{n+2}}{\Delta z^{*2}}\right)+S_{i,j}^{n+2} \qquad (5.21)$$

This equation can be written as:

$$C\theta_{i,j-1}^{n+2}-D\theta_{i,j}^{n+2}+C\theta_{i,j+1}^{n+2}=L_j^{n+1} \qquad (5.22)$$

Where

$$C=\frac{\Delta\tau}{\mathrm{Pr}\Delta z^{*2}}$$

$$D=\frac{2\Delta\tau}{\mathrm{Pr}\Delta z^{*2}}+1$$

$$L_j^{n+1}=-\left(\theta_{i,j}^{n+1}+\frac{\Delta\tau}{\mathrm{Pr}\Delta y^{*2}}\left(\theta_{i+1,j}^{n+1}-2\theta_{i,j}^{n+1}+\theta_{i-1,j}^{n+1}\right)+S_{i,j}^{n+2}\Delta\tau\right)$$

5.2.AC (MHD) pumping

Now the ADI numerical method can also be used to solve the AC energy equation with the same steps

$$St^2\frac{\partial\theta}{\partial\tau}=\frac{1}{p_r}\left(\frac{\partial^2\theta}{\partial y^{*2}}+\frac{\partial^2\theta}{\partial z^{*2}}\right)+S\left(y^*,z^*,\tau\right) \qquad (5.23)$$

Where the source term is:

$$S\left(y^*,z^*,\tau\right)=Ha^2E_c\left(\frac{\sin\left(2\pi\tau+\phi\right)}{Ha^2}+u^*\sin\left(2\pi\tau\right)\right)^2$$

Firstly, we treat the y derivative in equation (5.23) implicitly.

$$St^2\frac{\theta_{i,j}^{n+1}-\theta_{i,j}^{n}}{\Delta\tau}=\frac{1}{\mathrm{Pr}}\left(\frac{\theta_{i+1,j}^{n+1}-2\theta_{i,j}^{n+1}+\theta_{i-1,j}^{n+1}}{\Delta y^{*2}}+\frac{\theta_{i,j+1}^{n}-2\theta_{i,j}^{n}+\theta_{i,j-1}^{n}}{\Delta z^{*2}}\right)+S_{i,j}^{n+1} \qquad (5.24)$$

This equation can be written as:

$$A\theta_{i-1,j}^{n+1}-B\theta_{i,j}^{n+1}+A\theta_{i+1,j}^{n+1}=K_i^n \qquad (5.25)$$

Where

$$A=\frac{\Delta\tau}{St^2\,\mathrm{Pr}\Delta y^{*2}}$$

$$B=\frac{2\Delta\tau}{St^2\,\mathrm{Pr}\Delta y^{*2}}+1$$

$$K_i^n=-\left(\theta_{i,j}^{n}+\frac{\Delta\tau}{St^2\,\mathrm{Pr}\Delta z^{*2}}\left(\theta_{i,j+1}^{n}-2\theta_{i,j}^{n}+\theta_{i,j-1}^{n}\right)+\frac{S_{i,j}^{n+1}\Delta\tau}{St^2}\right)$$

Now treat the z derivative in equation (5.23) implicitly.

$$St^2\frac{\theta_{i,j}^{n+2}-\theta_{i,j}^{n+1}}{\Delta\tau}=\frac{1}{\mathrm{Pr}}\left(\frac{\theta_{i+1,j}^{n+1}-2\theta_{i,j}^{n+1}+\theta_{i-1,j}^{n+1}}{\Delta y^{*2}}+\frac{\theta_{i,j+1}^{n+2}-2\theta_{i,j}^{n+2}+\theta_{i,j-1}^{n+2}}{\Delta z^{*2}}\right)+S_{i,j}^{n+2} \qquad (5.26)$$

This equation can be written as:

$$C\theta_{i,j-1}^{n+2}-D\theta_{i,j}^{n+2}+C\theta_{i,j+1}^{n+2}=L_j^{n+1} \qquad (5.27)$$

Where

$$C=\frac{\Delta\tau}{St^2\,\mathrm{Pr}\Delta z^{*2}}$$

$$D=\frac{2\Delta\tau}{St^2\,\mathrm{Pr}\Delta z^{*2}}+1$$

$$L_j^{n+1}=-\left(\theta_{i,j}^{n+1}+\frac{\Delta\tau}{St^2\,\mathrm{Pr}\Delta y^{*2}}\left(\theta_{i+1,j}^{n+1}-2\theta_{i,j}^{n+1}+\theta_{i-1,j}^{n+1}\right)+\frac{S_{i,j}^{n+2}\Delta\tau}{St^2}\right)$$

Chapter 6
Developing flow solution (pressure correction method)

6.1 Introduction

The pressure correction method which is widely used technique for incompressiple viscous CFD applications (Anderson, 1995) is applied to solve the previous two-dimensional incompressible Navier-Stokes equations in non-dimensional form. The technique is included in an algorithm called SIMPLE (semi-implicit method for pressure-linked equations).

6.2 Staggered Grid

For discretization of differential equations a uniform staggered grid where the pressures and velocities are calculated at different grid points in the x and y directions is used. In figure (6.1) a staggered grid for rectangular area is sketched. Primitive variables (u, v and p) are placed in different places. The velocity component u is calculated at the solid grid points, labeled (i-1/2,j), (i+1/2,j), etc., and the velocity component v is calculated at the open grid points, labeled (i,j-1/2), (i,j+1/2), etc., and the pressures are calculated at the triangular grid points, labeled (i-1,j), (i,j), etc.

That simple model of staggered grid gives us possibility to use simple discretization with second order accuracy.

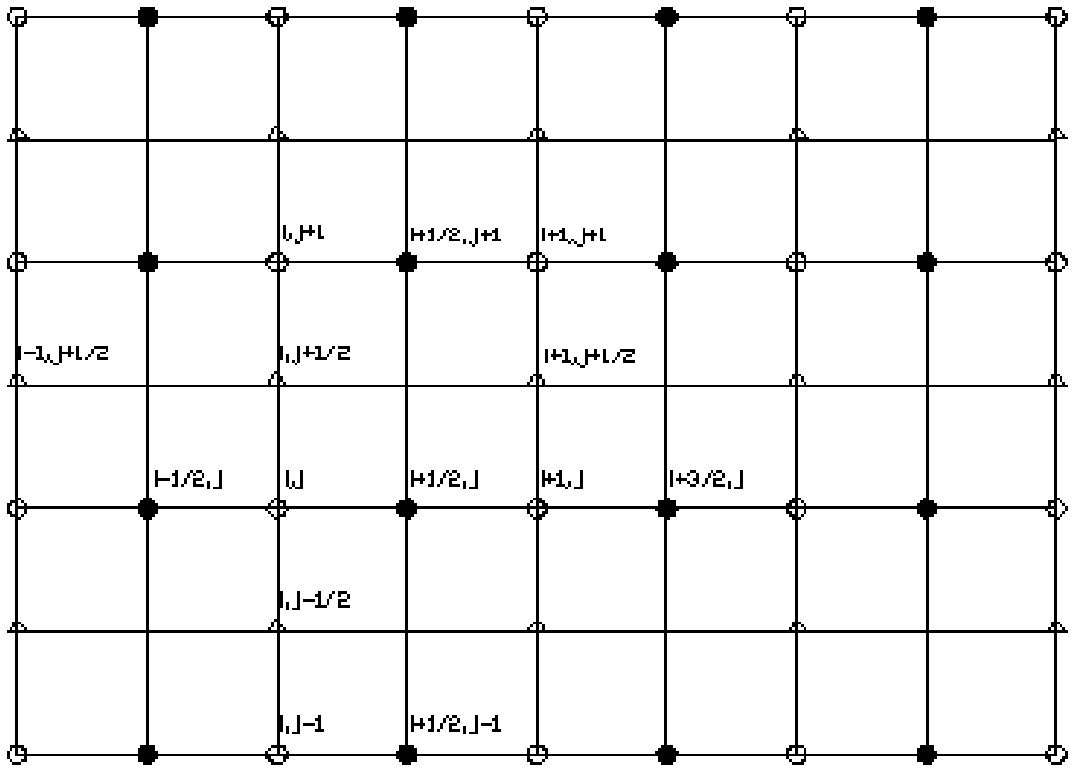

Figure 6.1: Staggered grid used for descritization

6.3 Descritization

The nonlinear terms in the left hand side of the Navier-Stockes equations can be ignored because Reynolds number is small. Hence the resulting system of equations becomes:

$$\frac{\partial u^*}{\partial x^*}+\frac{\partial v^*}{\partial y^*}=0 \tag{6.1}$$

$$\frac{\partial u^*}{\partial \tau}=-\frac{\partial p^*}{\partial x^*}+\frac{\partial^2 u^*}{\partial x^{*2}}+\frac{\partial^2 u^*}{\partial y^{*2}}+1-Ha^2u^* \tag{6.2}$$

$$\frac{\partial v^*}{\partial \tau}=-\frac{\partial p^*}{\partial y^*}+\frac{\partial^2 v^*}{\partial x^{*2}}+\frac{\partial^2 v^*}{\partial y^{*2}} \tag{6.3}$$

we have only three equations for the three dependent variables $u^*, v^*,$ and p^* which

have to be discretized on a grid. First we have momentum equations (6.2) and (6.3). These equations can be discretized on staggered grid and written as follows:

x-momentum: about (i+1/2,j)

$$\frac{u^{n+1}_{i+\frac{1}{2},j}-u^{n}_{i+\frac{1}{2},j}}{\Delta t}=\frac{p^{n}_{i+1,j}-p^{n}_{i,j}}{\Delta x}+\frac{u^{n}_{i+\frac{3}{2},j}-2u^{n}_{i+\frac{1}{2},j}+u^{n}_{i-\frac{1}{2},j}}{(\Delta x)^2}$$
$$+\frac{u^{n}_{i+\frac{1}{2},j+1}-2u^{n}_{i+\frac{1}{2},j}+u^{n}_{i+\frac{1}{2},j-1}}{(\Delta y)^2}+1-Ha^2u^{n}_{i+\frac{1}{2},j} \qquad (6.4)$$

y-momentum: about (i,j+1/2)

$$\frac{v^{n+1}_{i,j+\frac{1}{2}}-v^{n}_{i,j+\frac{1}{2}}}{\Delta t}=\frac{p^{n}_{i,j+1}-p^{n}_{i,j}}{\Delta y}+\frac{v^{n}_{i+1,j+\frac{1}{2}}-2v^{n}_{i,j+\frac{1}{2}}+v^{n}_{i-1,j+\frac{1}{2}}}{(\Delta x)^2}+\frac{v^{n}_{i,j+\frac{3}{2}}-2v^{n}_{i,j+\frac{1}{2}}+v^{n}_{i,j-\frac{1}{2}}}{(\Delta y)^2} \qquad (6.5)$$

from equation (6.4),

$$u^{n+1}_{i+\frac{1}{2},j}=(1-Ha^2\Delta t)u^{n}_{i+\frac{1}{2},j}-\Delta t\left[-\frac{u^{n}_{i+\frac{3}{2},j}-2u^{n}_{i+\frac{1}{2},j}+u^{n}_{i-\frac{1}{2},j}}{(\Delta x)^2}-\frac{u^{n}_{i+\frac{1}{2},j+1}-2u^{n}_{i+\frac{1}{2},j}+u^{n}_{i+\frac{1}{2},j-1}}{(\Delta y)^2}\right]$$
$$-\frac{\Delta t}{\Delta x}(p^{n}_{i+1,j}-p^{n}_{i,j})+\Delta t \qquad (6.6)$$

or,

$$u^{n+1}_{i+\frac{1}{2},j}=(1-Ha^2\Delta t)u^{n}_{i+\frac{1}{2},j}-\Delta t(A-1)-\frac{\Delta t}{\Delta x}(p^{n}_{i+1,j}-p^{n}_{i,j}) \qquad (6.7)$$

where

$$A=-\frac{u^n_{i+\frac{3}{2},j}-2u^n_{i+\frac{1}{2},j}+u^n_{i-\frac{1}{2},j}}{(\Delta x)^2}-\frac{u^n_{i+\frac{1}{2},j+1}-2u^n_{i+\frac{1}{2},j}+u^n_{i+\frac{1}{2},j-1}}{(\Delta y)^2} \tag{6.8}$$

in y-mom

$$v^{n+1}_{i,j+\frac{1}{2}}=v^n_{i,j+\frac{1}{2}}-\Delta t\left[-\frac{v^n_{i+1,j+\frac{1}{2}}-2v^n_{i,j+\frac{1}{2}}+v^n_{i-1,j+\frac{1}{2}}}{(\Delta x)^2}-\frac{v^n_{i,j+\frac{3}{2}}-2v^n_{i,j+\frac{1}{2}}+v^n_{i,j-\frac{1}{2}}}{(\Delta y)^2}\right] \tag{6.9}$$
$$-\frac{\Delta t}{\Delta y}\left(p^n_{i,j+1}-p^n_{i,j}\right)$$

or

$$v^{n+1}_{i,j+\frac{1}{2}}=v^n_{i,j+\frac{1}{2}}-\Delta tB-\frac{\Delta t}{\Delta y}\left(p^n_{i,j+1}-p^n_{i,j}\right) \tag{6.10}$$

where

$$B=-\frac{v^n_{i+1,j+\frac{1}{2}}-2v^n_{i,j+\frac{1}{2}}+v^n_{i-1,j+\frac{1}{2}}}{(\Delta x)^2}-\frac{v^n_{i,j+\frac{3}{2}}-2v^n_{i,j+\frac{1}{2}}+v^n_{i,j-\frac{1}{2}}}{(\Delta y)^2} \tag{6.11}$$

Similar to the DC developing flow, the pressure correction method can be used to solve the two-dimensional incompressible developing Navier-Stokes equations in AC MHD pump.

The nonlinear terms in the left hand side of the Navier-Stockes equations also can be ignored. Hence the resulting system of equations becomes:

$$\frac{\partial u^*}{\partial x^*}+\frac{\partial v^*}{\partial y^*}=0 \tag{6.12}$$

$$St^2\frac{\partial u^*}{\partial \tau}=-\frac{\partial p^*}{\partial x^*}+\frac{\partial^2 u^*}{\partial x^{*2}}+\frac{\partial^2 u^*}{\partial y^{*2}}+\sin(2\pi\tau)\sin(2\pi\tau+\phi)-Ha^2u^*\sin^2(2\pi\tau) \tag{6.13}$$

$$St^2\frac{\partial v^*}{\partial \tau}=-\frac{\partial p^*}{\partial y^*}+\frac{\partial^2 v^*}{\partial x^{*2}}+\frac{\partial^2 v^*}{\partial y^{*2}} \tag{6.14}$$

Now the momentum equations (6.13) and (6.14) can be descritized and written as follows:

x-momentum: about $(i+1/2,j)$

$$St^2\frac{u^{n+1}_{i+\frac{1}{2},j}-u^{n}_{i+\frac{1}{2},j}}{\Delta\tau}=-\frac{p^n_{i+1,j}-p^n_{i,j}}{\Delta x}+\frac{u^n_{i+\frac{3}{2},j}-2u^n_{i+\frac{1}{2},j}+u^n_{i-\frac{1}{2},j}}{(\Delta x)^2}+\frac{u^n_{i+\frac{1}{2},j+1}-2u^n_{i+\frac{1}{2},j}+u^n_{i+\frac{1}{2},j-1}}{(\Delta y)^2}$$
$$+\sin(2\pi\tau^{n+1})\sin(2\pi\tau^{n+1}+\phi)-Ha^2u^n_{i+\frac{1}{2},j}\sin^2(2\pi\tau^{n+1}) \tag{6.15}$$

y-momentum: about $(i,j+1/2)$

$$St^2\frac{v^{n+1}_{i,j+\frac{1}{2}}-v^{n}_{i,j+\frac{1}{2}}}{\Delta\tau}=-\frac{p^n_{i,j+1}-p^n_{i,j}}{\Delta y}+\frac{v^n_{i+1,j+\frac{1}{2}}-2v^n_{i,j+\frac{1}{2}}+v^n_{i-1,j+\frac{1}{2}}}{(\Delta x)^2}+\frac{v^n_{i,j+\frac{3}{2}}-2v^n_{i,j+\frac{1}{2}}+v^n_{i,j-\frac{1}{2}}}{(\Delta y)^2} \tag{6.16}$$

Equation (6.15) can be written as:

$$u_{i+\frac{1}{2},j}^{n+1}=\left(1-Ha^2\frac{\Delta\tau}{St^2}\sin^2\left(2\pi\tau^{n+1}\right)\right)u_{i+\frac{1}{2},j}^{n}+\frac{\Delta\tau}{St^2}\sin 2\pi\tau^{n+1}\sin\left(2\pi\tau^{n+1}+\phi\right)$$
$$+\frac{\Delta\tau}{St^2}\left(\frac{u_{i+\frac{3}{2},j}^{n}-2u_{i+\frac{1}{2},j}^{n}+u_{i-\frac{1}{2},j}^{n}}{(\Delta x)^2}+\frac{u_{i+\frac{1}{2},j+1}^{n}-2u_{i+\frac{1}{2},j}^{n}+u_{i+\frac{1}{2},j-1}^{n}}{(\Delta y)^2}\right)-\frac{\Delta\tau}{St^2\Delta x}\left(p_{i+1,j}^{n}-p_{i,j}^{n}\right) \tag{6.17}$$

or,

$$u_{i+\frac{1}{2},j}^{n+1}=\left(1-Ha^2\frac{\Delta\tau}{St^2}\sin^2\left(2\pi\tau^{n+1}\right)\right)u_{i+\frac{1}{2},j}^{n}$$
$$-\frac{\Delta\tau}{St^2}A+\frac{\Delta\tau}{St^2}\sin 2\pi\tau^{n+1}\sin\left(2\pi\tau^{n+1}+\phi\right)-\frac{\Delta\tau}{St^2\Delta x}\left(p_{i+1,j}^{n}-p_{i,j}^{n}\right) \tag{6.18}$$

where

$$A=-\frac{u_{i+\frac{3}{2},j}^{n}-2u_{i+\frac{1}{2},j}^{n}+u_{i-\frac{1}{2},j}^{n}}{(\Delta x)^2}-\frac{u_{i+\frac{1}{2},j+1}^{n}-2u_{i+\frac{1}{2},j}^{n}+u_{i+\frac{1}{2},j-1}^{n}}{(\Delta y)^2} \tag{6.19}$$

in y-mom

$$v_{i,j+\frac{1}{2}}^{n+1}=v_{i,j+\frac{1}{2}}^{n}+\frac{\Delta\tau}{St^2}\left(\frac{v_{i+1,j+\frac{1}{2}}^{n}-2v_{i,j+\frac{1}{2}}^{n}+v_{i-1,j+\frac{1}{2}}^{n}}{(\Delta x)^2}+\frac{v_{i,j+\frac{3}{2}}^{n}-2v_{i,j+\frac{1}{2}}^{n}+v_{i,j-\frac{1}{2}}^{n}}{(\Delta y)^2}\right) \tag{6.20}$$
$$-\frac{\Delta\tau}{St^2\Delta y}\left(p_{i,j+1}^{n}-p_{i,j}^{n}\right)$$

or

$$v_{i,j+\frac{1}{2}}^{n+1} = v_{i,j+\frac{1}{2}}^{n} - \frac{\Delta\tau}{St^2} B - \frac{\Delta\tau}{St^2 \Delta y}\left(p_{i,j+1}^{n} - p_{i,j}^{n}\right) \tag{6.21}$$

where

$$B = -\frac{v_{i+1,j+\frac{1}{2}}^{n} - 2v_{i,j+\frac{1}{2}}^{n} + v_{i-1,j+\frac{1}{2}}^{n}}{(\Delta x)^2} - \frac{v_{i,j+\frac{3}{2}}^{n} - 2v_{i,j+\frac{1}{2}}^{n} + v_{i,j-\frac{1}{2}}^{n}}{(\Delta y)^2} \tag{6.22}$$

6.4 Poisson Equation

At beginning $p = p^*$

Equations (6.7) and (6.10) become:

$$u_{i+\frac{1}{2},j}^{*n+1} = \left(1 - Ha^2 \Delta t\right) u_{i+\frac{1}{2},j}^{*n} - \Delta t\left(A^* - 1\right) - \frac{\Delta t}{\Delta x}\left(p_{i+1,j}^{*n} - p_{i,j}^{*n}\right) \tag{6.23}$$

$$v_{i,j+\frac{1}{2}}^{*n+1} = v_{i,j+\frac{1}{2}}^{*n} - \Delta t B^* - \frac{\Delta t}{\Delta y}\left(p_{i,j+1}^{*n} - p_{i,j}^{*n}\right) \tag{6.24}$$

Now subtract equation (6.23) from (6.7) yields:

$$u'^{n+1}_{i+\frac{1}{2},j} = \left(1 - Ha^2 \Delta t\right) u'^{n}_{i+\frac{1}{2},j} - \Delta t\left(A' - 1\right) - \frac{\Delta t}{\Delta x}\left(p'^{n}_{i+1,j} - p'^{n}_{i,j}\right) \tag{6.25}$$

and subtract (6.24) from (6.10) yields:

$$v'^{n+1}_{i,j+\frac{1}{2}} = v'^{n}_{i,j+\frac{1}{2}} - \Delta t B' - \frac{\Delta t}{\Delta y}\left(p'^{n}_{i,j+1} - p'^{n}_{i,j}\right) \tag{6.26}$$

Let us arbitrarily set $A', B', u'^{n}, and v'^{n} = 0$ then equations (6.25) and (6.26) become:

$$u'^{n+1}_{i+\frac{1}{2},j} = \Delta t - \frac{\Delta t}{\Delta x}\left(p'^{n}_{i+1,j} - p'^{n}_{i,j}\right) \tag{6.27}$$

and

$$v'^{n+1}_{i,j+\frac{1}{2}} = -\frac{\Delta t}{\Delta y}\left(p'^{n}_{i,j+1} - p'^{n}_{i,j}\right) \tag{6.28}$$

but

$$u'^{n+1}_{i+\frac{1}{2},j} = u^{n+1}_{i+\frac{1}{2},j} - u^{*n+1}_{i+\frac{1}{2},j} \tag{6.29}$$

and

$$v'^{n+1}_{i,j+\frac{1}{2}} = v^{n+1}_{i,j+\frac{1}{2}} - v^{*n+1}_{i,j+\frac{1}{2}} \tag{6.30}$$

Substitute (6.29) into (6.27) and (6.30) into (6.28) :

$$u^{n+1}_{i+\frac{1}{2},j} = u^{*n+1}_{i+\frac{1}{2},j} + \Delta t - \frac{\Delta t}{\Delta x}\left(p'^{n}_{i+1,j} - p'^{n}_{i,j}\right) \tag{6.31}$$

and

$$v^{n+1}_{i,j+\frac{1}{2}} = v^{*n+1}_{i,j+\frac{1}{2}} - \frac{\Delta t}{\Delta y}\left(p'^{n}_{i,j+1} - p'^{n}_{i,j}\right) \tag{6.32}$$

Now descritize the continuity equation around the point (*i*,*j*) :

$$\frac{u_{i+\frac{1}{2},j} - u_{i-\frac{1}{2},j}}{\Delta x} + \frac{v_{i,j+\frac{1}{2}} - v_{i,j-\frac{1}{2}}}{\Delta y} = 0 \tag{6.33}$$

Substitute (6.31) and (6.32) into (6.33) :

$$\frac{u^{*n+1}_{i+\frac{1}{2},j}+\Delta t-\frac{\Delta t}{\Delta x}\left(p'^{n}_{i+1,j}-p'^{n}_{i,j}\right)-u^{*}_{i-\frac{1}{2},j}-\Delta t+\frac{\Delta t}{\Delta x}\left(p'_{i,j}-p'_{i-1,j}\right)}{\Delta x}+\frac{v^{*}_{i,j+\frac{1}{2}}-\frac{\Delta t}{\Delta y}\left(p'_{i,j+1}-p'_{i,j}\right)-v^{*}_{i,j-\frac{1}{2}}+\frac{\Delta t}{\Delta y}\left(p'_{i,j}-p'_{i,j-1}\right)}{\Delta y}=0 \tag{6.34}$$

$$ap'_{i,j}+b\left(p'_{i+1,j}+p'_{i-1,j}\right)+c\left(p'_{i,j+1}+p'_{i,j-1}\right)+d=0 \tag{6.35}$$

where

$$a=\frac{2\Delta t}{\Delta x^2}+\frac{2\Delta t}{\Delta y^2}$$

$$b=\frac{-\Delta t}{\Delta x^2}$$

$$c=\frac{-\Delta t}{\Delta y^2}$$

$$d=\frac{u^{*}_{i+\frac{1}{2},j}-u^{*}_{i-\frac{1}{2},j}}{\Delta x}+\frac{v^{*}_{i,j+\frac{1}{2}}-v^{*}_{i,j-\frac{1}{2}}}{\Delta y}$$

Similar to DC the Poisson equation can be developed for AC pumping. It will be:

$$ap'_{i,j}+b\left(p'_{i+1,j}+p'_{i-1,j}\right)+c\left(p'_{i,j+1}+p'_{i,j-1}\right)+d=0 \tag{6.36}$$

where

$$a=\frac{2\Delta\tau}{St^2\Delta x^2}+\frac{2\Delta\tau}{St^2\Delta y^2}$$

$$b=\frac{-\Delta\tau}{St^2\Delta x^2}$$

$$c=\frac{-\Delta\tau}{St^2\Delta y^2}$$

$$d=\frac{u^*_{i+\frac{1}{2},j}-u^*_{i-\frac{1}{2},j}}{\Delta x}+\frac{v^*_{i,j+\frac{1}{2}}-v^*_{i,j-\frac{1}{2}}}{\Delta y}$$

6.5 SIMPLE algorithm

SIMPLE algorithm is one of the fundamental algorithm to solve incompressible Navier-Stockes equations.

The step by step procedure for the SIMPLE algorithm is as follows:

1 First we have to guess initial values of the pressure p^* and set initial values of velocities u^*, v^*.

2 The values of u^{*n+1}, v^{*n+1} will be obtained at all appropriate internal grid points.

3 Substitute these values of u^{*n+1}, v^{*n+1} into the pressure-correction equation, and solve for P' (using relaxation technique) at all interior grid points.

4 Calculate P^{n+1} at all internal grid points from the equation

$$P^{n+1} = P^{*n} + P'$$

5 The values of P^{n+1} obtained in step 4 are used to solve the momentum equations again. Return to step 2 and substitute P^{n+1} as P^{*} in equations (6.23) and (6.24).

6 Repeat steps 2 to 5 until convergence is achieved

That iterative procedure is rather simple - we use equation (6.35) for all interior points on a grid. After that one step of iterative procedure is done. Then we check if solution converges. We can do it simply to check maximum change of pressure on a grid. If it is bigger than ε we continue iterative process. Solution should finish when pressure is converged.

The method with a large amount of time steps is employed until the steady state solution is achieved.

The numerical results using SIMPLE algorithm can be verified by comparing the transient fully developed axial velocity comes from developing flow solution with that comes from fully developed flow. The SIMPLE algorithm and the program used to solve for velocities and pressure is included in appendix A.

Chapter 7
Results and Discussion

7.1.Fully developed flow

The dimensionless governing equations (3.23-3.28) are solved analytically and numerically for a DC and AC fully developed flow. In this section, the transient velocity and temperature profiles and the effect of different parameters on these profiles will be discussed. To study the effect of these parameters analytical and numerical solutions for the velocity and temperature profiles are computed for different values of Hartmann number, aspect ratio, Prandtl number, and Eckert number.

In addition, the transient velocity profile in AC fully developed flow and the effect of Hartmann number and Stanton number on the behavior of the transient velocity will be discussed.

Hartmann number effect

The effect of Hartmann number on the dimensionless velocity, and dimensionless temperature profiles is shown in Figures (7.1) and (7.2) respectively. The effect of increasing Ha is to retard the flow and then reduce the velocity and the temperature. This means that controlling the electrical conductivity and magnetic flux density will allow to control the velocity and temperature in the channel. Also, It is seen that at low Hartman number the velocity and temperature profiles are parabolic, and as the Ha increases, the profiles flatten. It is seen that the same effect of Ha on the velocity profile is observed on temperature profile, and that the heat generated from the electric current and magnetic flux will cause an increase of the temperature from the initial state. In Figures (7.3), and (7.4) the transient behavior of

the dimensionless centerline velocity, and dimensionless centerline temperature is plotted for different Hartman numbers. It is observed that increasing Ha will decrease the time required to reach steady state conditions.

Figures (7.5) and (7.6) illustrate the effect of Hartmann number on the transient velocity and temperature profiles for the AC pumping. It is seen that Hartmann number has the same effect as in DC pumping. It is noticed in AC pumping that the velocity and temperature have pulsating profiles, where the pulse volume decreases as Ha increases and this is due to the decrease in magnitude of the velocity.

Prandtl number and Eckert number effect

Figures (7.7) and (7.8) depict the transient temperature for different values of the Prandtl number for DC and AC pumping, respectively. It is observed that the temperature increases and the time required to reach steady state increases as P_r increases because with increasing Pr the rate of diffusion of viscous effects increases. Figures (7.9) and (7.10) illustrate the effect of the Eckert number ($Ec=u_0^2/C_pT_w$) on the temperature. It is seen that the Eckert number has the same effect on transient temperature as the prandtl number and this because with increasing Ec the kinetic energy increases.

Aspect ratio effect

Figure (7.11) and (7.12) illustrate the effect of the aspect ratio on the velocity and temperature at the mid height of the channel. It is seen that as the aspect ratio increases, the height of the channel increases which allow to increase the velocity and temperature. This means that controlling the conduit width will allow to control the velocity and temperature.

Stanton number effect

Figures (7.13) and (7.14) depict the transient dimensionless velocity u and dimensionless temperature at different Stanton numbers. It is seen that as the Stanton number increases the pulsed volume decreases and this because the diffusion time increases compared with forcing period. This means that at high frequency, the flow seems to be continuous instead of pulsating flow. It is noticed also that the effect of increasing St is to increase the time required to reach steady state.

phase angle effect

The transient velocity u at different phase angle is shown in figure (7.15). This figure illustrate the effect of the phase angle on the flow direction. The figure shows that at phase angle $\phi=0$, the fluid flows in positive direction while it flows in the opposite direction at $\phi=180^{o}$, and there is no flow at high frequencies when $\phi=90^{o}$. It is concluded that the direction and the magnitude of the flow can be controlled by the phase shift between the electrical and magnetic fields.

A comparison of the analytical and numerical results for the centerline steady-state velocity and temperature is shown below in table (7.1) at different Hartman numbers. Another comparison for the steady-state velocity and temperature at different dimensionless Y coordinate is shown in figure (7.16). The analytical and numerical results seems to be in very good agreement.

A comparison between the numerical and analytical results of a steady AC fully developed flow is shown in figure (7.17). It is seen that the results are in very good agreement.

Table 7.1. Comparison of analytical and numerical methods for steady-state dimensionless centerline velocity and temperature.

	Velocity		Temperature ($\times 10^{-5}$)	
Hartman number	**Analytical solution**	**Numerical solution**	**Analytical solution**	**Numerical solution**
2	0.0904	0.0901	2.7953	2.8964
4	0.0574	0.0572	1.2534	1.2943
6	0.0348	0.0347	0.78006	0.8208
8	0.022	0.0218	0.52224	0.5341
10	0.0147	0.0146	0.36775	0.3710

A Comparison of present results and published analytical results (Zhong et al. 2002) for steady state DC fully developed flow velocity with α=1 is shown in figure (7.18). It is shown that there is a very good agreement between the results.

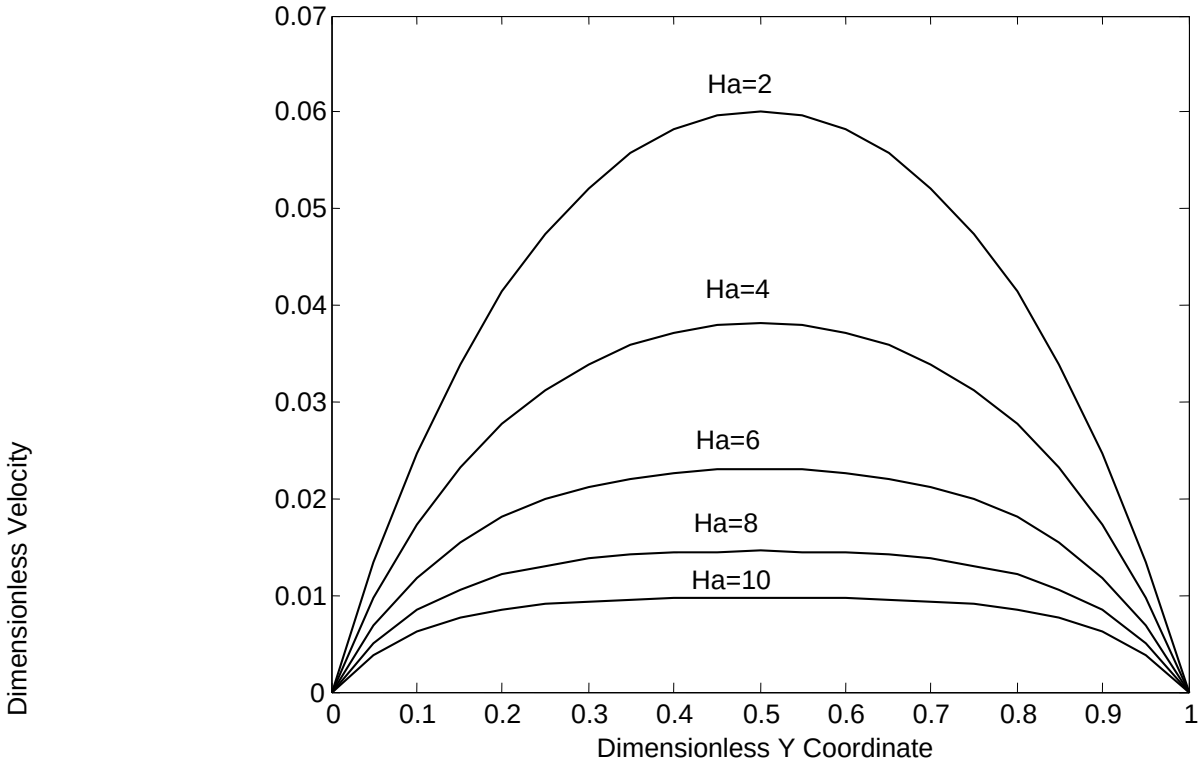

Figure 7.1: Variation of the dimensionless steady mid width velocity with the dimensionless Y coordinate at different Hartman numbers with α=1

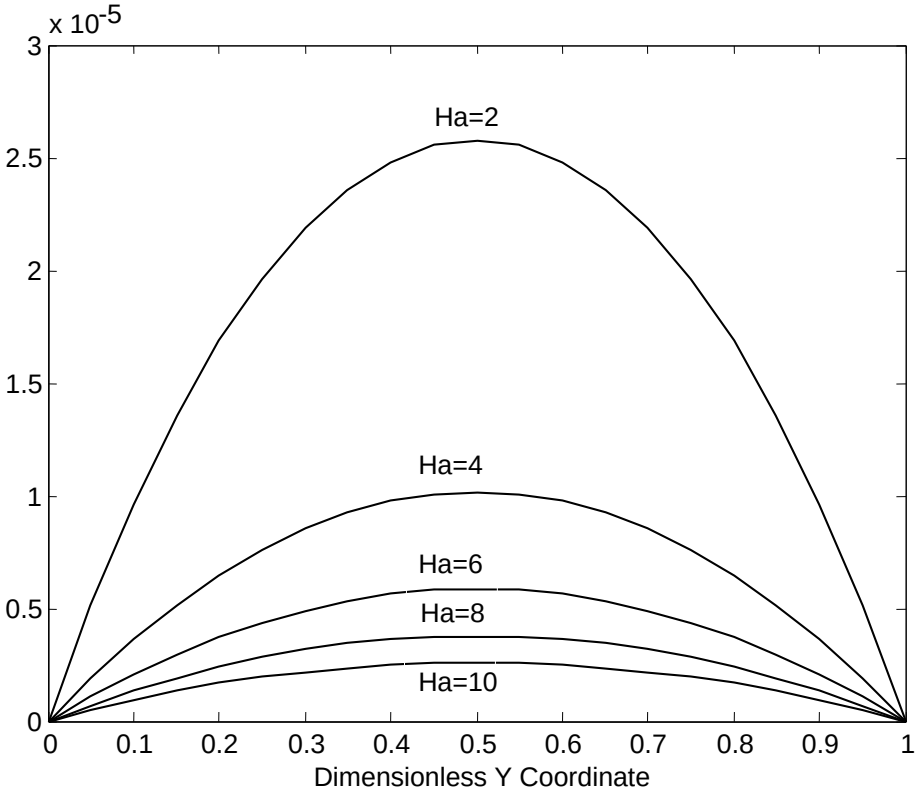

Figure 7.2: Variation of the dimensionless steady mid width temperature with the dimensionless Y coordinate at different Hartman numbers with α=1, Ec=0.01 and Pr=0.1

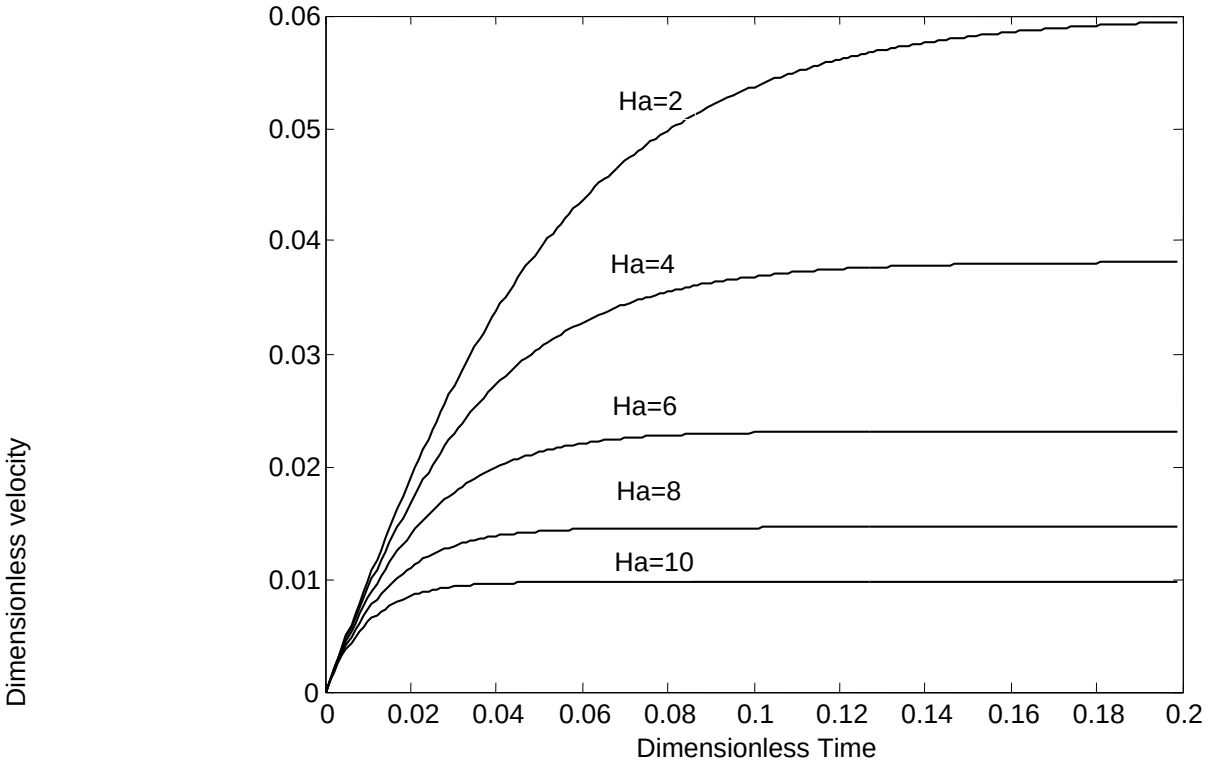

Figure 7.3: Transient behavior of the centerline velocity at different Hartman numbers with α=1

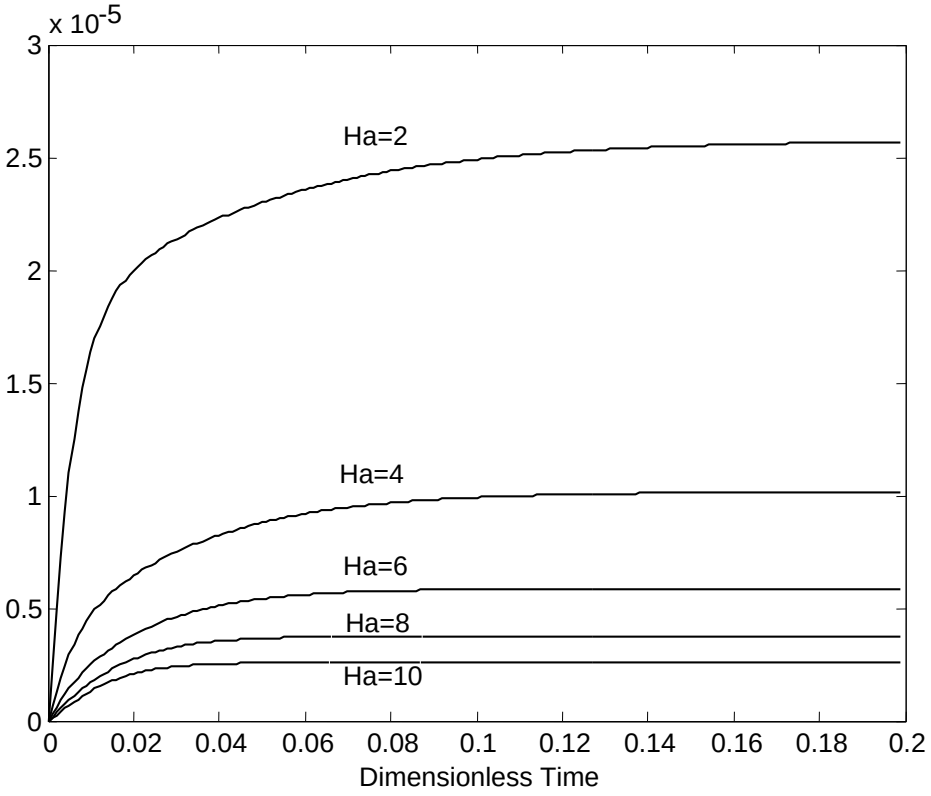

Figure 7.4: Transient behavior of the centerline dimensionless temperature at different Hartman numbers with α=1, Ec=0.01 and Pr=0.1

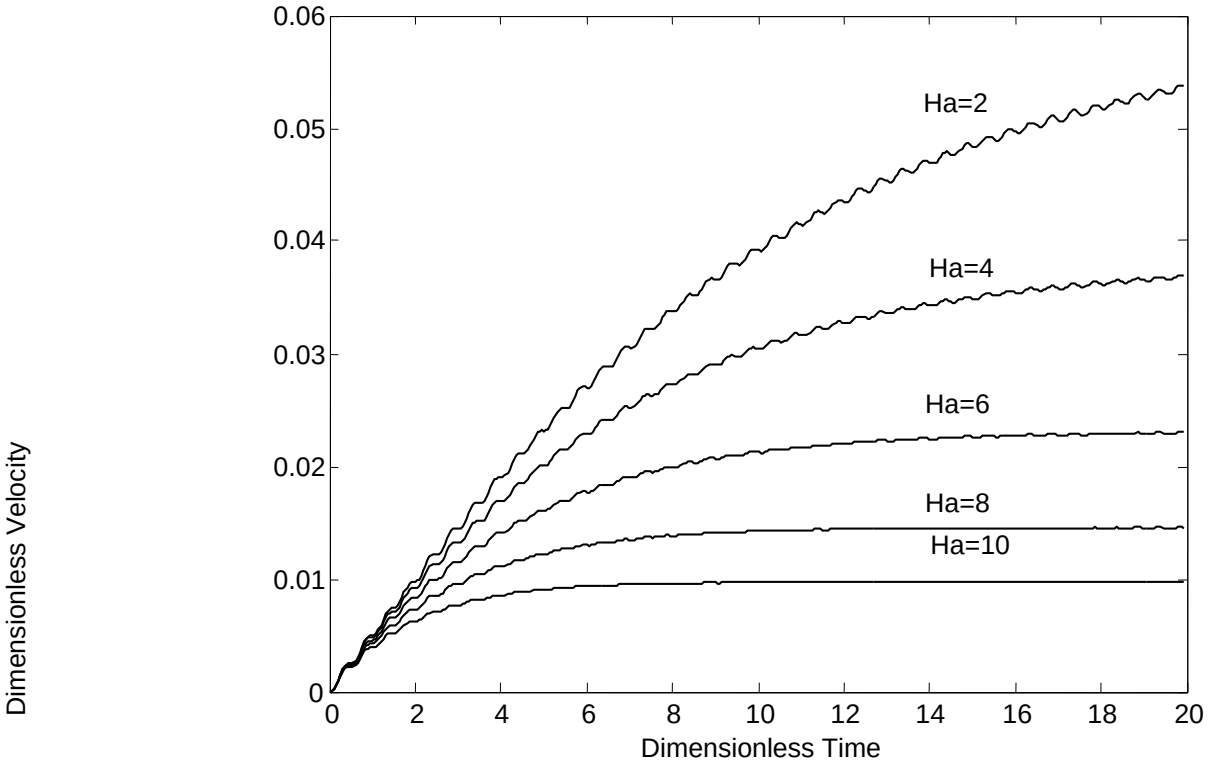

Figure 7.5: Transient behavior of the centerline dimensionless velocity at different Hartman numbers for the AC pumping with α=1, St=10 and φ=0.

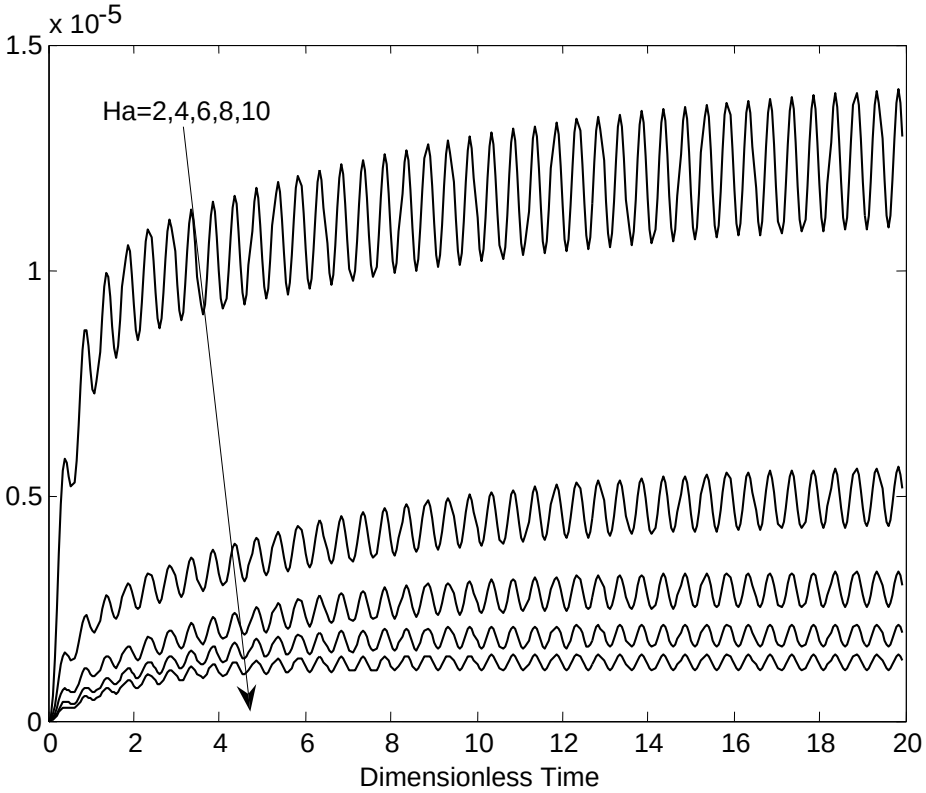

Figure 7.6: Transient behavior of the centerline dimensionless temperature at different Hartman numbers for the AC pumping with α=1, *Ec*=0.01, *Pr*=0.1, St=10 and φ=0.

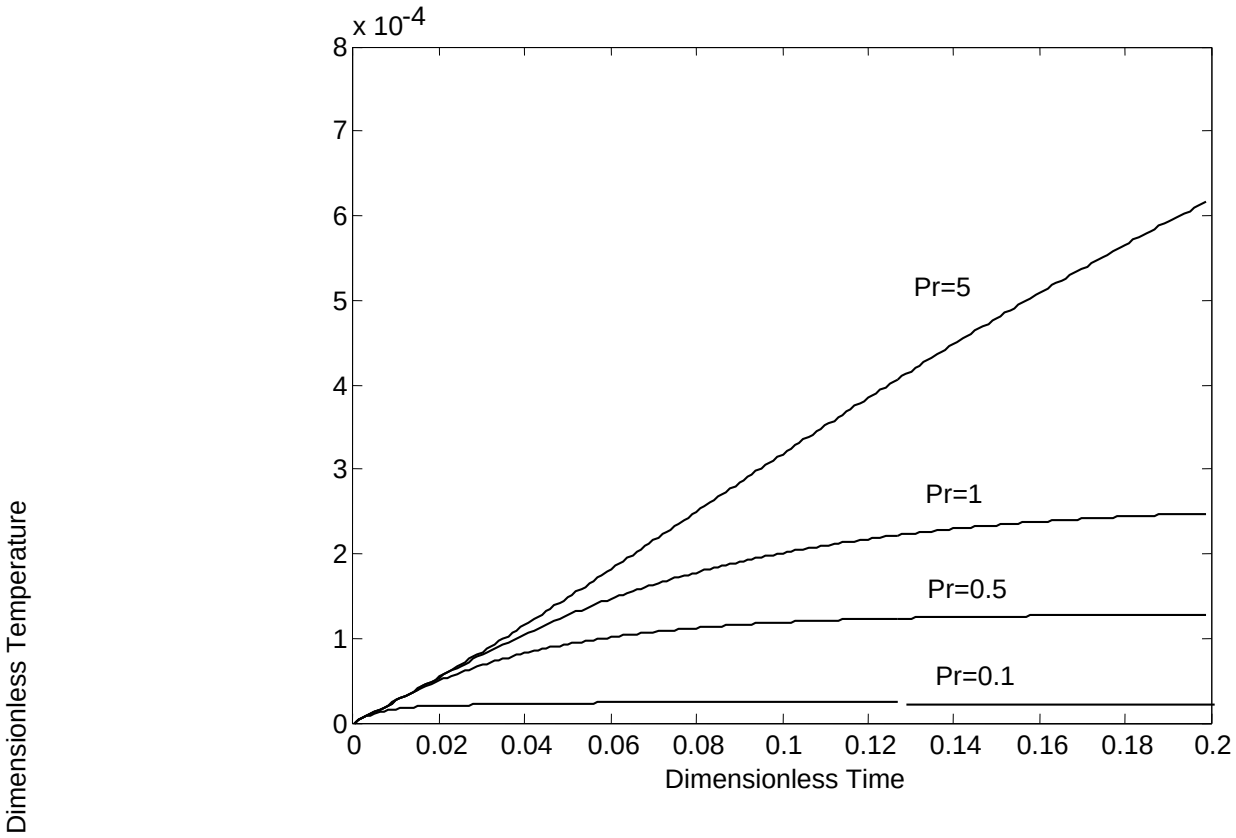

Figure 7.7: Transient behavior of the centerline temperature at different Prandtl numbers for DC pumping with α=1, Ec=0.01 and Ha=2.

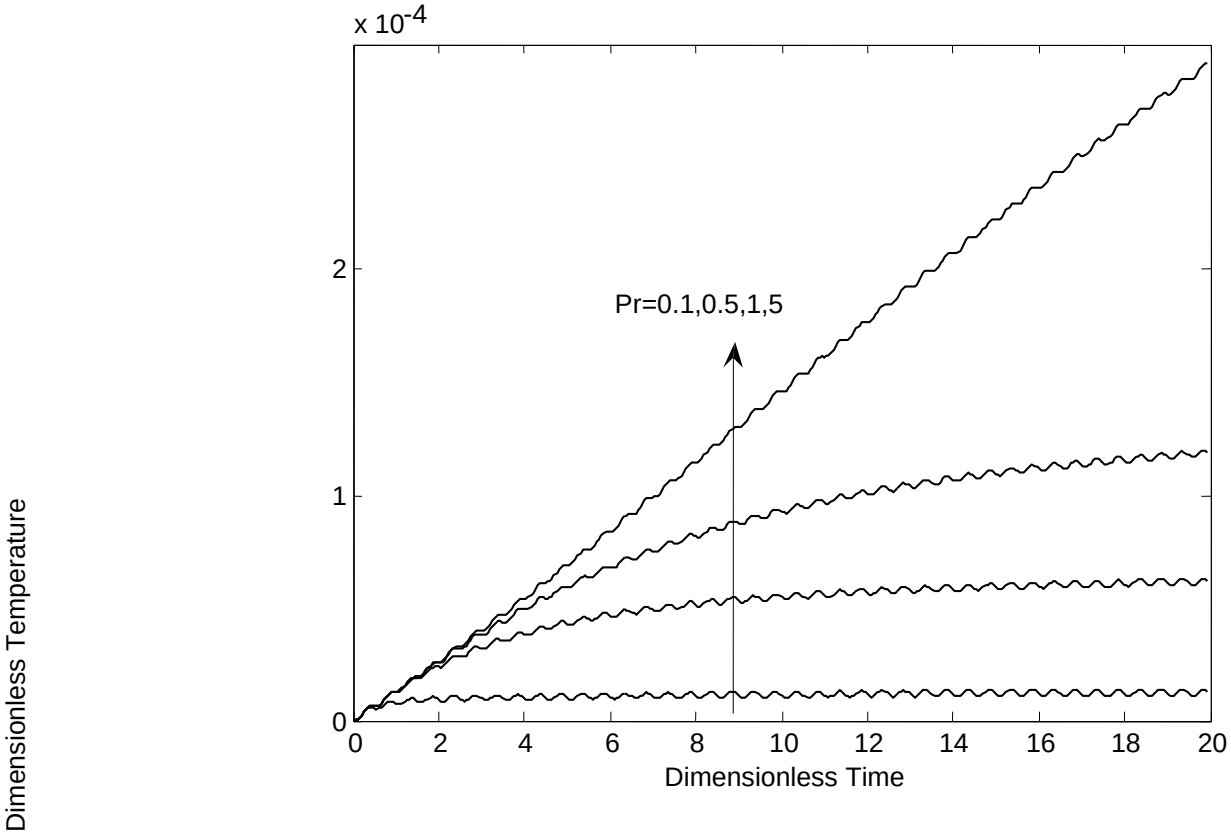

Figure 7.8: Transient behavior of the centerline temperature at different Prandtl numbers for AC pumping with α=1, *Ec*=0.01, *Ha=2*, St=10 and φ=0.

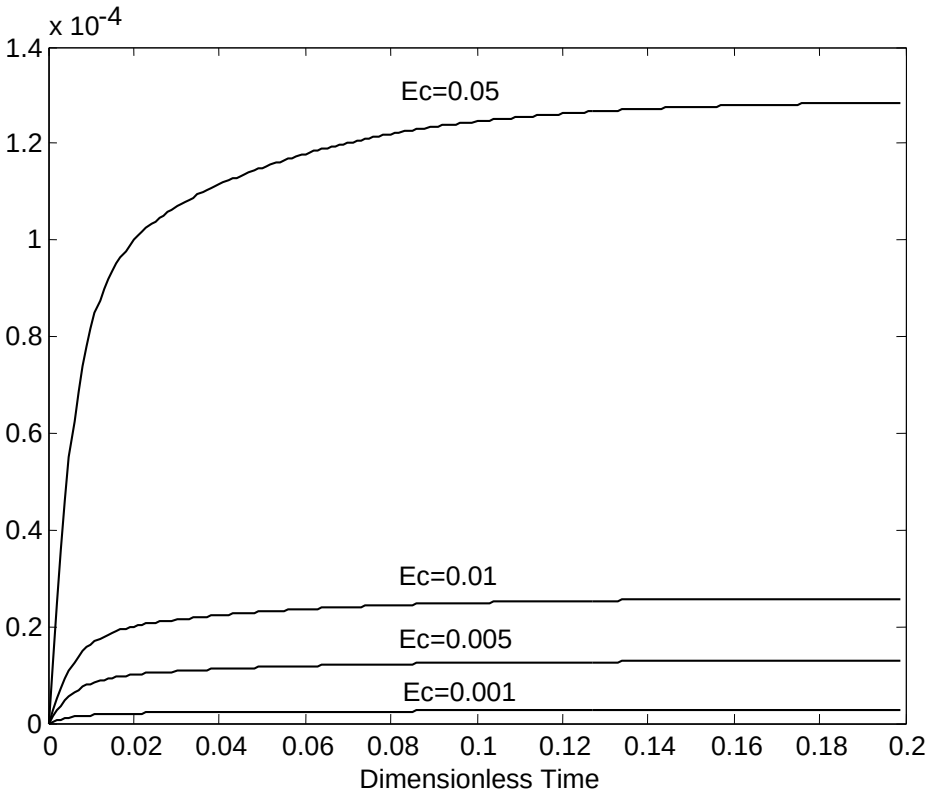

Figure 7.9: Transient behavior of the centerline temperature at different Eckert numbers with α=1, *Ha=2* and *Pr*=0.1

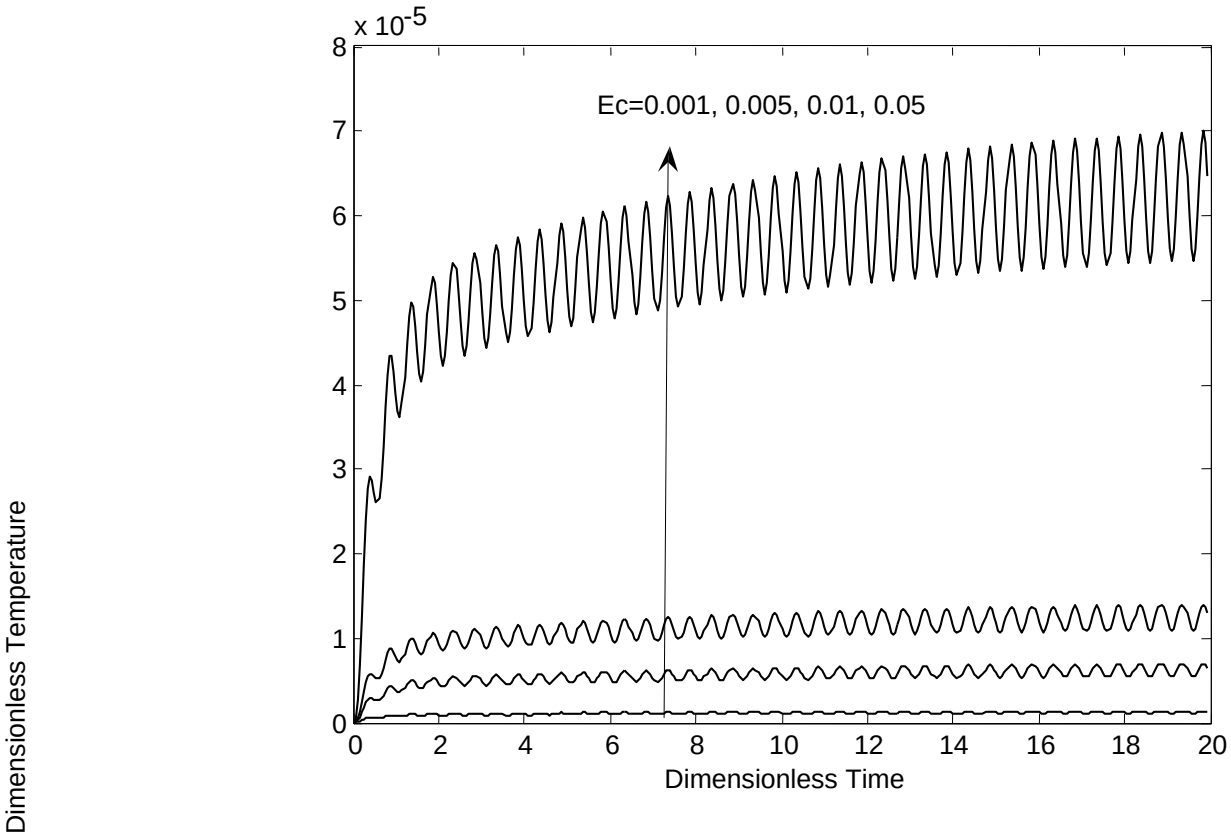

Figure 7.10: Transient behavior of the centerline temperature at different Eckert numbers for AC pumping with α=1, *Ha=2, Pr*=0.1, St=10 and φ=0.

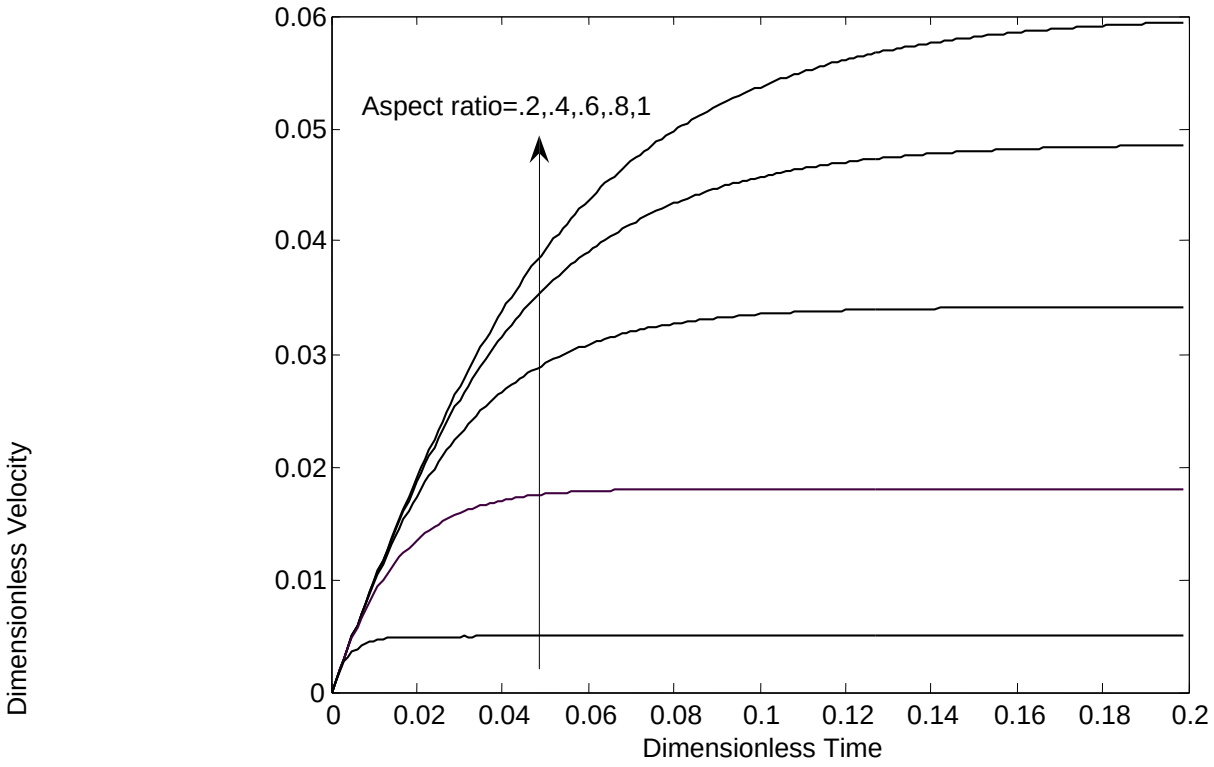

Figure 7.11: Transient behavior of the centerline dimensionless velocity at different aspect ratio with *Ha=2*.

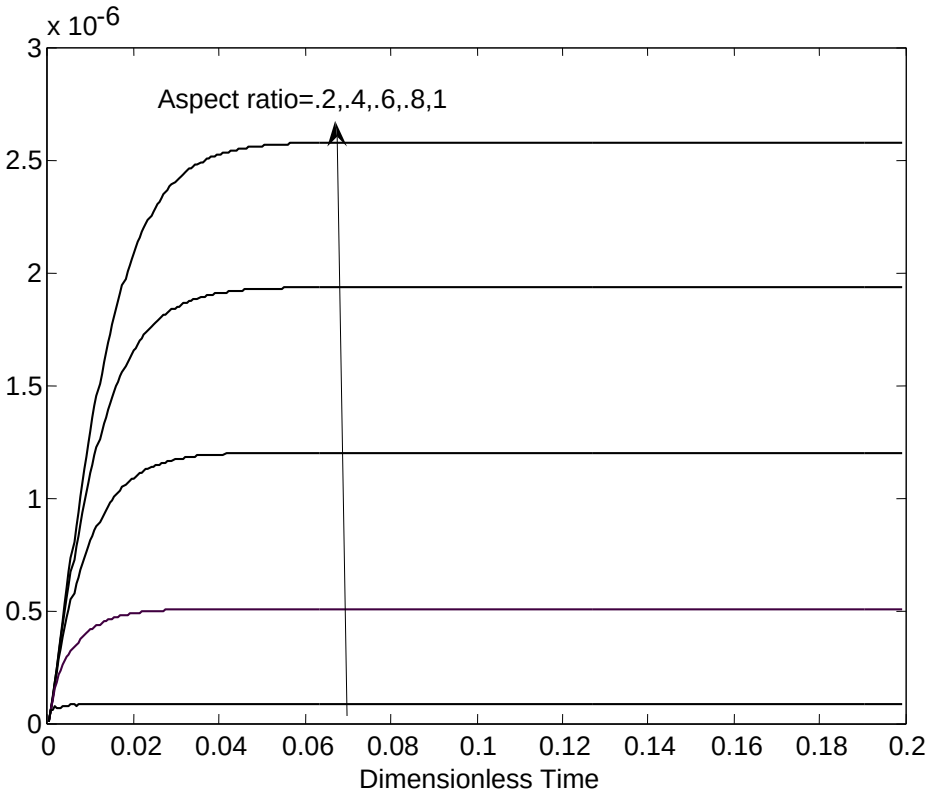

Figure 7.12: Transient behavior of the centerline dimensionless temperature at different aspect ratio with *Ha*=2, *Ec*=0.01 and *Pr*=0.1

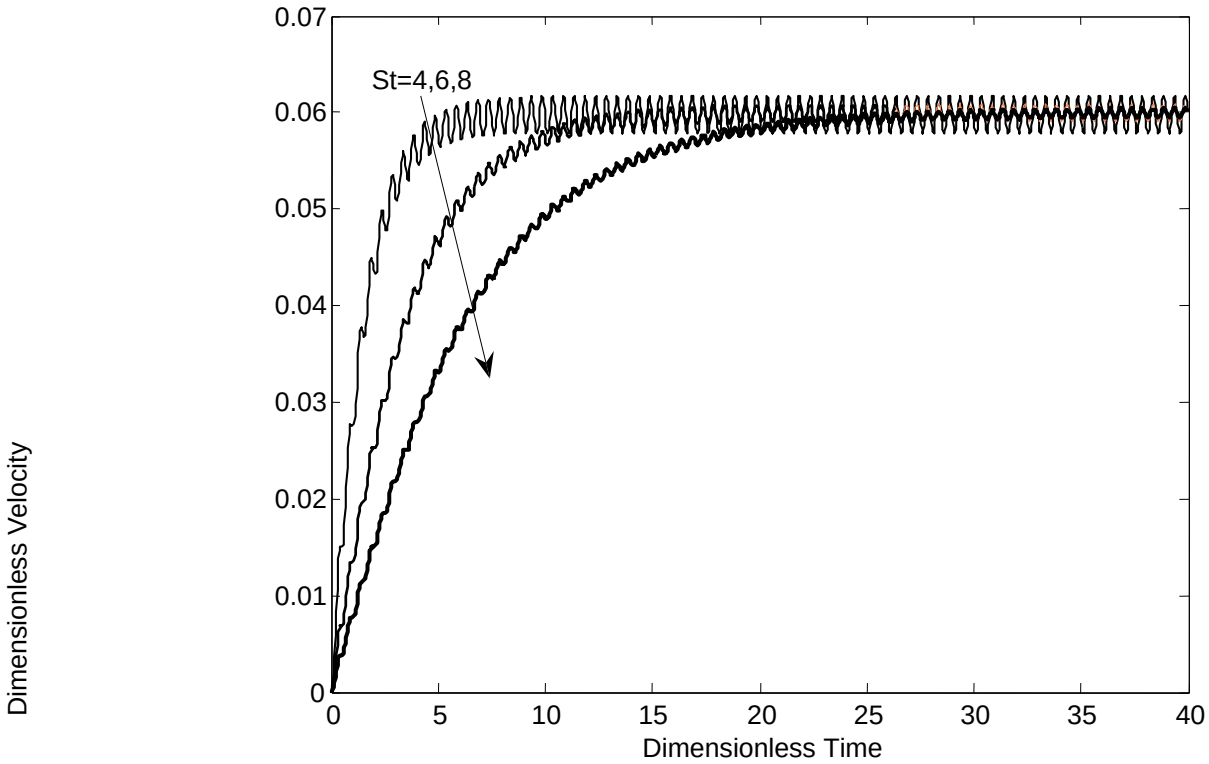

Figure 7.13: Transient behavior of the centerline dimensionless velocity at different Stanton number for AC pumping with α=1, *Ha=2* and φ=0.

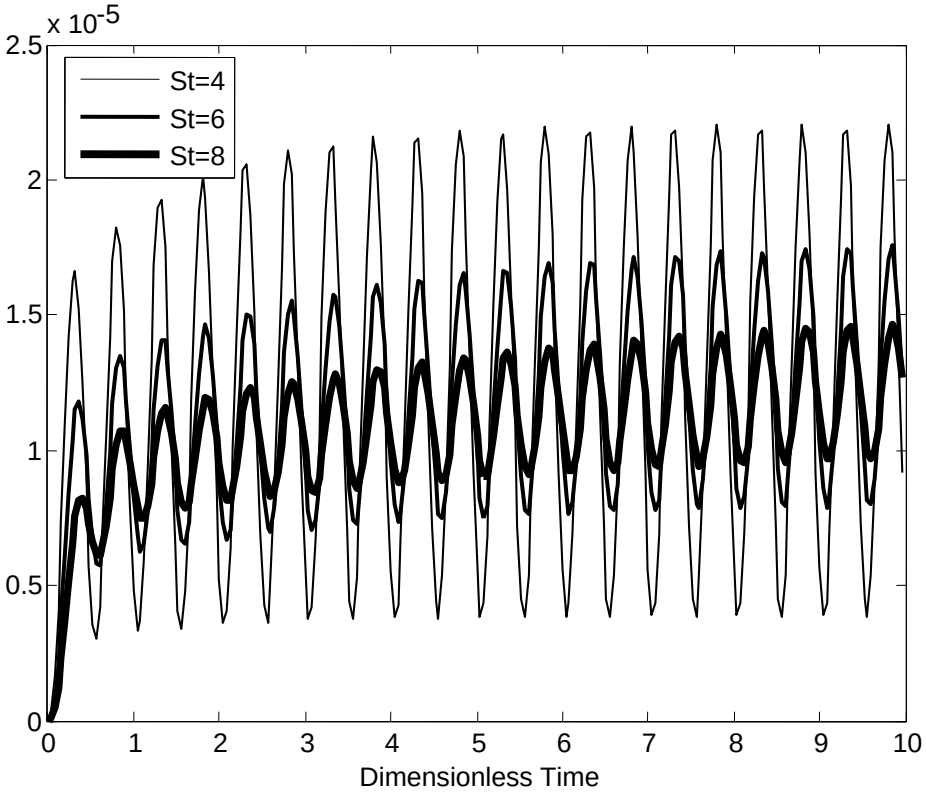

Figure 7.14: Transient behavior of the centerline dimensionless temperature at different Stanton number for AC pumping with α=1, Ec=0.01, Pr=0.1, Ha=2 and φ=0.

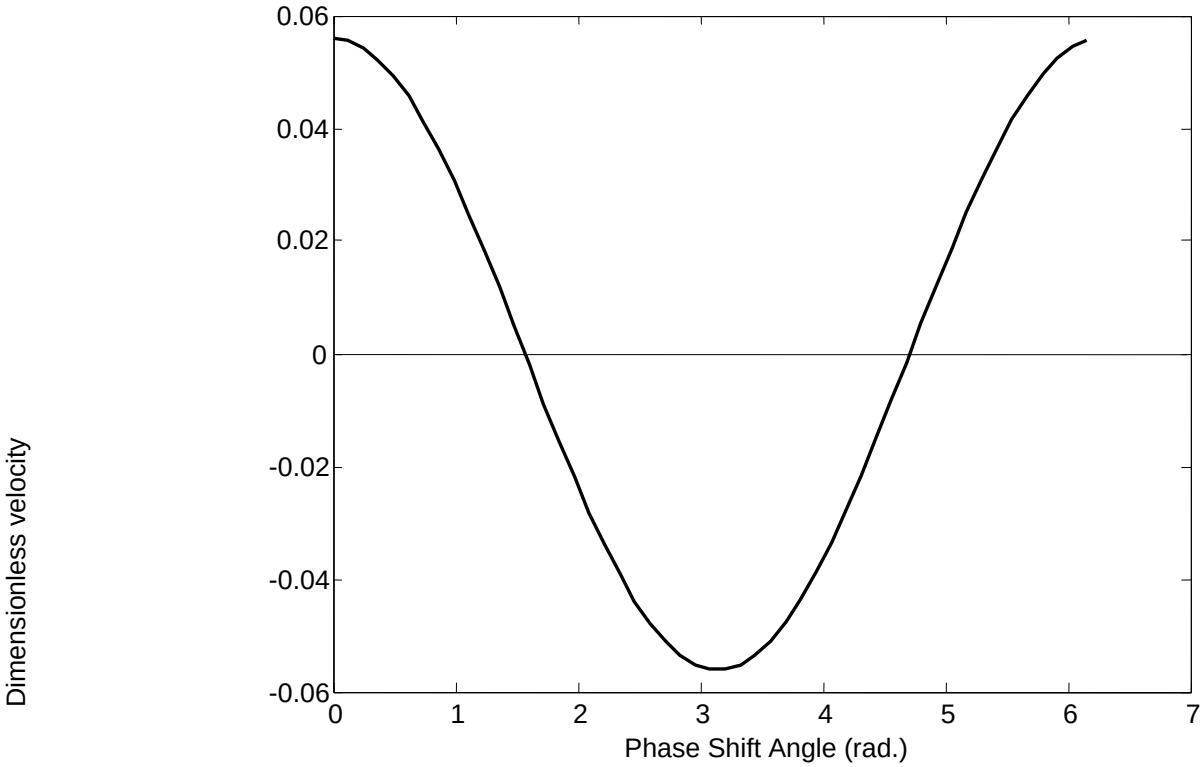

Figure 7.15: Effect of phase shift angle on the dimensionless centerline velocity for AC pumping with α=1, *Ha=2 and* St=10

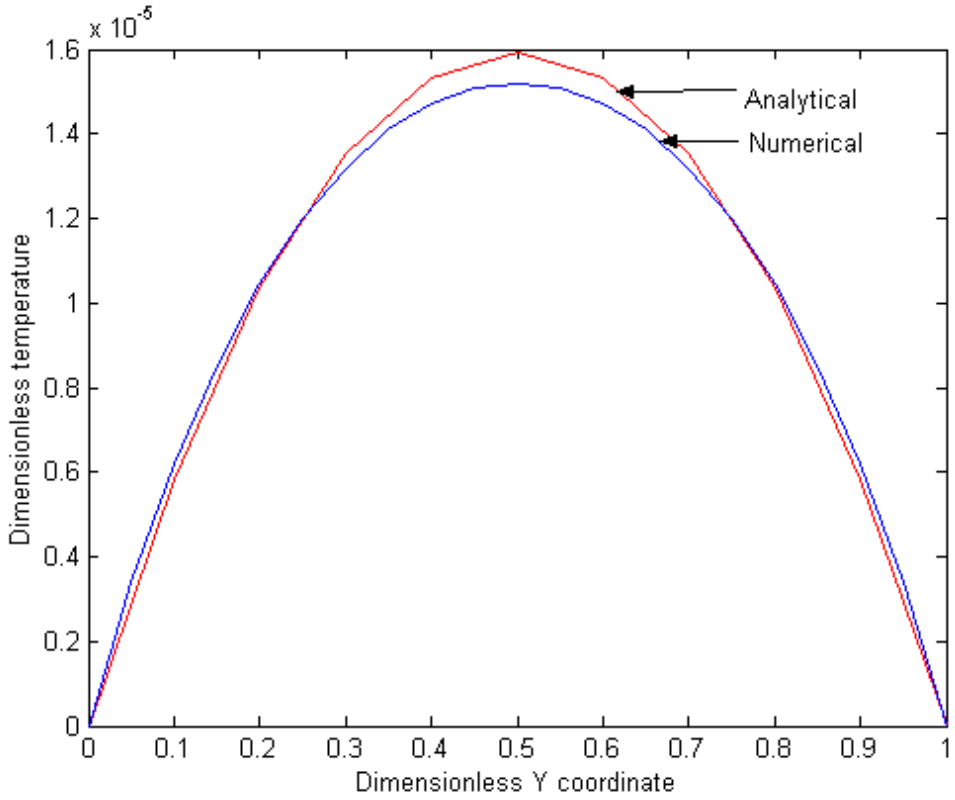

Figure 7.16: Comparison of analytical and numerical methods for steady state temperature with α=1, *Ec*=0.01, *Pr*=0.1 and *Ha*=3.

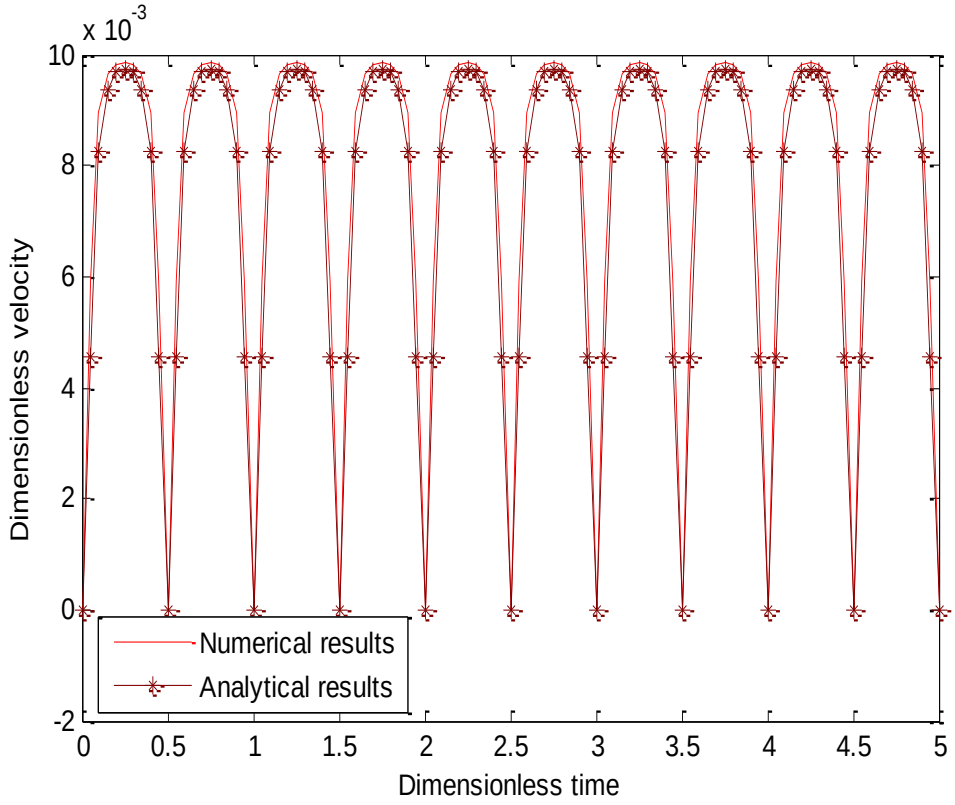

Figure 7.17: Comparison of analytical and numerical methods for steady state AC fully developed flow velocity with α=1, *Ha=10* and φ=0.

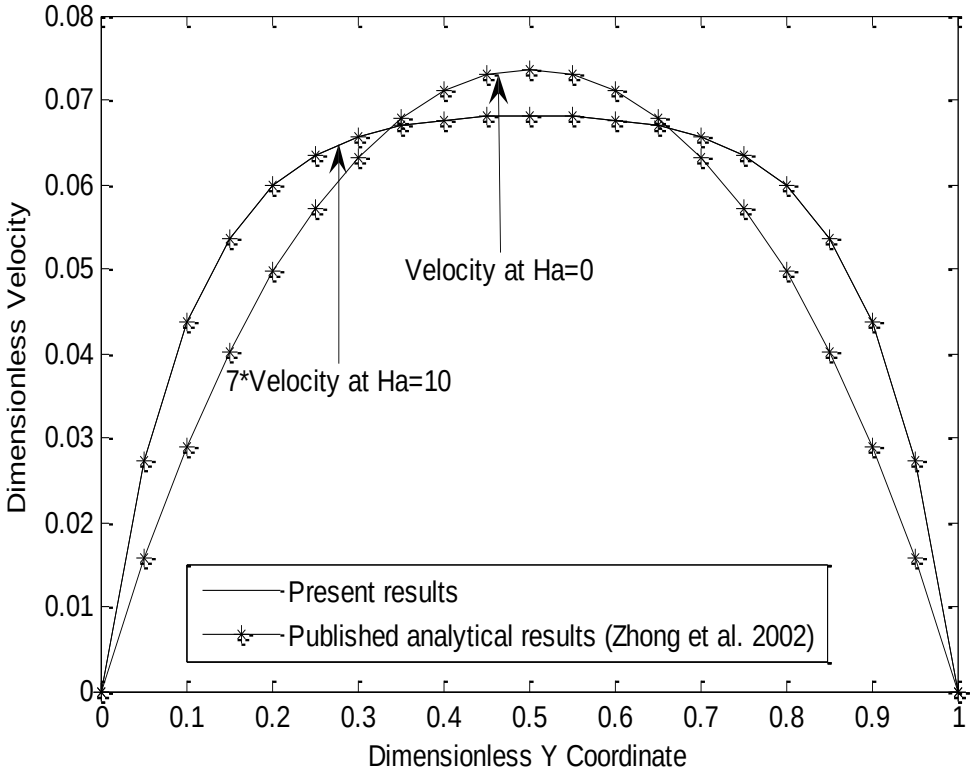

Figure 7.18: Comparison of present results and published analytical results (Zhong et al. 2002) for steady state DC fully developed flow velocity with α=1.

.7.2 Developing flow

The dimensionless governing equations (3.29-3.33) and (3.36-40) are solved analytically and numerically for a DC and AC developing flow. In this section, the transient velocity profile, and the effect of Hartmann number and Stanton number on the behavior of the transient velocity and the entrance length in DC and AC developing flow is studied. To study the effect of these parameters the pressure correction method and SIMPLE algorithm are applied to solve for the velocity profiles at different values of Hartmann number and Stanton number.

Hartmann number effect

Figure (7.19) and (7.20) illustrate the effect of Hartmann number on the velocity profile and the entrance region length. It is seen that the mid width velocity components U and V decreases as the Hartmann number increases, which means that a slightly conductive fluid is enough to propel the fluid. It is also seen that the axial velocity U increases and the velocity component V decreases until they reach the fully developed region which is influenced by the Hartmann number and this is due to the effect of Hartmann number on the Lorentz force. This means that controlling the electrical conductivity and magnetic flux density will allow to control the entrance region length.

Figure (7.21) depict the dimensionless pressure P which decreases as the Hartmann number increases. It is noticed that the pressure increases at the channel inlet and then decreases until reaching a constant pressure gradient at the channel fully developed region.

The variation of velocity component U with the dimensionless Y coordinate is shown in figure (7.22) at different Hartmann numbers. It is seen that at low Hartman number the Axial velocity (U) profile is parabolic, and as the Ha increases, the profiles flatten.

The effect of Hartmann number on the transient behavior of the mid width dimensionless centerline velocity components U and V is shown in Figures (7.23) and (7.24). It is seen that the effect of increasing Ha is to decrease the time required to reach steady state.

The effect of Hartmann number on the behavior of the transient velocity for AC pumping is also discussed. Figures (7.25), (7.26) and (7.27) illustrate the effect of Hartmann number on the dimensionless transient velocity components profiles and dimensionless pressure, respectively. It is seen that the mid width velocity components U and V affected in the same way as in DC pumping. It is noticed also that the velocities have pulsating behavior.

Stanton number effect

Figures (7.28), (7.29) and (7.30) depict the transient dimensionless velocity components, and the dimensionless pressure at different Stanton numbers. It is seen that as the Stanton number increases the pulsed volume decreases. This means that at high frequency, the flow seems to be continuous instead of pulsating flow.

Phase angle effect

The transient velocity component u at different phase angle is shown in figure (7.31). This figure illustrate the effect of the phase angle on the flow direction. The figure shows that at phase angle $\phi=0$, the fluid flows in positive direction while it flows in the opposite direction at $\phi=180^{o}$, and there is no flow at high frequencies when $\phi=90^{o}$. It is concluded that the direction and the magnitude of the flow can be controlled by the phase shift between the electrical and magnetic fields.

A comparison of the transient fully developed axial velocity comes from developing flow solution (SIMPLE algorith) with that comes from fully developed flow solution (ADI method) is shown in figure (7.32). It is seen that there is a good agreement between the two profiles.

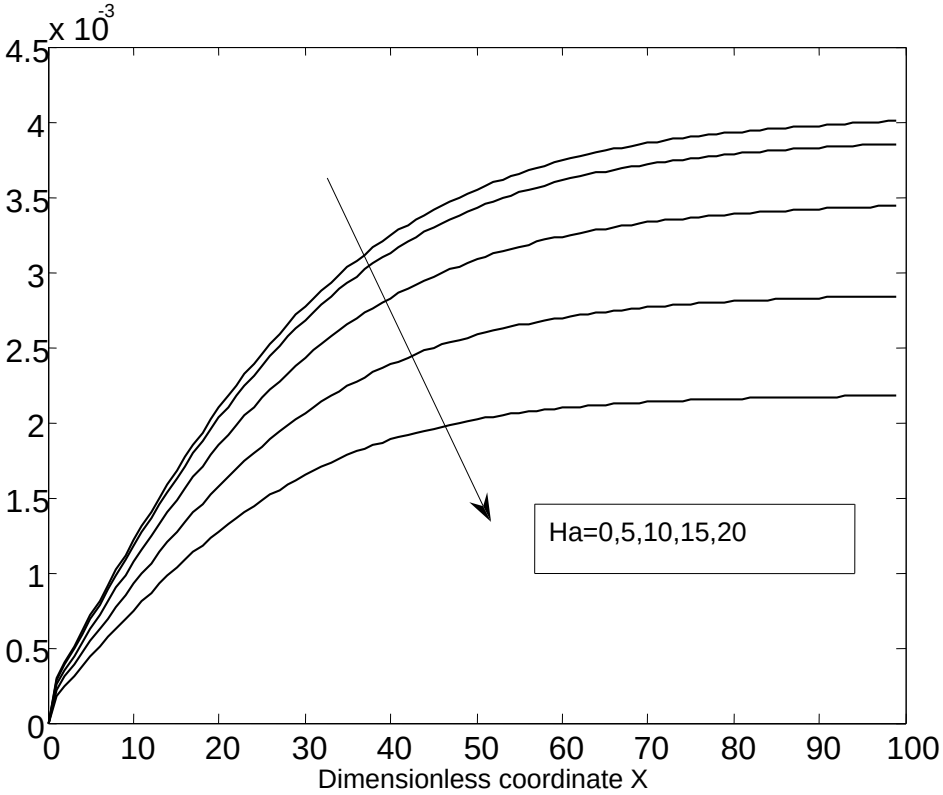

Figure 7.19: Variation of the dimensionless mid width axial velocity U with the dimensionless X coordinate at different Hartman numbers with α=1 and *Re=0.*

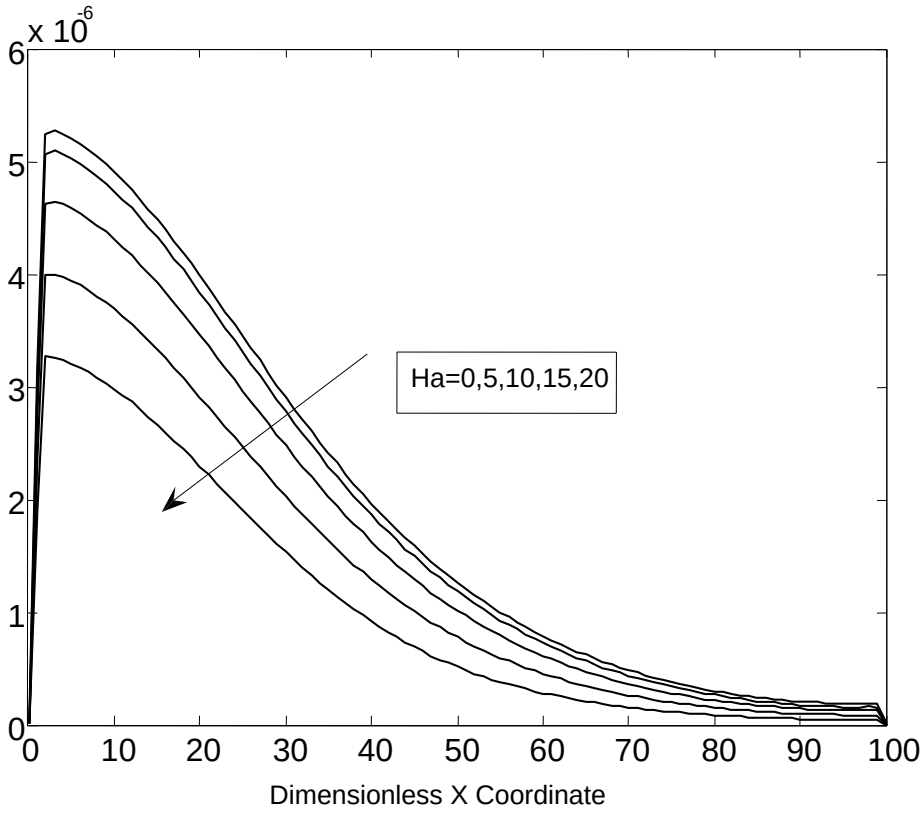

Figure 7.20: Variation of the dimensionless mid width velocity component V with the dimensionless X coordinate at different Hartman numbers α=1 and *Re=0.*

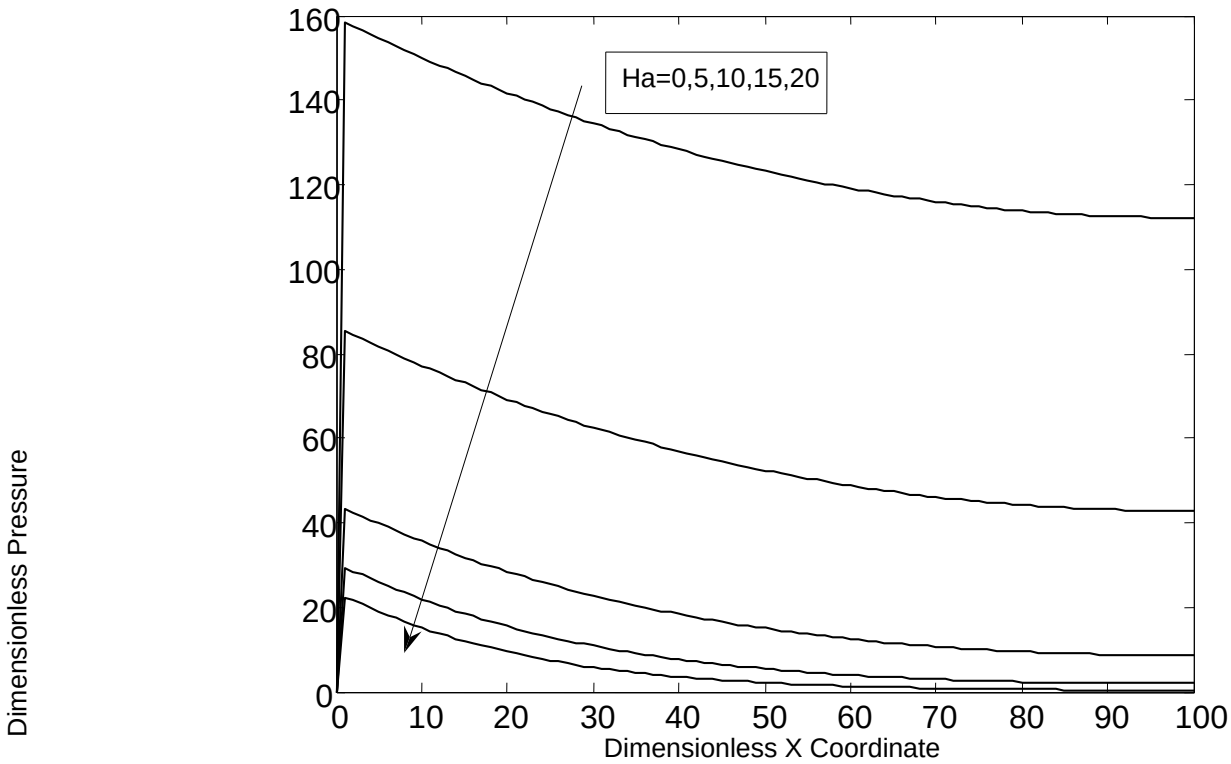

Figure 7.21: Variation of the dimensionless pressure P with the dimensionless X coordinate at different Hartman numbers α=1 and *Re=0.*

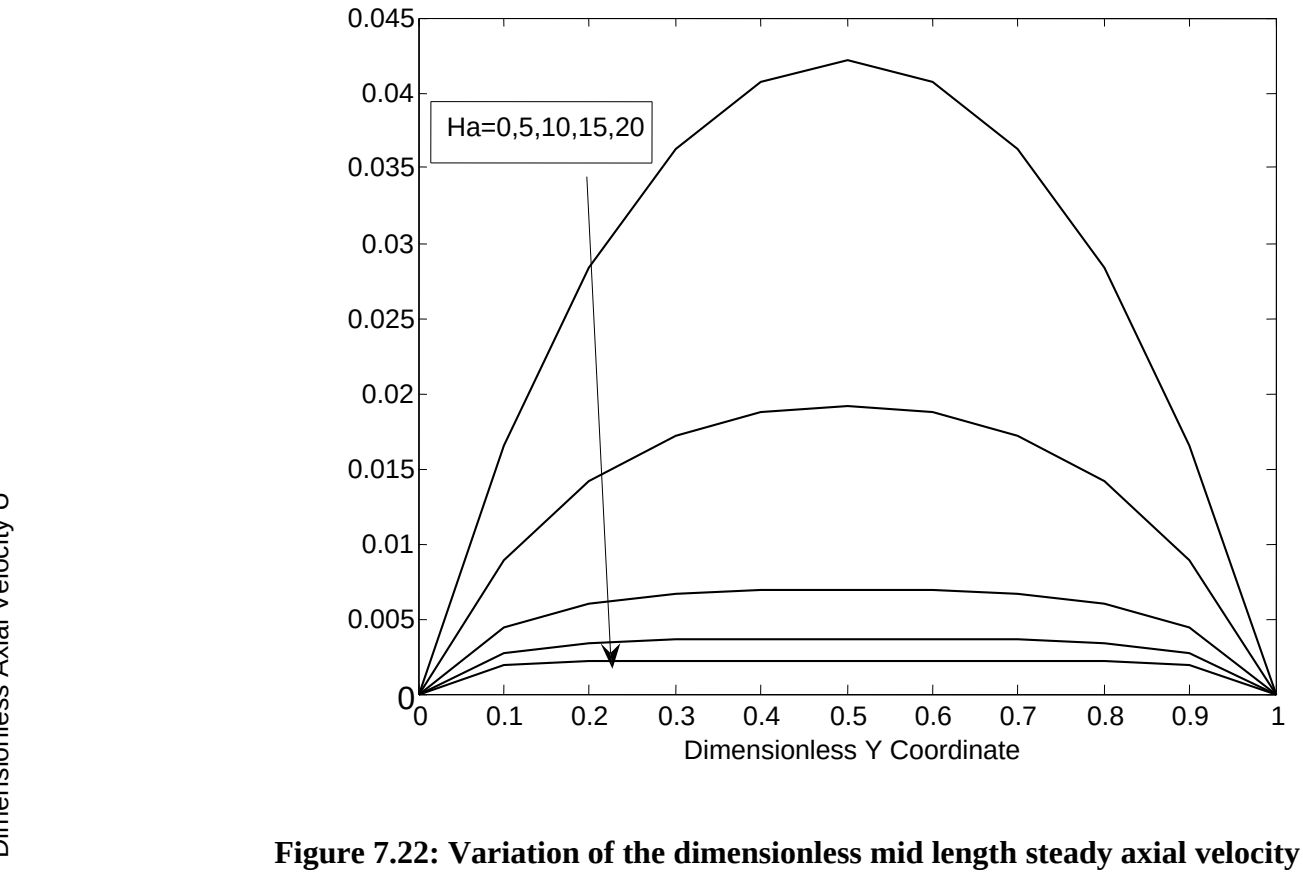

Figure 7.22: Variation of the dimensionless mid length steady axial velocity U with the dimensionless Y coordinate at different Hartman numbers α=1 and *Re=0.*

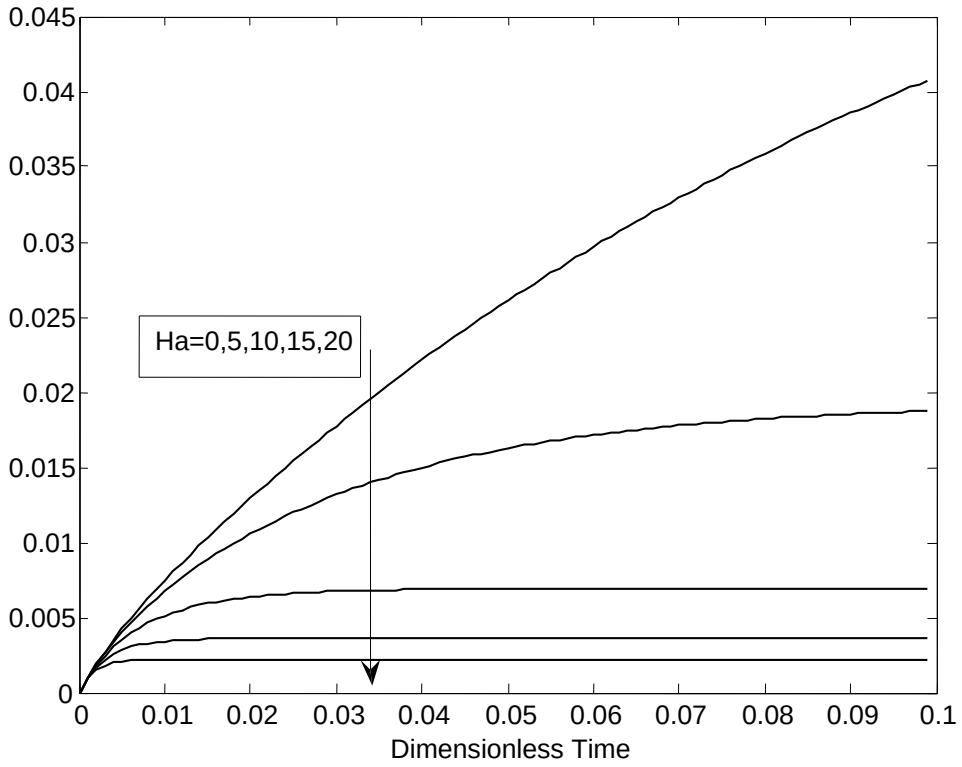

Figure 7.23: Transient behavior of the mid length centerline axial velocity U at different Hartman numbers α=1 and *Re=0.*

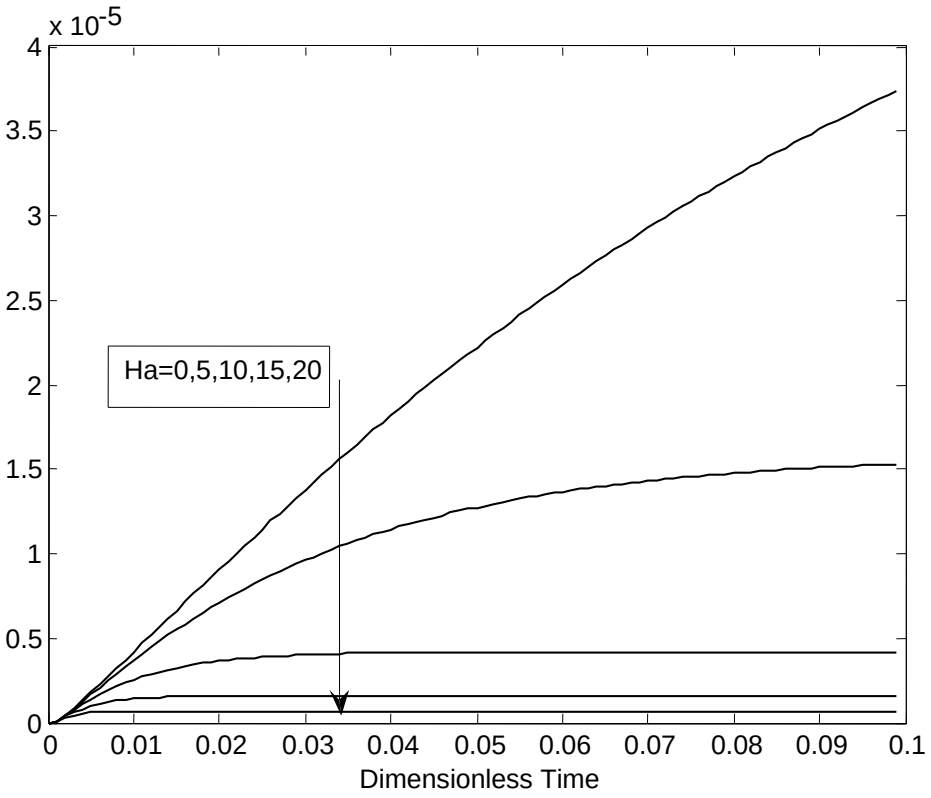

Figure 7.24: Transient behavior of the mid length centerline velocity component V at different Hartman numbers α=1 and *Re=0.*

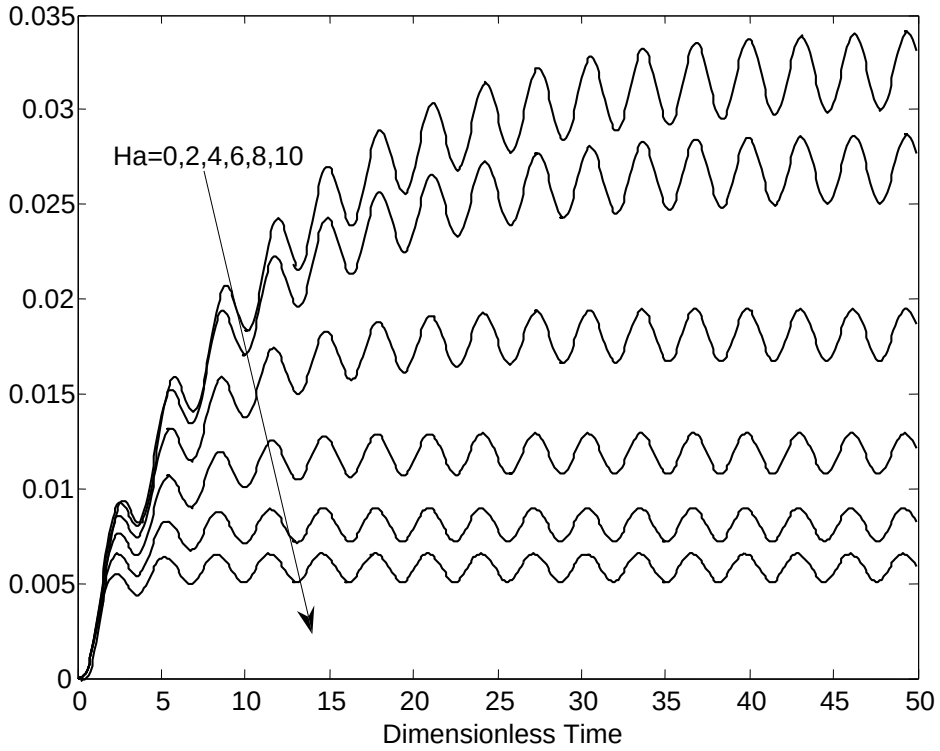

Figure 7.25: Transient behavior of the mid length centerline axial velocity U at different Hartman numbers for AC pumping α=1, *Re=0,* St=10 and φ=0.

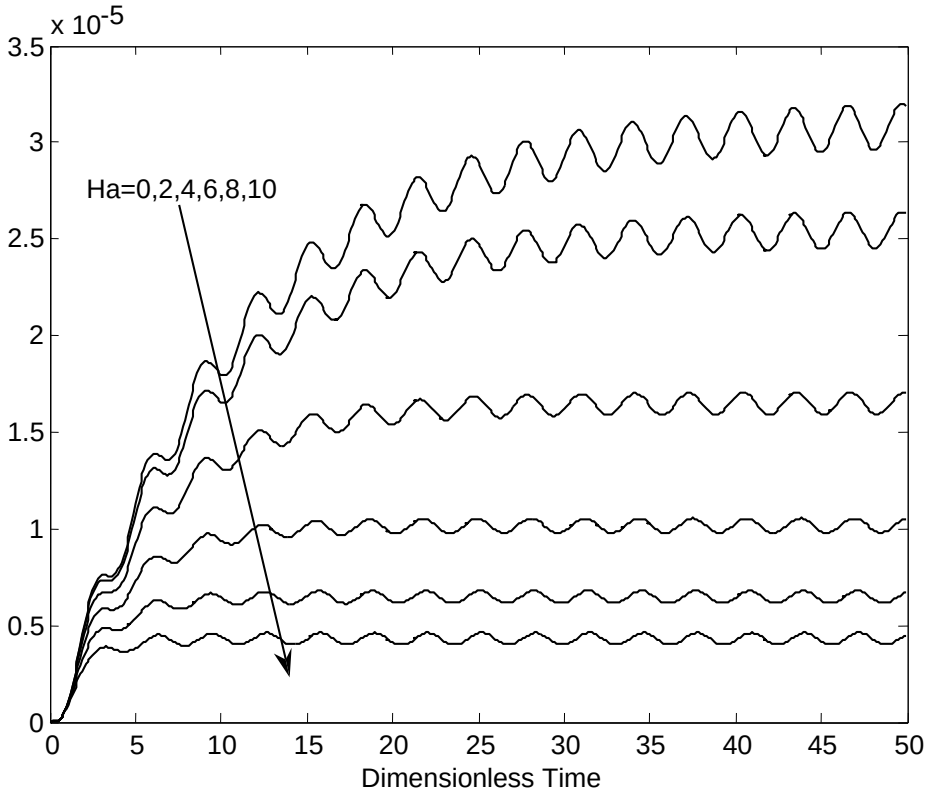

Figure 7.26 Transient behavior of the mid length centerline velocity component V at different Hartman numbers for AC pumping α=1, *Re=0,* St=10 and φ=0.

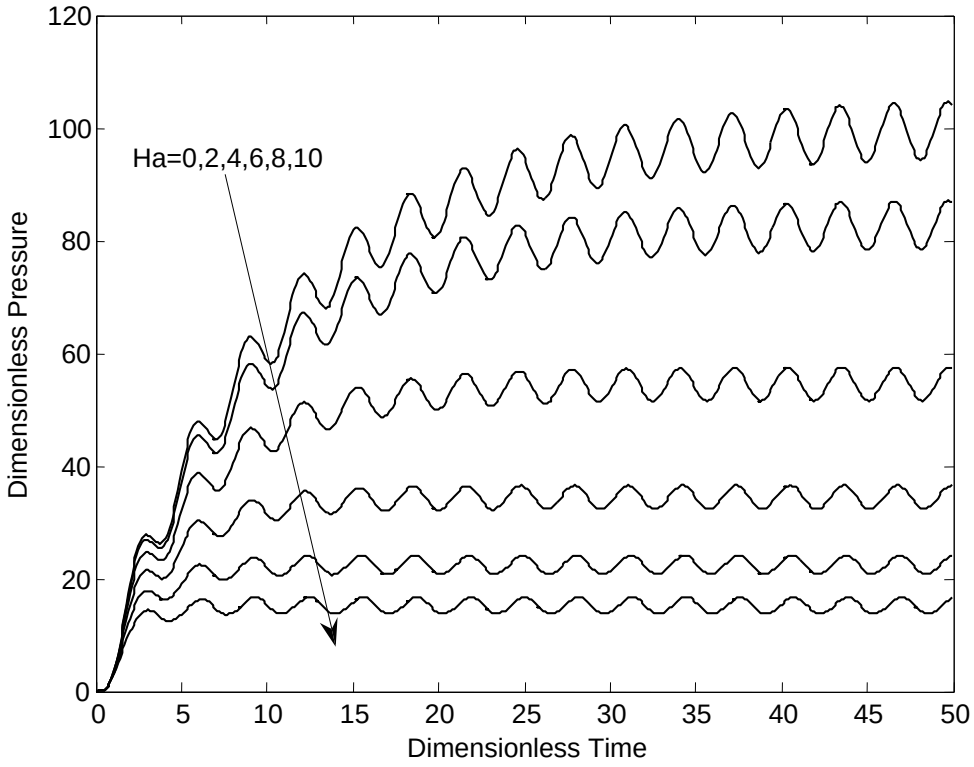

Figure 7.27: Transient behavior of the dimensionless pressure at different Hartman numbers for AC pumping α=1, *Re=0,* St=10 and φ=0.

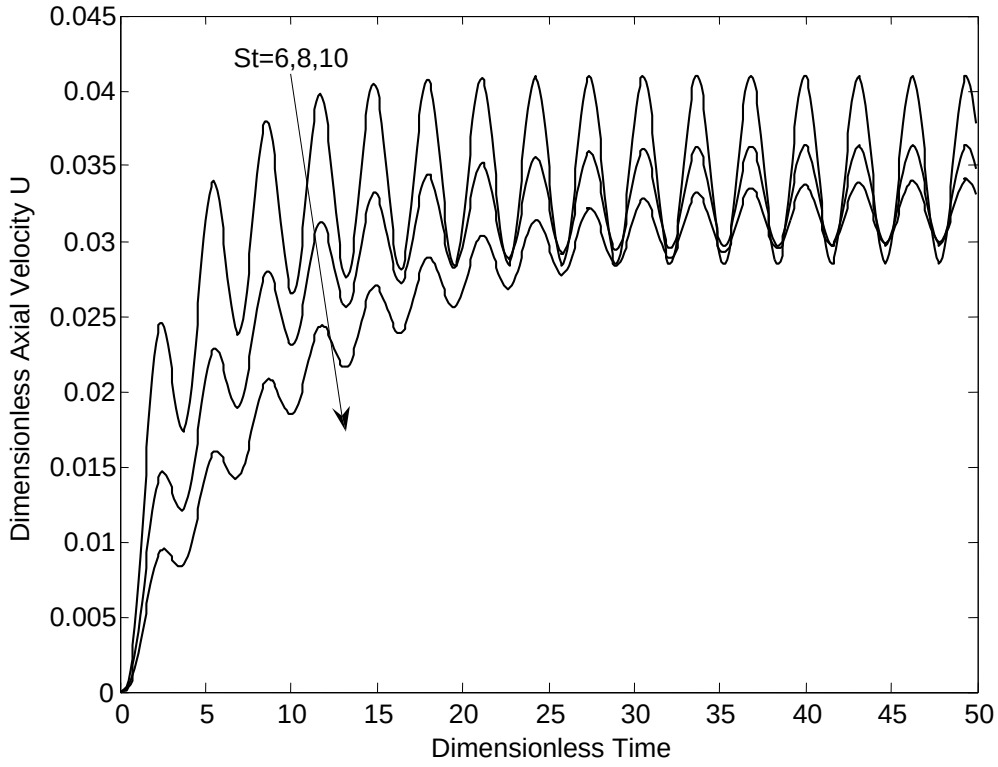

Figure 7.28: Transient behavior of the axial velocity u at different Stanton numbers for AC pumping with α=1, *Re=0, Ha*=0 and φ=0.

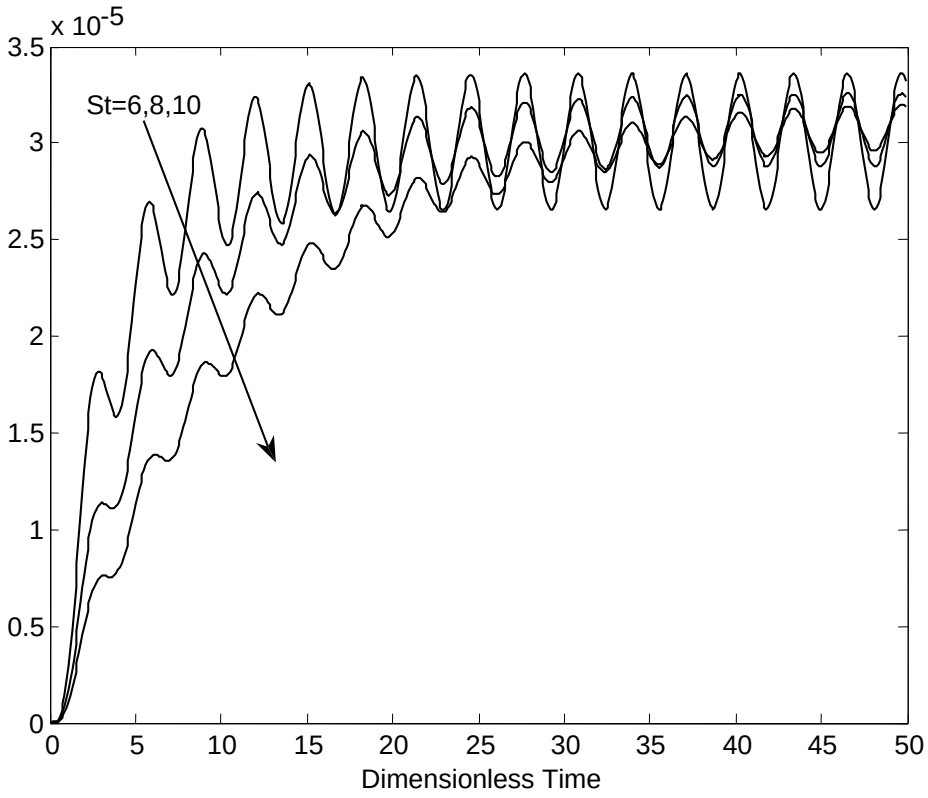

Figure 7.29: Transient behavior of the dimensionless velocity v at different Stanton numbers with α=1, *Re=0, Ha*=0 and φ=0.

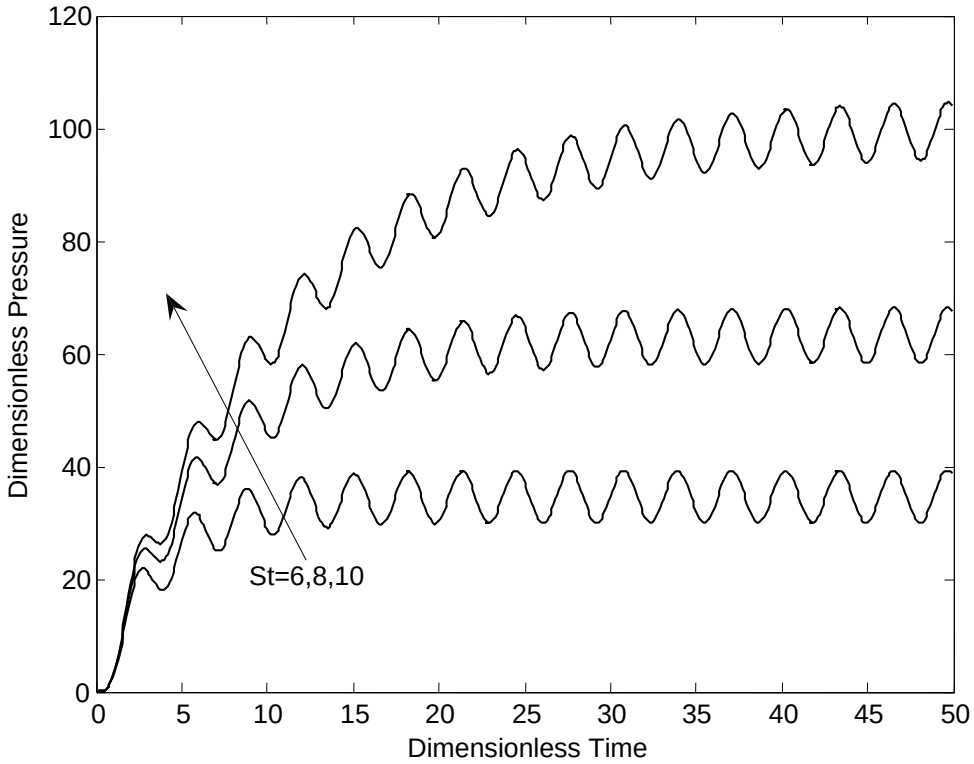

Figure 7.30: Transient behavior of the dimensionless pressure at different Stanton numbers with α=1, Re=0, Ha=0 and φ=0.

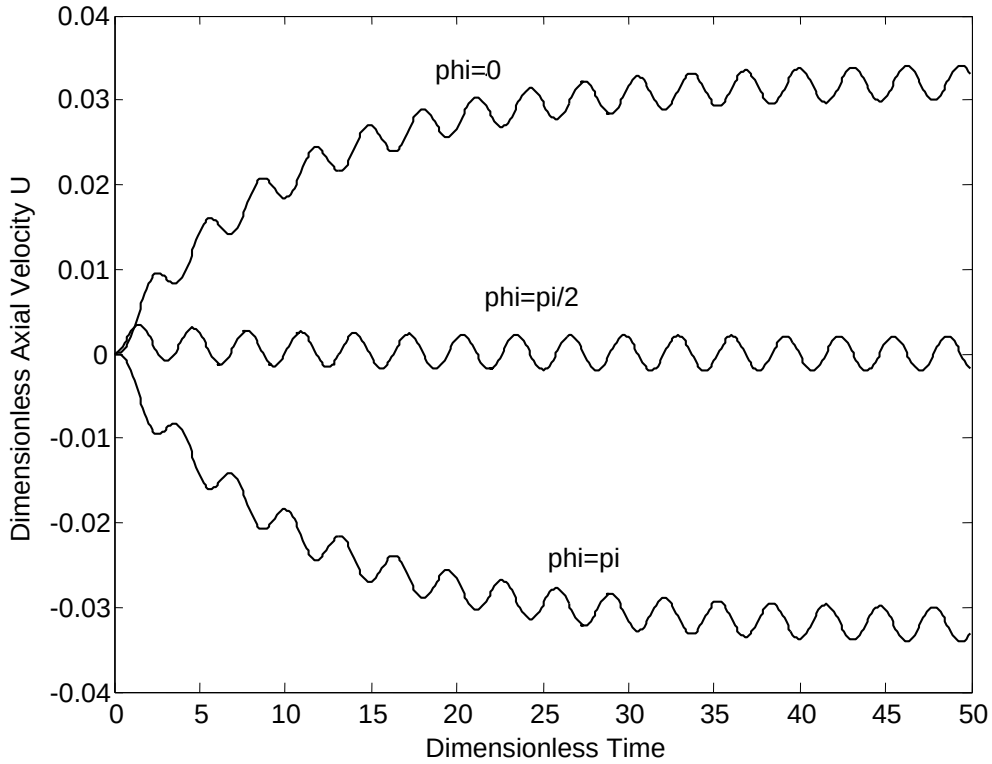

Figure 7.31: Transient behavior of the axial velocity u at different phase angles with α=1, *Re=0, Ha*=0 and *St*=10.

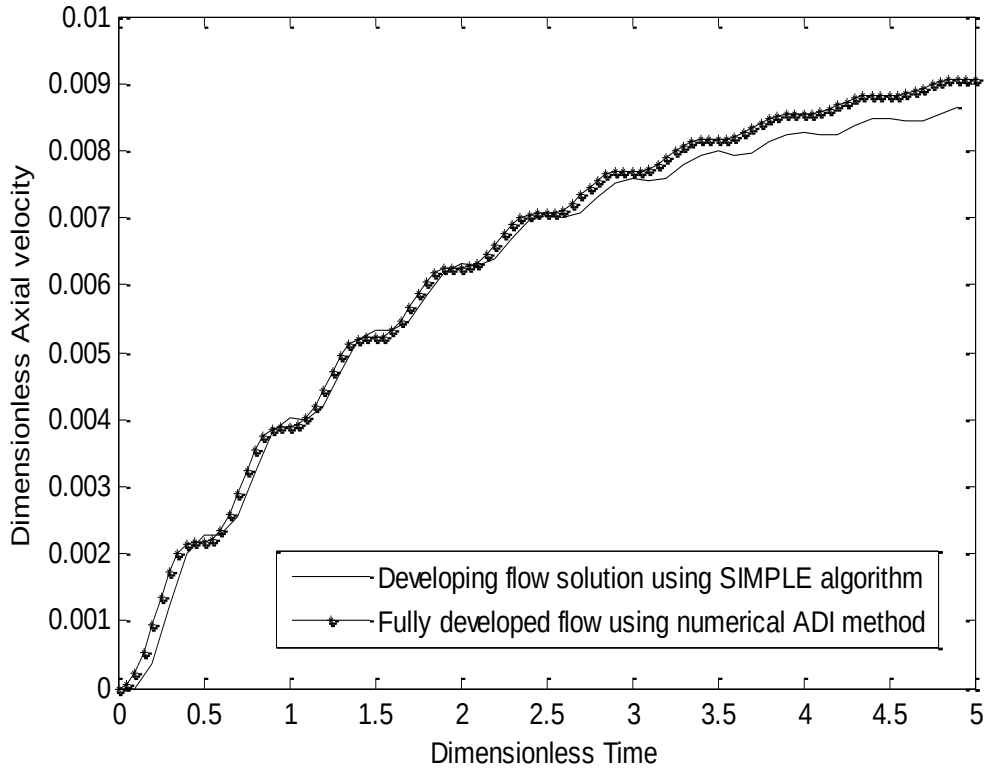

Figure 7.32: Comparison of transient velocity for fully developed flow and developing flow solutions with α=1, *Re=0, Ha*=10, *St*=10 and φ=0.

.7.3 Pump design

It is known that the MHD micropump is used to propel different types of conducting fluids in many applications with different flow rates. Hence, the main step in the design of the MHD micropump is a good selection of the magnitude of certain parameters to be suitable for the desired pressure and flow rate.

In this section, different magnitudes of electrical conductivity, applied voltage, magnetic flux and aspect ratios are taken as a study case to show their effect on controlling the flow velocity. The following tables show the effect of these parameters on the steady fully developed flow velocity.

Table 7.2 Electrical conductivity effect (B=0.5 T and V=10 volts)

fluid	Electrical conductivity	Maximum velocity (m/s)	Pressure difference (Pa)	Flow rate (µl/min)
Saline solution	2.2e-3	7e-6	0.323	0.002
Sea water	4	0.0122	587	4.1

Table 7.3 Voltage effect (sea water with σ=4 siemens/m and B=0.5T)

Voltage (volts)	Maximum velocity (m/s)	Pressure difference (Pa)	Flow rate (µl/min)
0.5	0.003	146.7	1.03
5	0.0305	1467	10.3

Table 7.4 Magnetic flux effect (sea water with σ=4 siemens/m and V=10 volts)

Magnetic flux density (Tesla)	Maximum velocity (m/s)	Pressure difference (Pa)	Flow rate (µl/min)
0.1	0.0024	117.3	0.82
0.5	0.0122	587	4.1

Table 7.5 Aspect ratio effect (sea water with σ=4 siemens/m, V=10 volts and B=0.5T)

Aspect ratio (height/width)	Maximum velocity (m/s)	Pressure difference (Pa)	Flow rate (μl/min)
0.5	0.0122	587	4.1
1	0.0315	585	21.27

In table (7.2) low and medium values of electrical conductivity for two different fluids are taken to show their effect on the steady flow velocity. It is seen that using high conducting fluid yields high flow rate with high pressure. Tables (7.3) and (7.4) show the effect of voltage and magnetic flux on the flow rate and pressure difference for sea water. It is noticed that controlling the voltage and magnetic flux will allow to control the flow rate and pressure with linear relation between them.

The effect of aspect ratio (height/width) is shown in table (7.5). It is seen that the flow rate increases as the height of the channel relative to width increases and a suitable value of the aspect ratio must be selected to predict the desired flow rate. From figure (7.19) it is noticed that for a low conductive liquids the suitable channel length can be taken about 100 times of the channel width to reach the fully developed region.

The relations between the flow rate, pressure difference and the induced electric current are shown in figures (7.33) and (7.34). In these figures the results were obtained for sea water by changing the magnetic flux density B, or the applied voltage with keeping constant other parameters (h=75μm, w=150μm, L=22mm and σ=4 $siemens/m$). It is seen from this figure that increasing the current will increase the flow rate and the pressure difference linearly.

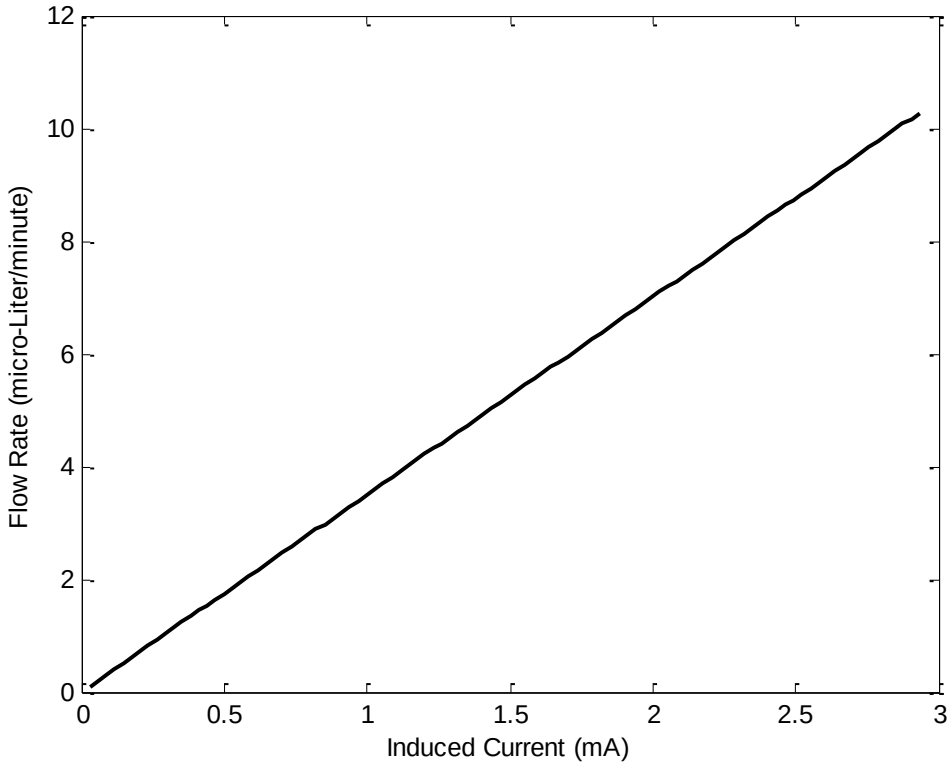

Figure 7.33: Variation of pressure difference with flow rate-system curve (h=75*μm*, w=150*μm*, L=22*mm* and σ=4 *siemens/m*)

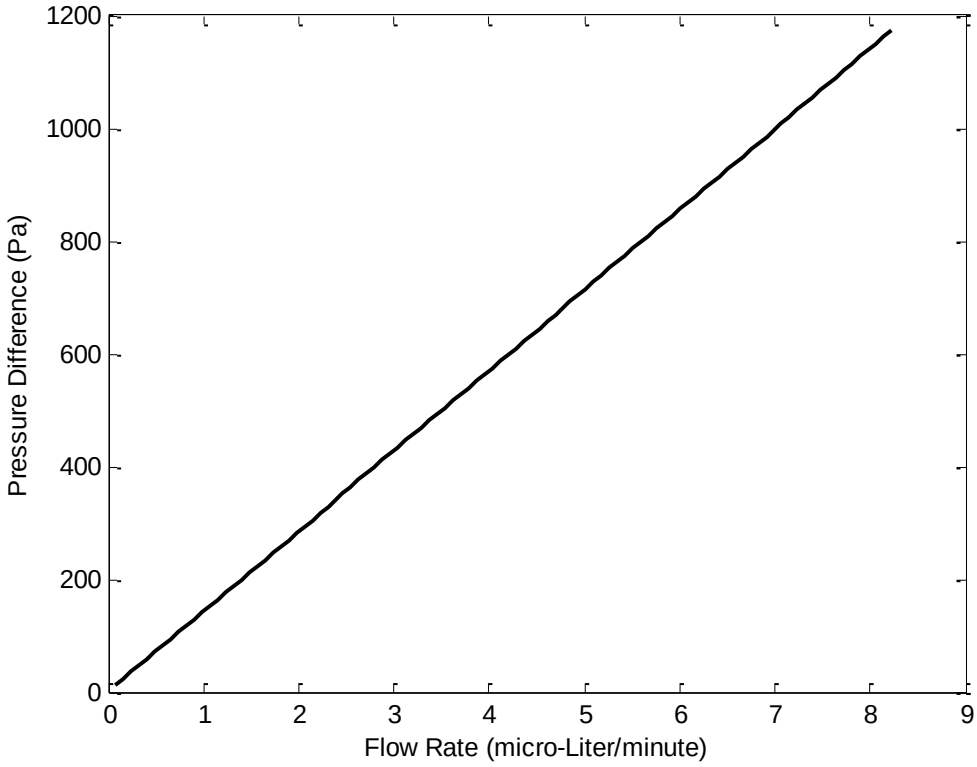

Figure 7.34: Variation of pressure difference with flow rate-system curve (h=75*μm*, w=150*μm*, L=22*mm* and σ=4 *siemens/m*)

Chapter 8

Conclusions and Recommendations

Analytical and numerical methods to predict the fully developed flow velocity and temperature distribution in a magnetohydrodynamic (MHD) micropump has been presented. The analytical results are found in very good agreement with the numerical results. Also a numerical method to predict the velocity distribution in a developing magnetohydrodynamic (MHD) micropump flow has been presented. The effect of fluctuating Lorentz force on the Ac magnetohydrodynamic micropump flow is studied for both developing and fully developed flow

In this study, the effect of Hartman number, aspect ratio, Prandtl number, Eckert number, Stanton number and phase angle on the transient velocity and temperature profiles was investigated. The following conclusions can be summarized in the following points:

1- It is seen that at low Hartman number the velocity profiles in the MHD micropump using Lorentz force are parabolic, and these profiles are similar to that produced by external pressure gradient.

2- It is seen that the velocity decreases as the Hartmann number increases, which means that a slightly conductive fluid is enough to propel the fluid

3- It is seen from the transient behavior that the effect of increasing Ha is to decrease the time required to reach steady state.

4- It is seen that that the heat generated from the electric current and magnetic flux will cause an increase of the temperature from the initial state, and the same effect of Ha on the velocity profile is observed on temperature profile.

5- It is seen that the velocity and temperature increases as the aspect ratio increases. This means that controlling the conduit width will allow to control the velocity and temperature.

6- It is noticed that controlling the flow and the temperature can be achieved by controlling the potential difference, the magnetic flux, aspect ratio and by a good choice of the electrical conductivity.

7- It is observed that the temperature increases and the time required to reach steady state increases as P_r and Eckert number ($Ec=u_0^2/C_pT_w$) increases.

8- It is noticed in AC pumping that the velocity and temperature have pulsating profiles. And as the Stanton number increases the pulsed volume decreases. This means that at high frequency, the pulsed volume is small which yields a continuous flow instead of pulsating flow.

9- It is noticed also that the effect of increasing St is to increase the time required to reach steady state.

10- The magnitude and direction of the flow can be controlled by the phase shift between the electrical and magnetic fields. It is noticed that at phase angle $\phi=0$, the fluid flows in positive direction while it flows in the opposite direction at $\phi=180^o$

The following recommendations can be followed in future work:

1- It is recommended to take into account the effect of the different parameters discussed previously on the flow and temperature in the design of the AC MHD micropump.

2- It is recommended to take into account the temperature rise and it's effect on the velocity profile in the design of the AC MHD micropump.

3- It is recommended to solve the same problem with variable properties, especially the viscosity.

4- It is recommended to solve the same problem for a three-dimensional laminar flow.

REFERENCES

Anderson, J. (1995). **Computational fluid dynamics- The basics with applications**. McGraww-Hill.

Attia, H. (2001) Influence of temperature dependent viscosity on the MHD-chnnel flow of dusty fluid with heat transfer. **Acta Mechanica**, (151), 89-101.

Bau, H., Zhong, J., and Yi, M. (2001). A minute magneto hydro dynamic (MHD) mixer. **Sensors and Actuators**, (79), 207–215.

Bessaih, R. and Kadji, M. (1999). Numerical study of disk driven rotating MHD flow of a liquid metal in a cylindrical enclosure. **Acta Mechanica**, (135), 153-167.

Bohm, S., Olthuis, W., and Bergveld, P. (1999) A plastic micropump constructed with conventional techniques and Materials. **Sensors and Actuators**, (77), 223–228

Brener, K. and Park J. (2004). Actuation and control of a turbulent channel flow using Lorentz forces. **Physics of fluids**, (4),

Debesset, S., Hayden, C., Dalton, C., Eijkel, J., and Manz, A. (2004). An Ac electroosmatic micropump for circular chromatographic applications**. Lab Chip**, (4), 396-400.

Eijkel, J., Dalton,C., Hayden,C., Burt,J., and Manz,A. (2003). A circular ac magnetohydrodynamic micropump for chromatographic applications. **Sensors and Actuators**, (92), 215-221.

Elwenspoek, M., Lammerink, T., Miyakei, R. and Ruitman, J. (1994) .Towards integrated microliquid handling systems. **J. Micromech. Microeng**, (4), 227-245.

Holman, J. (1976) **Heat transfer**. 4th edition, McGrawHill.

Homsy, A., Koster, S., Eijkel, J., Berg, A., Lucklum, F., Verpoorte, E., and Rooij, F. (2005). A high current density DC magnetohydrodynamic (MHD) micropump. **Lab Chip**, (5), 466-471.

Jang, J. Lee, S. (1998). MHD_Magnetohydrodynamic.micropump using Lorentz force. MEMS Symposium, **ASME International Mechanical Engineering Congress and Exposition**, Anaheim, California, Nov. 15–20, 439–443.

Jang, J., and Lee,S. (2000). Theoretical and experimental study of MHD (magnetohydrodynamic) micropump. **Sensors and Actuators**, (80), 84–89.

Jun, T. and Kim, C. (1998) Valveless pumping using traversing vapor bubbles in microchannels, **Journal of applied physics**, (83), 5658-5664.

Khalzov, I. and Smolyakov, A. (2006). On the calculation of steady-state magnetohydrodynamic flows of liquid metals in circular ducts of a rectangular cross section. **Technical physics**, (51), 26-33.

Koch, M., Harris, N., Evans, A., White, N., and Brunnschweiler, A. (1998). A novel micromachined pump based on thick-film piezoelectric actuation. **Sensors and Actuators** A, (70), 98-103.

Lemoff, A., Lee, A., Miles, R., and McConaghy, C. (1999). An AC Magnetohydrodynamic Micropump: Towards a True Integrated Microfluidic System. **Int. Conf. on Solid-State Sensors and Actuators** , 1126–1129.

Lemoff, A., and Lee, A. (2000).An AC Magnetohydrodynamic Micropump. **Sensors and Actuators**, (63), 178–185.

Lemoff, A., and Lee, A. (2003). An ac magnetohydrodynamic microfluidic switch for micro total analysis systems. **Biomedical Microdevices**, 5(1), 55-60.

Nguyen, N., Huang, X., and Chuan, T.(2002). MEMS-micropumps: a review . **Transactions of the ASME**,(124), 384-392.

Patankar,S. (1980). **Numerical heat transfer and fluid flow**. Hemisphere, Washington DC.

Patel, V. and Kassegne, K. (2006). Electroosmosis and thermal effects in magnetohydrodynamic (MHD) micropumps using 3D MHD equations. **Sensors and Actuators B**.

.

Qian,S., and Bau,H.(2005). Magnetohydrodynamic flow of RedOx electrolyte. **Physics of Fluids**, (17), 067105.

Qian, S., Zhu, J. and Baua,. (2002) A stirrer for magnetohydrodynamically controlled minute fluidic networks. **Physics if fluids**, 14(10), OCTOBER

Ramos, J. and Winowich, N. (1986). Magnetohydrodynamic channel flow study, Physics **of fluids**, (4), 992-997.

Reyes, D., Lossifidis, D., Auroux, P., and Manz, A. (2002). Micro total analysis systems.1. introduction, theory, and technology. **Analytical chemistry**, (74), 2623-2636.

Satou, S., Fujisaki, K., and Furukawa, T. (2004). Consideration of the AC-part force of electromagnetic stirring in MHD calculation. **International journal of applied electromagnetics and mechanics**, (19), 653-657.

Schomburg, W., Fahrenberg, J. , Maas D., and Rapp, R. (1993) Active valves and pumps for Microfluidics. **J. Micromech. Mioroeng**, (3), 216-218.

Schomburg, W., Vollmer, J., and Menz, W. (1994) Microfluidic components in LIGA technique. **J. Micromech. Microeng**, (4), 186-191.

Shoji S, Esashi M, Schoot B. and Rooij N. (1992). A study of high-pressure micropump for integrated chemical analysis systems, **Sensors and Actuators** . (32), 335-339

Shoji, S., and Esashi, M.(1994). Microflow devices and systems. **J. Micromech. Microeng**, (4), 157-171.

Ueno, K. (1991) Inertia effect in two-dimensional MHD channel flow under a traveling sine wave magnetic field. **Phys. Fluids A**, 3 (12), December

Ueno, K. (1993) Effect of turnaround lines of magnetic flux in two-dimensional MHD channel flow under a traveling sine wave magnetic field. **Phys. Fluids** A. 5 (2), February

Ullmann, A. (1998) The piezoelectric vave-less pump-performance enhancement analysis. **Sensors and actuators**, (69), 97-105.

Lintel H., Pol, F. and Bouwstra, S. (1988). A piezoelectric micropump based on micromachining of silicon **Sensors Actuators**, (15), 153-67.

White, F. (1979). **Fluid mechanics**. McGrawHill

Woias, P. (2005). Micropumps-past, progress and future prospects. **Sensors and Actuators** B, (105), 28-38.

Yi, M., Qian, S., and Bau, H.(2002). A magnetohydrodynamic chaotic stirrer. **J.Fluid Mech**., (468), 153-177.

Zeng, S., Chen, C., Mikkelsen, J., and Santiago, J. (2001). Fabrication and characterization of electroosmatic micropumps. **Sensors and Actuators** B, (79), 107-114.

Zaky, A., and Hawley, R. (1974) **Fundamentals of electromagnetic field theory**. Harrap, London.

Zhong, J. Yi, M., and Bau, H. (2002). Magneto hydrodynamic (MHD) pump fabricated with ceramic tapes. **Sensors and Actuators**, (96), 59–66.

Appendices
Appendix A

Programs

A-1 ADI numerical technique

The following program is performed to solve the 2-d navier stockes equations and energy equation in an incompressible viscous fully developed flow in a Magnetohydrodynamic micropump with Fluctuating Lorentz force using a numerical marching technique which is the ADI method.

```
%%=================================================================
=========
%       function [x] = thomas(a,b,c,cwrk,r,n)
%-----------------------------------------------------------------------
% solve tridiagonal system with thomas algorithm.  tri(a,b,c)*x = r.
% solution returned in r array.
% input
%   a,b,c   arrays containing the tridiag matrix (these are not changed)
%   r       array containing the right hand side (destroyed in call)
%   n       size of the system
% output
%   x       solution returned in x array
% work
%   cwrk    work array so that original matrix is not destroyed
%-----------------------------------------------------------------------

%-----------------------------------------------------------------------
% forward elimination
clear
 alpha=1;
n=19;
dz=alpha/20;
dy=1/20;
dt=.05;
ke=101;
%B=0.44;
%segma=2.2e-3;
%V=2;
%mu=1.09e-3;
%den=1025;
%nu=mu/den;
%Ha=B*w*sqrt(segma/mu);
%Ti=300;
Ha=10;
st=10;
```

```
phi=0;
pr=0.1;
pstar=0;
Ec=0.05;
N=1-pstar;
for k=1:ke
t(k)=dt*(k-1);
end
for j=1:21
      for i=1:21
         u(i,j,1)=0;
      end
   end
   %-----------------
for k=1:ke
   for i=1:21
         u(i,1,k)=0;
         u(i,21,k)=0;
      end
   end
   %-------------------
   for k=1:ke
   for j=1:21
         u(1,j,k)=0;
         u(21,j,k)=0;
      end
   end
   %---------------
for k=2:ke
   %%%%%%%%%%%
  chek=(-1)^k;
   if chek>0;
   for j=2:20
      %------------
a(1,j,k)=0;
c(n,j,k)=0;
for i=1:n
   b(i,j,k)=-(1+2*dt/(st^2*dy^2)+Ha^2*(dt/st^2)*sin(2*pi*t(k))^2);
end
for i=2:n
   a(i,j,k)=dt/(st^2*dy^2);
end
for i=1:n-1
   c(i,j,k)=dt/(st^2*dy^2);
end
%-----------
end
```

```
for j=2:20
   for i=1:21
u(i,j,1)=0;
end
end
    for j=2:20
   for i=1:n
   r(i,j,k)=-(u(i+1,j,k-1)+(dt/st^2*dz^2)*(u(i+1,j+1,k-1)-2*u(i+1,j,k-1)+u(i+1,j-1,k-
1))+(dt/st^2)*(sin(2*pi*t(k))*sin(2*pi*t(k)+phi)-pstar));
end
end
   %-------------------
   for j=2:20
      %------------------------
fac(1,j,k)   = 1.0/b(1,j,k);
cwrk(1,j,k) = c (1,j,k)* fac(1,j,k);
r(1,j,k)    = r(1,j,k) * fac(1,j,k);

for i = 2:n
   fac (i,j,k)    = 1.d0/( b(i,j,k) - a(i,j,k)*cwrk(i-1,j,k) );

   cwrk(i,j,k) =                  c (i,j,k)  * fac(i,j,k);
   r(i,j,k)    = ( r(i,j,k) - r(i-1,j,k) * a (i,j,k)) * fac(i,j,k);
end
%-----------------------------------------------------------------------
% back substitution
% put solution into x array, r(n) already has solution
x(n,j,k) = r(n,j,k);
for i = n-1:-1:1
   x(i,j,k) = r(i,j,k) - cwrk(i,j,k)*x(i+1,j,k);
end
%-----------------------------------------------------------------------
% end of thomas
end
for j=2:20
   for i=1:n
      u(i+1,j,k)=x(i,j,k);
   end
end
%---------------------------------------------------------------
%  End of the first step of the ADI method in i with different j
else
for i=2:20
      %------------
a(i,1,k)=0;
c(i,n,k)=0;
for j=1:n
```

```
    b(i,j,k)=-(1+2*dt/(st^2*dz^2)+Ha^2*(dt/st^2)*sin(2*pi*t(k))^2);
end
for j=2:n
    a(i,j,k)=dt/(st^2*dz^2);
end
for j=1:n-1
    c(i,j,k)=dt/(st^2*dz^2);
end
%-----------
end
 for i=2:20
    for j=1:21
%r(i,j,1)=0;
u(i,j,1)=0;
end
end
 %---------------------------------------
   for i=2:20
    for j=1:n
    r(i,j,k)=-(u(i,j+1,k-1)+(dt/st^2*dy^2)*(u(i+1,j+1,k-1)-2*u(i,j+1,k-1)+u(i-1,j+1,k-
1))+(dt/st^2)*(sin(2*pi*t(k))*sin(2*pi*t(k)+phi)-pstar));
end
end
    %-------------------
    for i=2:20
        %------------------------
fac(i,1,k)   = 1.0/b(i,1,k);
cwrk(i,1,k) = c (i,1,k)* fac(i,1,k);
r(i,1,k)    = r(i,1,k) * fac(i,1,k);

for j = 2:n
    fac (i,j,k)    = 1.d0/( b(i,j,k) - a(i,j,k)*cwrk(i,j-1,k) );

    cwrk(i,j,k) =                  c (i,j,k)  * fac(i,j,k);
    r(i,j,k)    = ( r(i,j,k) - r(i,j-1,k) * a (i,j,k)) * fac(i,j,k);
end
%------------------------------------------------------------------------
% back substitution
% put solution into x array, r(n) already has solution
x(i,n,k) = r(i,n,k);
for j = n-1:-1:1
    x(i,j,k) = r(i,j,k) - cwrk(i,j,k)*x(i,j+1,k);
end
%------------------------------------------------------------------------
% end of thomas
end
for i=2:20
```

```
   for j=1:n
      u(i,j+1,k)=x(i,j,k);
   end
end
%-----------------------------------------------
end
end
%.....................................................
for k=1:ke
   for j=1:21;
      for i=1:21;
         u1(i,j,k)=u(i,j,k);
      end
   end
end
%#################################################################
% Now solve for the temperature profile
%#################################################################
for k=1:ke
   for j=1:21
      for i=1:21
        s(i,j,k)=Ha^2*Ec*((sin(2*pi*t(k)+phi)/Ha^2)+u1(i,j,k)*sin(2*pi*t(k)))^2;
      end
   end
end
for j=1:21
      for i=1:21
         th(i,j,1)=0;
      end
   end
   %-----------------
for k=1:ke
   for i=1:21
         th(i,1,k)=0;
         th(i,21,k)=0;
      end
   end
   %-------------------
   for k=1:ke
   for j=1:21
         th(1,j,k)=0;
         th(21,j,k)=0;
      end
   end
   %---------------
for k=2:ke
```

```
    %%%%%%%%%%%%
   chek=(-1)^k;
    if chek>0;
    %%%%%%%%%%%%
     for j=2:20
       %------------
a(1,j,k)=0;
c(n,j,k)=0;
for i=1:n
    b(i,j,k)=-(1+2*dt/(st^2*pr*dy^2));
end
for i=2:n
    a(i,j,k)=dt/(st^2*pr*dy^2);
end
for i=1:n-1
    c(i,j,k)=dt/(st^2*pr*dy^2);
end
%-----------
end
 for j=2:20
    for i=1:21
%r(i,j,1)=0;
th(i,j,1)=0;
end
end
 for j=2:20
    for i=1:n
    r(i,j,k)=-(th(i+1,j,k-1)+(dt/(st^2*pr*dz^2))*(th(i+1,j+1,k-1)-2*th(i+1,j,k-1)+th(i+1,j-1,k-
1))+s(i+1,j,k)*dt/st^2);
end
end
    %-------------------
    for j=2:20
       %------------------------
fac(1,j,k)   = 1.0/b(1,j,k);
cwrk(1,j,k) = c (1,j,k)* fac(1,j,k);
r(1,j,k)    = r(1,j,k) * fac(1,j,k);

for i = 2:n
    fac (i,j,k)    = 1.d0/( b(i,j,k) - a(i,j,k)*cwrk(i-1,j,k) );

    cwrk(i,j,k) =                 c (i,j,k)  * fac(i,j,k);
    r(i,j,k)    = ( r(i,j,k) - r(i-1,j,k) * a (i,j,k)) * fac(i,j,k);
end
%---------------------------------------------------------------------
% back substitution
% put solution into x array, r(n) already has solution
x(n,j,k) = r(n,j,k);
```

```
for i = n-1:-1:1
   x(i,j,k) = r(i,j,k) - cwrk(i,j,k)*x(i+1,j,k);
end
%-------------------------------------------------------------------
% end of thomas
end
for j=2:20
   for i=1:n
      th(i+1,j,k)=x(i,j,k);
   end
end
%-------------------------------------------------------------
%  End of the first step of the ADI method in i with different j
else
for i=2:20
      %------------
a(i,1,k)=0;
c(i,n,k)=0;
for j=1:n
   b(i,j,k)=-(1+2*dt/(st^2*pr*dz^2));
end
for j=2:n
   a(i,j,k)=dt/(st^2*pr*dz^2);
end
for j=1:n-1
   c(i,j,k)=dt/(st^2*pr*dz^2);
end
%-----------
end
 for i=2:20
   for j=1:21
%r(i,j,1)=0;
th(i,j,1)=0;
end
end
 %---------------------------------------
 for i=2:20
   for j=1:n
   r(i,j,k)=-(th(i,j+1,k-1)+(dt/(st^2*pr*dy^2))*(th(i+1,j+1,k-1)-2*th(i,j+1,k-1)+th(i-1,j+1,k-
1))+s(i,j+1,k)*dt/st^2);
end
end
   %------------------
   for i=2:20
      %-----------------------
fac(i,1,k)   = 1.0/b(i,1,k);
cwrk(i,1,k) = c (i,1,k)* fac(i,1,k);
r(i,1,k)    = r(i,1,k) * fac(i,1,k);
```

```
for j = 2:n
   fac (i,j,k)    = 1.d0/( b(i,j,k) - a(i,j,k)*cwrk(i,j-1,k) );

   cwrk(i,j,k) =                  c (i,j,k)  * fac(i,j,k);
   r(i,j,k)    = ( r(i,j,k) - r(i,j-1,k) * a (i,j,k)) * fac(i,j,k);
end
%---------------------------------------------------------------------
% back substitution
% put solution into x array, r(n) already has solution
x(i,n,k) = r(i,n,k);
for j = n-1:-1:1
   x(i,j,k) = r(i,j,k) - cwrk(i,j,k)*x(i,j+1,k);
end
%---------------------------------------------------------------------
% end of thomas
end
for i=2:20
   for j=1:n
      th(i,j+1,k)=x(i,j,k);
   end
end
%-----------------------------------------------
end
end
%#####################################################################
for i=1:21
   y(i)=(i-1)*dy;
end
for j=1:21
   z(j)=(j-1)*dz;
end

%=====================================================
% to plot the centerline velocity and temperature with time:
for k=1:ke
   uk(k)=u1(11,11,k);
   thk(k)=th(11,11,k) ;
   sk(k)=s(11,11,k);
end
```

A-2 SIMPLE algorithm

The following program is performed to solve the 2-d navier stockes equations in an incompressible viscous flow in a Magnetohydrodynamic micropump with Fluctuating Lorentz force using a numerical marching technique which is the PRESSURE CORRECTION METHOD

```
%-------------------------------------------------------------------
%   1) set the dimensionless parameters and other required quantites:
clear
w=1;
l=100;
nx=100;
ny=10;
ke=50;
dt=0.1;
dx=(l/w)/nx;
dy=1/ny;
Re=0;
Ha=10;
st=10;
phi=0;
a=(2*dt/(st^2*dx^2))+(2*dt/(st^2*dy^2));
b=-dt/(st^2*dx^2);
c=-dt/(st^2*dy^2);
%-------------------------------------------------------------------
%   2) Guess values of P* at all the pressure grid points.
for k=1:ke
          t(k)=dt*(k-1);
for i=1:2:2*nx+1
   for j=1:2:2*ny+1
  pst(i,j,k)=0;
end
end
for i=3:2:2*nx+1;
       for j=1:2:2*ny+1
          pr(i,j,k)=0;
       end
   end
end
%  initial conditions of the velocities at time equal zero(k=1)
for i=2:2:2*nx
   for j=1:2:2*ny+1
      ust(i,j,1)=0;
   end
end
for i=1:2:2*nx+1
   for j=2:2:2*ny
```

```
       vst(i,j,1)=0;
   end
end
%---------
for k=2:ke
   for m=1:100
   % Boundary conditions of the velocities:
 % Boundary conditions at the left
for j=1:ny;
      vst(1,2*j,k)=0;
      ust(2,1,k)=0;
      ust(2,2*j+1,k)=0;
  end
% Boundary conditions at the bottom
for i=1:nx-1;
      ust(2*i+2,1,k)=0;
      vst(3,2,k)=0;
      vst(2*i+3,2,k)=0;
  end
% Boundary conditions at the top
for i=1:nx-1;
      ust(2*i+2,2*ny+1,k)=0;
      vst(3,2*ny,k)=0;
      vst(2*i+3,2*ny,k)=0;
  end
  % Boundary conditions at the right
for j=1:ny;
      vst(2*nx+1,2*j,k)=0;

  end
%-----------------------------------------------------------------------
%    3) Solve for u*(n+1) and v*(n+1) at all appropriate internal grid points.
  %

%------Calculate the star velocities in the interior points:
for i=4:2:2*nx-2;
   for j=3:2:2*ny-1;

       if i==2*nx-2
        % backword finite divided difference
  vsta(i,j,k-1)=(vst(i-1,j-1,k-1)+vst(i+1,j+1,k-1)+vst(i-1,j+1,k-1)+vst(i+1,j-1,k-1))/4;
      Ast(i,j,k-1)=Re*(ust(i,j,k-1)*((ust(i,j,k-1)-ust(i-2,j,k-1))/dx)+vsta(i,j,k-1)*((ust(i,j+2,k-
1)-ust(i,j-2,k-1))/(2*dy)))-(ust(i,j,k-1)-2*ust(i-2,j,k-1)+ust(i-4,j,k-1))/(dx^2)-(ust(i,j+2,k-1)-
2*ust(i,j,k-1)+ust(i,j-2,k-1))/dy^2;
      ust(i,j,k)=(1-((dt/st^2)*Ha^2*sin(2*pi*t(k-1))^2))*ust(i,j,k-1)-Ast(i,j,k-
1)*(dt/st^2)+(dt/st^2)*sin(2*pi*t(k-1))*sin(2*pi*t(k-1)+phi)-(dt/(st^2*dx))*(pst(i+1,j,k-1)-
pst(i-1,j,k-1));
```

```
else
   vsta(i,j,k-1)=(vst(i-1,j-1,k-1)+vst(i+1,j+1,k-1)+vst(i-1,j+1,k-1)+vst(i+1,j-1,k-1))/4;
        Ast(i,j,k-1)=Re*(ust(i,j,k-1)*((ust(i+2,j,k-1)-ust(i-2,j,k-1))/2*dx)+vsta(i,j,k-
1)*((ust(i,j+2,k-1)-ust(i,j-2,k-1))/(2*dy)))-(ust(i+2,j,k-1)-2*ust(i,j,k-1)+ust(i-2,j,k-
1))/(dx^2)-(ust(i,j+2,k-1)-2*ust(i,j,k-1)+ust(i,j-2,k-1))/dy^2;
      ust(i,j,k)=(1-((dt/st^2)*Ha^2*sin(2*pi*t(k-1))^2))*ust(i,j,k-1)-Ast(i,j,k-
1)*(dt/st^2)+(dt/st^2)*sin(2*pi*t(k-1))*sin(2*pi*t(k-1)+phi)-(dt/(st^2*dx))*(pst(i+1,j,k-1)-
pst(i-1,j,k-1));

end
end
end
%-----
for i=3:2:2*nx-1;
   for j=4:2:2*ny-2;


      usta(i,j,k-1)=(ust(i+1,j+1,k-1)+ust(i-1,j-1,k-1)+ust(i+1,j-1,k-1)+ust(i-1,j+1,k-1))/4;
Bst(i,j,k-1)=Re*(usta(i,j,k-1)*((vst(i+2,j,k-1)-vst(i-2,j,k-1))/2*dx)+vst(i,j,k-
1)*((vst(i,j+2,k-1)-vst(i,j-2,k-1))/(2*dy)))-(vst(i+2,j,k-1)-2*vst(i,j,k-1)+vst(i-2,j,k-
1))/(dx^2)-(vst(i,j+2,k-1)-2*vst(i,j,k-1)+vst(i,j-2,k-1))/dy^2;
vst(i,j,k)=vst(i,j,k-1)-Bst(i,j,k-1)*(dt/st^2)-(dt/(st^2*dy))*(pst(i,j+1,k-1)-pst(i,j-1,k-1));

end
end
%-------------------------------------------------------------------------
%   substitute the values of ust, and vst into pressure correction equation, and splve
% for pr at all interior grid points. (use Relaxation Technique).
%-----------------
 %----------------the first of relaxation (iteration)
for n=1:100
   %-------------------------------------
for i=3:2:2*nx-1;
      for j=3:2:2*ny-1;
         if i==2*nx-1
           d(i,j,k)=(vst(i,j+1,k)-vst(i,j-1,k))/dy;
         else
         d(i,j,k)=(ust(i+1,j,k)-ust(i-1,j,k))/dx+(vst(i,j+1,k)-vst(i,j-1,k))/dy;
      end
   end
end
%-----------------------------
%%%%%----------------------------
      for j=1:2:2*ny+1
       pr(1,j,k)=0;
   end
   for i=3:2:2*nx-3
```

```
    pr(i,3,k)=(-1/(a+c))*(b*(pr(i+1,3,k)+pr(i-1,3,k))+c*pr(i,5,k)+d(i,3,k));
    pr(i,1,k)=pr(i,3,k);
    pr(i,2*ny-1,k)= (-1/(a+c))*(b*(pr(i+1,2*ny-1,k)+pr(i-1,2*ny-1,k))+c*pr(i,2*ny-
3,k)+d(i,2*ny-1,k));
    pr(i,2*ny+1,k)=pr(i,2*ny-1,k);
    for j=5:2:2*ny-3
      pr(i,j,k)=(-1/a)*(b*(pr(i+2,j,k)+pr(i-2,j,k))+c*(pr(i,j+2,k)+pr(i,j-2,k))+d(i,j,k));
  end
end
pr(2*nx-1,3,k)=(-1/(a+b+c))*(b*pr(i-2,j,k)+c*pr(i,j+2,k)+d(i,j,k));
pr(2*nx-1,2*ny-1,k)=  (-1/(a+b+c))*(b*pr(i-2,j,k)+c*pr(i,j-2,k)+d(i,j,k));
pr(2*nx-1,1,k)=pr(2*nx-1,3,k);
pr(2*nx-1,2*ny+1,k)=pr(2*nx-1,2*ny-1,k);
for j=5:2:2*ny-3
   pr(2*nx-1,j,k)=(-1/a)*(b*(pr(i+2,j,k)+pr(i-2,j,k))+c*(pr(i,j+2,k)+pr(i,j-2,k))+d(i,j,k));

end
for j=1:2:2*ny+1
   pr(2*nx+1,j,k)=2*pr(2*nx-1,j,k)-pr(2*nx-3,j,k);
end
%pr
%end of relaxation
end
%
 %----------calculate the pressure
 for i=1:2:2*nx+1
        for j=1:2:2*ny+1
           p(i,j,k)=pr(i,j,k)+pst(i,j,k-1);
           pst(i,j,k-1)=p(i,j,k);
        end
     end
     for i=1:nx
   for j=1:ny+1
      xu(i)=dx*(i-1);
      yu(j)=dy*(j-1);
      u(i,j,k)=ust(2*i,2*j-1,k);
   end
end
for i=1:nx+1
   for j=1:ny
       xv(i)=dx*(i-1);
      yv(j)=dy*(j-1);
      v(i,j,k)=vst(2*i-1,2*j,k);
   end
end
for i=1:nx+1
   for j=1:ny+1
       xp(i)=dx*(i-1);
```

```
      yp(j)=dy*(j-1);
      pf(i,j,k)=p(2*i-1,2*j-1,k);
   end
end

         end

       end
       %==============================
      for k=1:ke;

      uk(k)=u(nx-4,ny/2,k);

    vk(k)=v(nx-4,ny/2,k);

      pk(k)=pf(nx-4,ny/2,k);
   end
```

نمذجة و تصميم مضخة كهرومغناطيسية دقيقة ذات تيار متناوب باستعمال قوى لورنتز

اعداد
مُصطفى رشيد عبد الله

المشرف
الدّكتور حمزه الدويري

Arabic Summary
ملخّص

تم عرض نموذج نظري يصف مضخة كهرومغناطيسية (MHD Micropump) . تدار المضخة باستخدام قوة لورينتز والتي تظهر كنتيجة للتفاعل بين مجال كهربائي ومجال مغناطيسي عمودي عليه، وتستخدم قوة لورينتز الناتجة لضخ سوائل ذات موصلية كهربائية داخل قناة دقيقة الأبعاد.
تم وضع نموذج رياضي يصف المرحلة الانتقالية لجريان رقائقي متطور بالكامل ولتوزيع درجات الحرارة، حيث تم وضع حلول تحليلية وأخرى عددية للسرعة ودرجة الحرارة تحت تأثير قوة لورينتز.
تم وضع حلول للمعادلات المتحكمة بشكل تحليلي باستخدام طريقة (Eigen Function Expansion) وحلول بشكل عددي باستخدام طريقة الفرق المحدود (ADI Finite Difference).
وجد أن هناك توافقا جيدا بين النتائج العددية والتحليلية. تم دراسة تأثير مجموعة من العوامل المختلفة على المرحلة الانتقالية والثابتة للسرعة ودرجة الحرارة وهذه العوامل هي: نسبة الإرتفاع للعرض، ورقم Hartmann ، ورقم Prandtl، ورقم Eckert.
بينت النتائج أن السيطرة على السرعة ودرجة الحرارة يمكن أن يتحقق من خلال السيطرة على فرق الجهد، والتدفق المغناطيسي، والإختيار الجيد للموصلية الكهربائية.
تم أيضا في هذه الدراسة وضع حلول عددية للمرحلة الإنتقالية لجريان رقائقي في مرحلة التطور باستخدام طريقة الفرق المحدود (Finite Difference) وخوارزمية (SIMPLE) .
تم دراسة تأثير رقم Hartmann على منحنى السرعة الإنتقالية وعلى طول منطقة المدخل للقناة. وقد وجد أن السيطرة على الموصلية الحرارية وشدة التدفق المغناطيسي ستؤدي إلى السيطرة على طول منطقة المدخل.
وتم دراسة تأثير قوة لورينتز المترددة على مضخة كهرومغناطيسية ذات تيار متناوب لحالتي الجريان المتطور والجريان في مرحلة التطور. وقد وجد أنه عند استخدام تردد عالي يكون الحجم النابض صغيرا ويؤدي ذلك إلى جريان مستمر بدلا من جريان متردد. وجد أيضا أن قيمة واتجاه الجريان يمكن التحكم بها من خلال السيطرة على تغيير المرحلة بين المجالين الكهربائي والمغناطيسي.